

DIGITAL SIGNAL ANALYSIS AND COMPRESSION TECHNIQUES USING WAVELETS

A Thesis

Submitted to the Kuvempu University for the Award of the Degree of

Doctor of Philosophy

in the Faculty of Science and Technology

by

Naveen kumar.R

Under the Guidance of

Dr. B.N.Jagadale



Department of Studies & Research in Electronics

School of Physical Sciences

Kuvempu University

Jnana Sahyadri, Shankaraghatta – 577 451

Shimoga, India

April, 2018

R/t
G21.381 32(a)
NAV

t-3994

Kuvempu University Library
Jnanasahyadri, Shankaraghatta

DECLARATION

I hereby declare that the work reported in this thesis is entirely original and has been carried out by me independently in the Department of Studies and Research in Electronics, Kuvempu University under the guidance of Dr. B.N. Jagadale, Department of Electronics, Kuvempu University, Shankaraghatta. I also declare that this work has not formed the basis for the award of any Degree, Diploma, Associate ship or similar title of any University or Institution.

April, 2018
Shankaraghatta




NAVEEN KUMAR.R

Department of Studies & Research in Electronics,
Kuvempu University,
Shankaraghatta - 577 451, India.

CERTIFICATE

This is to certify that the thesis entitled **DIGITAL SIGNAL ANALYSIS AND COMPRESSION TECHNIQUES USING WAVELETS** submitted by Mr. *Naveen kumar.R.* for the award of the degree of *Doctor of Philosophy* in the Faculty of Science and Technology, Kuvempu University Shankaraghatta, is based on the work carried out by him under my guidance and supervision. This thesis or any part of it has not been previously submitted, to the best of my knowledge, to any University or Institution for any other degree or diploma.

April, 2018
Shankaraghatta



Dr. B.N. Jagadale
Department of Electronics,
Kuvempu University,
Shankaraghatta - 577 451.
India.

Acknowledgement

Completion of this Doctoral thesis is actually long winded process, and a thesis is not an exclusive work of personage. This is possible by the support and encouragement of many resources, benefited from the insights and guidance of more than a few persons. Journey of these three years are fruitful and not have been completed without the help of countless peoples.

First and foremost, I feel grateful to thank my Ph.D. guide, Dr. B.N. Jagadale, Assistant professor, Dept. of PG studies and Research in Electronics, Kuvempu University, for his precious guidance, scholarly inputs and unswerving support I conventional throughout the research work. This wonderful journey is not fulfilling without his constant encouragement from the day I began my research work to till today. Still I remember the first day I approached him and he amiably agreed to serve as my guide for my Ph.D. at Kuvempu University. He is a kind person and a brilliant teacher to whom I indebted a great deal for the entire digital signal processing that I have learnt at research laboratory, Kuvempu University. During most difficult time's during the documentations of research articles and thesis, he gave me the moral support and good suggestion to resolve the problems. You have always been my leader in all the ups and downs throughout my research journey from past three years. I feel lucky to have an opportunity to work under your guidance since undertaking my master's degree.

I wish to express my gratitude to, Prof. J.S. Bhat, Karnataka University, Dharwad, for giving out his brilliant ideas and excellent advice in signal processing.

He deserves huge contentment for his expertise editing of documents for matters of grammar, syntax and spelling. Even in your busy schedule you found time to address my concerns, I have been grateful for everything you have done for me.

I also immense in this course was the support provided by Prof. Devaraju.J. T, Prof. Mrithyunjaya. V. Latte, Prof P.M. Hadalgi and Dr. A. M. Khan. I wish to convey my thankfulness for their moral support and they are taking part in constructive pondering pertained to my research work which has always been a productive experience.

No Research is accomplished without facilitated laboratories and library. My experience at research laboratory, Kuvempu university have been nothing short of wonderful. Many sweet memories of sleepless nights in laboratory with my research works always make me feel proud, I felt at home at research laboratory. Campus library is a pond of resources I used to update with current developments and publications in the field of signal processing. This time I express my thanks to library staffs and Electronics lab assistants of Kuvempu University for their support.

I am cordially conveying my all credit to my family, my father Ramadas.G, mother Jayapadma.M, wife Inchara.P. R, brother Kiran Kumar.R, and sister Asharani. R, my father in law Girish D.R for their huge support and encouragement in my every step. They have given potency for me to reach any goal I choose. Their moral support when things were bad and back-up when things were good makes me more consistent and confident. Their pride for me is my main goal in life. I am thankful to them for all their love, determined support, and outwardly unlimited belief in me during my Ph.D. work. They deserve far more credit than I can ever give them.

I am also blessed with an invaluable extended family and close, loving friends. I would like to finally acknowledge my father in law late sri. Mariyappa. D.V, my mother in law late Smt. Ramanjinamma and family who dreamt my career. My research was not possible without support of companion friends Sandeepa. K.S, Akash. K, Girish. K. C, Nirikshith, Mahesha. M.C, Avinash.K, Ramesh. M, Chathurmuka.V. S, Ganesha. K, Basavaraj. U.R., and Abhishek. T.E for their love, affection, and endless support. Thank you all for your support and interest in my journey. You made it all the more rewarding.

Naveen Kumar.R

*This Doctoral Dissertation is especially dedicated
to My Beloved family*

List of Figures

2.1	STFT computation by sliding a window	18
2.2	(a) sine wave; (b) mother wavelet (debauches)	19
2.3	Wavelet decomposition of function $Y(t)$ by scaling ($\tau = 2$) and shifting($\lambda = 0.4$)	21
2.4	CWT of function using Haar wavelet	23
2.5	Different families of wavelets	25
2.6	First level decomposition filter bank	33
2.7	Second level decomposition filter bank	33
2.8	First level reconstruction filter bank	34
2.9	Combination of Decomposition and reconstruction filter banks	34
3.1	Digital image with dimension	37
3.2	General block diagram of wavelet compression and decompression process	40
3.3	Two channel QMF	41
3.4	Level two wavelet decomposition	42
3.5	Level two wavelet reconstruction	43
3.6	The hard and soft threshold in wavelet	44
3.7	Root to descendent dependency in spatial domain	47
3.8	Transformation of image to set and	48
3.9	Quad tree partition of set 'S'	48
3.10	Octave partition of set 'I'	49
3.11	A block diagram of proposed hybrid image compression	54
3.12	A graphical representation of improved method to shrink wavelet coefficient	57
3.13	Input test images (a)Boat; (b)Lena; (c)Goldhill; (d)pepper	60
3.14	(a) Original boat image compressed at compression ratio of 80:1 using (b) SPIHT; (c)WDR; (d)JPEG2000 [137]; (e)Proposed method(Q=0.006)	60

4.1	Pipelined view of proposed lossy compression algorithm	69
4.2	The graph for different test images using DWT-DFRCT	71
4.3	(a)Original lena image(512X512) compressed by using proposed method at (b)20% with PSNR 36.23db; (c)40% with PSNR 35.29db;(d)60% with PSNR 35.08db; (e)80% with PSNR 33.29db;(f)85% with PSNR32.33db;	72
4.4	PSNR comparison of test images (1.Lena;2.Barbara; 3.cameraman; 4. rice; 5. IC) using DFRCT, DFRFT and DWT-DFRCT	73
4.5	A block view of proposed method	75
4.6	(a) Original Barbara image compressed using by DWT-DFRFT at compression ratio(b)20%;(c)40%;(d)60%; (e)70%;(f)80%	78
4.7	Comparison of proposed method with DFRCT and DFRST for barbara image at different compression percentage (50% to 90%);	79
4.8	Pipelined view of proposed compression technique	81
4.9	Original test images (a)Lung contusion(<i>XRAY</i> – 1); (b)MRSA lungs absess <i>X – Ray</i> (<i>XRAY</i> – 2) ; (c) <i>Pine – bone</i> (<i>MRI</i> – 1);(d) <i>knee_{uni}</i> (<i>MRI</i> – 2) ; (e) <i>PET</i> – 1; (f) <i>Lung</i> (<i>ULTR</i> – 1); (g) Thyroid structure (<i>ULTR</i> – 2); (h) <i>Skull</i> (<i>ULTR</i> – 3);	82
4.10	PSNR (a) and SSIM (b) varied along the Q-Factor	83
4.11	PSNR(a) and SSIM (b) varied along the Fractional order	84
4.12	PSNR (a) and SSIM (b) graphical comparison of proposed method with JPEG and JPEG2000	89
4.13	<i>XRay</i> – 2 image compression using JPEG2000 at compression percentage (a)20%; (b)40%; (c)60%; (d)80%; compression using JPEG at (e)20%; (f)40%; (g)60%; (h)80%; and compression by proposed method at (i)20%; (j)40%; (k)60%;(l)80%;	90

5.1	(a) Original lena (512X512) reconstructed with percentages of ranks (b)85% of ranks, (c) 65% of ranks, (d) 50% of ranks,(e)40%of ranks, (f)25% of ranks	97
5.2	(a) a block of wavelet coefficients processed by adaptive scanning ordered encode by SPIHT (b) Adaptive scanning order of the tree, where gray nodes are a significant node from the previous scanning	100
5.3	Generic representation of proposed MSVD- ASPIHT algorithm	101
5.4	Compression performance of proposed method with other compression technique with respect to PSNR and Compression ratio	105
5.5	(a) Uncompressed Deer image (512X512) (b) compressed by ASPIHT (c) compressed by JPEG2000 [184], (d) compressed by proposed method at 40:1	106
5.6	(a) Original lena image (512X512) is compressed by compression ratios of (b) 20:1; (c) 40:1; (d) 60:1 (e) 80:1 (f) 120:1using proposed MSVD-ASPIHT method	107
5.7	Performance evaluation of proposed method for fixed compression (20:1) with respect to PSNR and percentage of SVD ranks for deer image	108
5.8	Pipelined view of proposed MSVD-BTC image compression method	110
5.9	(a) Original Lena uncompressed image (b) Compressed at 0.125 BPP; (c) Compressed at 0.250 BPP; (d) Compressed at 0.500 BPP; (e) Compressed at 1.00BPP; (f) Compressed at1.250 BPP using proposed method	115
5.10	(a)Wavelet Pyramid decomposition of sub band with parent child relation;(b) flow of Significant mapping for wavelet coefficients	119
5.11	Channelized view of $MNSVD_{EZTW}$ method	120
5.12	Performance evaluation graph of proposed method with other compression method through respect to PSNR v/s Compression rate	124

- 5.13 (a) Uncompressed fireworks image is compressed by
compression ratios of (b) 30:1; (c) 70:1; (d) 90:1
using segmentation based rank one updated MNSVD-EZTW
method 125
- 5.14 Original Boat image compressed by (a) EZTW;
(b) Basic SPIHT; (c) JPEG; (d) proposed method at
compression rate 50:1 126

List of Tables

3.1	Frequently using image file formats and its properties [103]	40
3.2	Comparison of proposed method with other methods	60
4.1	Eigen values multiplied to DST kernel matrix to get DFRST	64
4.2	Eigen values multipliable to DCT kernel matrix to get DFRCT	65
4.3	Eigen values multipliable to DFT matrix to get DFRFT kernel matrix	67
4.4	MSE, PSNR at optimum wavelet decomposition level, quantization factor and opt compression proposed method for chosen compression percentage for lena image	71
4.5	MSE, PSNR comparison of proposed method with DFRCT and DFRFT	72
4.6	PRD and PSNR calculation of proposed method at different compression percentage for Barbara image	77
4.7	PRD and PSNR comparison of proposed method with DWT-DFRST and DWT-DFRCT	78
4.8	PSNR and SSIM of proposed method at different compression percentage for X-Ray images	83
4.9	PSNR and SSIM of proposed method at different compression percentage for MRI and PET image	86
4.10	PSNR and SSIM of proposed method at different compression percentage for Ultrasound images	87
4.11	PSNR Comparison of proposed method with JPEG and JPEG2000 at compression percentage 80	88
4.12	SSIM Comparison of proposed method with JPEG and JPEG2000 at compression percentage 80	88

5.1	Percentage of ranks used for specified singular values for reconstruction of lena image (8X8 block)	96
5.2	PSNR comparison for fixed compression ratio 20:1	102
5.3	PSNR comparison for fixed compression raio 40:1	103
5.4	PSNR comparison for fixed compression ratio 80:1	103
5.5	SSIM values for fixed compression ratio 20:1	103
5.6	SSIM values for fixed compression ratio 40:1	104
5.7	SSIM values for fixed compression ratio 80:1	104
5.8	Comparison of PSNR values for Barbara image at different BPP	114
5.9	Comparison of PSNR values for Lena image at different BPP	114
5.10	Comparison of PSNR values for goldhill image at different BPP	114
5.11	Comparison of PSNR values for Cameramen image at different BPP	114
5.12	Comparison of PSNR values for Jet plan image at different BPP	115
5.13	Comparison of PSNR values for pepper image at different BPP	115
5.14	PSNR comparison for fixed compression ratio 30:1	122
5.15	PSNR comparison for fixed compression raio 70:1	122
5.16	PSNR comparison for fixed compression ratio 90:1	122
5.17	SSIM values for fixed compression ratio 30:1	123
5.18	SSIM values for fixed compression ratio 70:1	123
5.19	SSIM values for fixed compression ratio 90:1	123

Abstract

Several applications like signal compression, enhancement, classification, recognition in the field of engineering field are constantly updating the signal processing technology. Signal processing techniques also have overlapping borders with areas of applications like, probability and statistics, decision theory and numerical analysis.

Signal compression, enhancement, and classifications use their own mathematical procedures for manipulation of signal, called as 'transforms'. There are several methods to represent the signal either in time, frequency and wavelet domain. Digital signal analysis by using time frequency representation (TFR) is a major developing research area in the field of digital signal processing (DSP). The Fourier transform (FT) assumes that the spectral characteristics of a signal do not change with time and hence it is not appropriate for the analysis of non-stationary signals. Also Short time Fourier transform has its limitations in analyzing the signal, due to fixed window size. Multiresolution analysis of wavelet transform makes it superior TFR for DSP applications. Smart communication systems in mobile, web applications are highly reliant on signal compression and coding technology to recover large amount of data.

Signal compression is another sub field in DSP, essential in developing advanced computer technology. It is a technique in which any source information, can be represented with a reduced number of bits without affecting its originality. Based on reconstruction capacity, it was classified as lossy and lossless compression methods. Multimedia and mobile applications are examples of having lossy

compression approaches, whereas, medical imaging, satellite and defense data handling applications use lossless compression techniques. Both lossy and lossless compression techniques are found their own significance in the field of specific signal processing applications. Identification of suitable TFR tool for signal compression application is one of the challenging tasks in DSP.

The present investigation is to develop new compression techniques for image data, by using TFR tool that includes wavelet transform and fractional transforms. However, coding of low frequency wavelet coefficients for compression is one of the challenging part of the present signal compression technology. It is found that, the combination of formal wavelet compression techniques with other compression techniques significantly improves the compression performance.

The thesis has two contributions in hybrid wavelet compression schemes and is targeted for high compression ratio along with better image quality. The thesis investigates the problems in present compression technology like JPEG2000 using wavelet transform. The advantages of wavelet mathematics with respect to time frequency plane creates a foundation for the development of new signal compression algorithm.

The main focus of this work is towards two dimensional signal compression and digital image compression using wavelet transform is explained by using general block diagram. The key features of wavelet in image compression using threshold techniques and progressive encoding schemes like EZTW, SPIHT, SPECK, WDR and ASWDR are discussed and a new compression algorithm with an improved neighbor shrink in DWT-DCT for grey scale image is developed. This compression results and their comparison with JPEG 2000 shows, significant improvements in image

compression. The idea of coding low frequency wavelet coefficients is extended by using fractional transforms and two compression algorithms DWT_DFRCT and DWT_DFRFT are developed by the combination of wavelet transform and fractional transforms. The lossy compression algorithm uses DFRCT to code low-frequency wavelet coefficients, but neglects, first level high frequency wavelet coefficients along with imaginary part of DFRCT to make it lossy approach. However, even though it is a lossy approach, the algorithm efficiently preserves the quality of reconstructed image. Another lossless compression algorithm was tried by using DFRTFT to code low frequency wavelet coefficients. The extension of this lossless method was tried in medical image compression. The method uses block based DFRFT to code low frequency wavelet coefficients. The results of these methods are compared with two dimensional DFRFT, DFRCT, DFRST and JPEG2000 and found that proposed algorithms show improvement in quality of reconstruction and compression percentage.

In the end, the thesis discusses a new approach for pre-processing procedure based on median based singular value decomposition (MSVD) is designed, which can improve the compression performance of wavelet based image compression technique. Basically, adaptive SPIHT, EZTW and binary tree coding algorithms operate at high compression ratio but they tend to lose image quality during reconstruction process. This could be improved by combination above methods with modified SVD. Median based SVD is used as pre-processing step for BTC and ASPIHT and mean based SVD is used for EZTW for gray scale image compression. The results show some significant improvement in compression performance in terms of PSNR and compression percentage.

The thesis is concluded with discussion on its limitations and future work

Contents

Acknowledgment	i
Abstract	iv
List of Figures	vii
List of Tables	xi
1 Introduction	
1.1 Introduction to Digital signal processing	01
1.2 Digital signal analysis in time-frequency domain	03
1.3 Signal compression	07
1.3.1 Definition	07
1.3.2 Types of signal compression techniques	07
1.4 Real time applications of signal compression	09
1.5 Challenges in wavelets for signal compression	10
1.6 Aim and objective of research	11
2 Digital signal analysis using wavelets	
2.1 History of wavelet	15
2.1.1 Fourier transform	16
2.1.2 Short time Fourier transform	17
2.2 Continuous wavelet transform	19
2.3 Discrete wavelet transform	23
2.4 Multiresolution analysis in wavelets	24
2.5 Wavelet decomposition	29
2.6 Wavelet reconstruction	32
2.7 Interpretation of wavelet filters	32
2.8 Summary	35

3	Two dimensional signal(Image) compression using wavelets	
3.1	Fundamentals of digital image	36
3.1.1	Digital image	36
3.1.2	Types of image	38
3.1.3	Image formats	39
3.2	Image compression using discrete wavelet transform	40
3.2.1	Wavelet decomposition using filter banks	41
3.2.2	Wavelet threshold for image compression	43
3.2.3	Wavelet based encoders for progressive image compression	45
3.2.4	Error metrics	51
3.3	Implementation of improved neigh shrink in hybrid wavelet transform for gray scale image compression	53
3.3.1	Previous work	53
3.3.2	Proposed hybrid compression technique	54
3.3.3	Results and discussions	59
3.4	Summary	61
4	Image compression techniques using wavelet and fractional transforms	
4.1	Introduction	62
4.2	Fractional transforms in image compression	62
4.3	Improved lossy image compression algorithm using DWT and DFRCT	68
4.3.1	Previous work	68
4.3.2	Flow of DWT-DFRCT algorithm	68
4.3.3	Results and discussions	70
4.4	Lossless image compression algorithm using DWT and DFRFT	74
4.4.1	Previous work	74
4.4.2	Flow of DWT-DFRFT algorithm	74
4.4.3	Results and discussions	77

4.5	Medical image compression algorithm using hybrid wavelet transform with block based DFRFT	
4.5.1	Introduction	80
4.5.2	Flow of Proposed method	80
4.5.3	Results and discussions	82
4.6	Summary	92
5	Hybrid compression schemes using modified singular value decomposition and wavelets	
5.1	Background	94
5.2	Median based rank one updated singular value decomposition for image compression(MSVD)	95
5.3	Hybrid gray scale image compression using MSVD and adaptive set partition hierarchical tree	98
5.3.1	SPIHT with adaptive coding order(ASPIHT)	98
5.3.2	Realization of MSVD-ASPIHT	100
5.3.3	Simulated results and discussions	102
5.4	Improved binary tree coding for gray scale image compression by using MSVD	109
5.4.1	Binary tree coding (BTC)	109
5.4.2	Realization of MSVD-BTC	110
5.4.3	Simulated results and discussions	113
5.5	Improved EZTW compression algorithm using mean based rank one updated SVD	116
5.5.1	Mean based rank one updated SVD(MNSVD)	116
5.5.2	Embedded zero tree wavelet (EZTW)	117
5.5.3	Realization of MNSVD-EZTW	119
5.5.4	Simulated results and discussions	121
5.6	Summary	127

6	Conclusion and future scope of research work	
6.1	Time frequency representation of signal in wavelet domain	128
6.2	Selection of wavelet for image compression	129
6.3	Image compression using hybrid wavelet transform	130
6.3.1	Wavelet with fractional transforms	130
6.3.2	Modified SVD in wavelet based progressive image compression	131
6.4	Contributions	132
6.5	Future work	132
	Bibliography	134
	Publications	157

Chapter 1

Introduction

1.1 Introduction to Digital Signal Processing

Digital signal processing (DSP) is cutting edge technology with wide range of applications in the field of science and technology. DSP plays a vital role in increasing computational speed and miniaturization of advanced digital computers. *It is compassion of every one's of present information technology and impact is felt all over the everywhere: in mobile technology, seismic pulsations, medical data analysis, and defense communication technology.* Naturally occurring sound waves, image signals, electromagnetic waves and vibrations are considered as signals which are manipulated by using DSP techniques [1-3].

DSP extends its applications beyond the boundaries of signal processing to other areas of science and technology, like medical science, business statistical analysis, mathematical modeling, genetics, and forensic science [4-6]. It became a powerful tool for designers to increase the efficiency of newly arriving technologies. Several ground-breaking signs of progress have been already made in wide range of applications [7,8]: *multi-rate signal processing in speech/audio technology, nonlinear signal processing in image recognition, a time frequency signal analysis in radar and sonar.*

In general, a signal is an entity which conveys information and is defined as function

of one or more independent variables. For example, a speech signal, where amplitude is function of an independent variable time, an image has intensity as function of two independent variables in spatial coordinates (x, y) . Most of digital signal processing concepts formed to analyze non stationary signals [9-12]. Naturally occurring most of the signals like speech, image, sensor waves, and vibrations are nonstationary signals. These signals are a convenient form of basic signals like sine, cosine, square waves and etc. and require specialized tools to process. This is where the time-frequency techniques come into picture.

Study of time-frequency techniques in signal analysis gain more attention in the field of DSP because of their characteristic features. Prior knowledge of features of signals is often advantageous to study and represent the signal in either time or frequency domain. A set of functions (transforms) are enough to extract the features of signals and represent them in a better way [13].

Digital signals obtained after sampling of analog signals through analog to digital (A/D) converters are loaded with redundancy which is will not make any significant contribution in reconstruction process [14]. Hence elimination of redundancy in digital signal and its compact coding increases the speed of computation and reduces the required storage space. In order to develop an efficient algorithm to analyze and characterization of digital signals, prior analysis of digital signals are very important.

1.2 Digital signal analysis in time-frequency domain

Digital signal analysis (DSA) deals with the study of digital signal characteristics, which are obtained through digitization of natural analog signals like sound waves, electric signals, image signals, and seismic vibrations. Basically, a sequence of a digital signal is represented either in time, frequency or in wavelets domain [15]. Time domain representation uses finite input response (FIR) or infinite input response(IIR) filters, whereas, frequency domain representation uses Fourier transform (FT) to analyze the frequency spectrum of the signal [16-20]. But in wavelet domain, signals are represented both in time and frequency domains.

A French mathematician 'Jean-batiste Joseph Fourier' (1807) made an important contribution in DSA by introducing an equation for frequency representation to analyze the behavior of discontinuous signals [21]. He represented, any discontinuous function with the sum of continuous functions and he termed it as Fourier transform (FT).

$$X(f) = \int_{-\infty}^{\infty} x(t)e^{-j2\pi ft} dt \quad (1.2.1)$$

FT is a powerful tool which acts as sliding door for the signal and convert them into their frequency segments [22, 23]. However, the biggest limitation of FT is that, it presumes that the spectral characteristics of signals are not varying with time and hence it is ineffective in analyzing non-stationary signals. In order to get spectral characteristics at different time scale, a time-frequency representation (TFR) was introduced. This is done by application of small window for non-stationary signals and then computing FT for windowed signal, and is referred as short time Fourier transform (STFT) [24]. STFT for

any sequence of signal is given by,

$$w(n, \phi) = \sum_{-\infty}^{\infty} x(m)h(n-m)e^{-j\phi m} \quad (1.2.2)$$

Here, the STFT analyze the behavior of the signal by using the sliding window [25]. However use of windows cause unexpected truncation of signals in STFT, leading to Gibb's phenomenon and reduces the time/frequency resolution [26].

A famous quadratic TFR representation method introduced by Ville [27], as Wigner Ville distribution (WVD) resolves the problems caused by STFT. The WVD $S_f(n, \phi)$ of any discrete signal $S(n)$ s given by,

$$S_f(n, \phi) = 2 * \sum_{k=-\infty}^{\infty} e^{-j2k\phi} f(n+k)f^*(n-k) \quad (1.2.3)$$

WVD returns, many useful signal analyzing properties like marginal properties, instantaneous frequency and group delay [28]. Most common difficulty in applying WVD to discrete signal is aliasing effect in time-frequency plane due to the periodic disproportion between band limit signal and Wigner distribution [29]. This effect can be overcome by sampling the band limited signal twice of its maximum frequency [30]. Another hurdle in time frequency analysis of signal using WVD is, counterfeit structure formation of '*cross term interference*' due to its bilinear form, which reduces the time-frequency resolution [31]. Many attempts have been made by a researchers to suppress the cross term interference in time-frequency representation by smoothing the window and optimizing the kernel for the limited set of signals [32-35].

Fractional Fourier transform (FRFT) became the superior alternative to the FT in time-frequency representation. Use of chirp signal as an orthonormal basis and better interpretation as rotational angles in time-frequency plane made FRFT more advantageous

in a study of discrete signals [36]. For finite input samples $y(n)$ at sampling intervals Δu closed form of discrete FRFT (DFRFT) $Y_\alpha(m)$ at sampling interval Δt is written as,

$$Y_\alpha(m) = \sum_{n=-N}^N F_\alpha(m, n)y(n) \quad (1.2.4)$$

where normalized kernel $F_\alpha(m)$ is given by,

$$F_\alpha(m) = \sqrt{\frac{|\sin\alpha| - j \operatorname{sgn}(\sin\alpha) \cos\alpha}{2M+1} \frac{e^{j \frac{\cos\alpha}{2} m^2 \Delta n^2} e^{j \frac{\cos\alpha}{2} n^2 \Delta t^2} e^{-\frac{j 2n\pi m}{2M+1}}}{den}} \quad (1.2.5)$$

This DFRFT computational method is straightforward and uses two chirp multiplication and one FFT operation [37]. The most common approach for computation of DFRFT [38] is by computing fractional power (rotational angle) for the DFT kernel matrix. This method gives theoretical justification for DFRFT but doesn't comply with rotational rules, and finds itself in difficulty during signal reconstruction using inverse transform. DFRFT implementation introduced in [39] uses the orthogonal DFT Hermite Eigenvectors to relate the FRFT, and preserves the rotational properties of a signal in the time-frequency plane.

Discrete wavelet transform (DWT) is a dominant approach in processing digital signals with its time-varying spectra. It processes the signal by using scaling and shifting operations of 'mother wavelets' [40]. Mathematical representation of Haar wavelet for infinite sum of large numbered functions is given by,

$$f(t) = \sum_{k=-\infty}^{\infty} x_k \phi(t-k) + \sum_{k=-\infty}^{\infty} \sum_{j=0}^{\infty} y_{j,k} \psi(2^j t - k) \quad (1.2.6)$$

where, x_k and $y_{j,k}$ are the coefficients to be computed by using scale function $\phi(t)$ and Haar wavelet function $\psi(t)$. Basically scale function $\phi(t)$ is a unit pulse

$$\phi(t) = \begin{cases} 1, & \text{if } 0 \leq t \leq 1. \\ 0, & \text{otherwise.} \end{cases} \quad (1.2.7)$$

Haar wavelet, is a step function,

$$\psi(t) = \begin{cases} 1, & \text{if } 0 \leq t \leq 0.5. \\ -1, & \text{if } 0.5 \leq t \leq 1. \end{cases} \quad (1.2.8)$$

In DWT multiresolution analysis, the signal with higher frequency is analyzed by using a window with high time resolution and low-frequency resolution. Similarly, at lower frequencies, the analysis is done with a window of poor time resolution and high-frequency resolution [41]. If we compare all these methods, the cross term interference in bilinear transform WVD, made it less attractive in time-frequency analysis. STFT suffers from fixed window size and time-frequency tradeoff. However, FRFT also affected by its limited rotational angles and time-frequency tradeoffs. But multiresolution property, choice of orthonormal basis functions, optional sampling rate, and perfect reconstruction filters made DWT more attractive and efficient in a digital signal analysis in the time-frequency plane. Time-frequency analysis uses distributive functions to map the energy of digital signal on time-frequency plane. The time frequency distribution (TFD) is used to extract features like power spectrum, energy, harmonic feature, noise etc. [42-44] from the signal. It also facilitate to analyze the frequency varying nonstationary signals such as seismic waves, speech, image, radar, sonar and mechanical vibrations etc [45-47]. TFD techniques are very effective in energy characterization of signal in time-frequency plane, which helps to extract significant information from the signal. Applications like speech/image modeling, speech/image compression, watermarking, recognition, restoration etc., use time-frequency representation techniques to process the source information [48-51]. Hence, by developing new algorithms by using TFR techniques a significant contribution can be made in the field of science and technology.

1.3 Signal compression

Handling of large data is a most familiar problem in modern data communication system. Large data, refers to the signal, which requires a large number of the memory location to store and process. Signal processing techniques are necessary to manipulate and format the signals digitally, which in turn help in reducing the memory required to store these processed signal and ease the communication process.

1.3.1 Definition

Nonstationary signals are finite time-varying spectra with compact signal boundaries. Even then there exist some signal components which are repeatedly occurring in a spectrum forms redundancy and process of efficient removal of such undesirable components and coding of the signal without affecting original signal is considered as signal compression. Formally, *a process of representation or coding of any finite signals with reduced number of bits without affecting its originality is termed as signal compression* [52].

The compression technology always finds itself in significant role in designing new computer technologies as it enhances the efficiency of any digital computational device by increasing its computational speed and also reduces the size of the device.

1.3.2 Types of signal compression techniques

Based on reconstruction capability, the compression techniques are broadly classified as lossy and lossless compression techniques. In compression process, signal is encoded and is reconstructed from decoder during decompression. If reconstructed signal resembles its source signal then it is called as lossless compression technique, otherwise it is called as

lossy compression technique [53].

a. Lossy compression Techniques

In lossy compression, the compressed data will not be identical, bit-for-bit with the original data. This method is also called Perceptive coding as it utilizes the fact that some information is truly irrelevant in that the intended recipient will not be able to perceive that, it is missing. In most cases, information that is close to irrelevant is neglected, which results in loss of quality of the reconstructed signal. However, this quality loss is small and is fine, as we think of the data reduction [54]. The main objective of lossy compression is to get maximum benefit, i.e., compression ratio (CR) or bit rate reduction, at a reduced cost, i.e., loss in quality [55]. An example for application of lossy compression technique is, joint photographic expert group (JPEG) image file, which is commonly used for photographs. The JPEG compression, allows designers to decide how much loss can be introduced and make a trade-off between file size and image quality [56].

b. Lossless compression techniques

Lossless compression technique, works by removing the redundant information present in a signal. This would be the ideal compression technique as there is no loss of information. Every single bit of data, that was in original data file, will remain after the file is decompressed and all the information is completely restored.

However, lossless compression has two common drawbacks, as, it offers small compression ratio, using it alone is not economically viable. Also, it does not produce stable output data rate as the compression ratio is very much dependent on the input data [57]. Lossless techniques that are used in general are run-length encoding (RLE) and entropy encoding[58], graphics interchange file (GIF).

1.4 Real-time applications of signal compression

Signal compression has unlimited applications, since it is a necessary tool to create smart embedded systems and to develop high speed communication devices. Signal compression has become an integral part of computing systems and some real time applications in which compression techniques used are as follows.

a. *Astronomical and communication applications:* Signals and images captured in space are suffered by blur due to rapid change in refractive index of the atmosphere. 1D and 2D signals captured by spaceship are degraded due to motion variations of a source with respect to a spaceship. Storage of large information for long period in smart devices is possible only due to compression techniques. To avoid network trafficking, the only solution is to compress and code the signal with low bit rate. This technique is used in high definition television (HDTV), three dimensional TV (3DTV), personnel computers (PC)[59]. Incremental cost-effectiveness ratio (ICER) is wavelet-based image compression file format used by the NASA Mars rovers. The mars exploration rovers spirit (MER-A) and Opportunity (MER-B) both use ICER technology [60].

b. *Medical imaging:* Today a lot of hospitals handle their medical image data with computers. The use of computers and a network makes it possible to distribute the image data among the staff efficiently. As the healthcare is computerized, new techniques and applications are developed, and the medical resonance imaging (MRI) and computed tomography (CT) techniques are among them. MR and CT produce sequences of images (image stacks) for every cross-section of an object. The amount of data produced by these techniques is vast and this might be a problem when sending the data over a network. To overcome this, image data can be compressed. For two-dimensional data, there exist

many compression techniques such as JPEG, GIF and the new wavelet-based JPEG2000 [61,62].

c. Defense and investigation: Many defense applications require signal compression, such as naval commands, to handle communication between boat with navy base. We can improve the sound amplification and ranging (SONAR) performance by pulse compression. In visually guided missiles, which may obtain distorted images from cameras mounted on missiles, due to the effects of pressure differences in environment. Compression methods are used to restore X-ray images of aircraft parts to improve aviation inspection procedures. It is also used to improve the RADAR image quality [63,64].

1.5 Challenges in wavelets for signal compression

The most common challenging part of signal compression is to reduce the size of a signal without affecting the signal quality during signal transmission. But there is an ambiguity between compression percentage and quality in a reconstruction of signals [65]. In this situation, some compression techniques are developed to enhance the compression performance based on their requirement for specific applications.

In image compression, the lack of spatial adaptive quantization may result in serious blurring problem, in areas with subtle texture. Secondly, wavelets don't seem to code visual energy of image effectively [66]. Thus wavelet codecs have a tendency to look much blurrier than discrete cosine transform (DCT) -based codec, however, the peak signal to noise ratio (PSNR) likes blur, and is often seen as a beneficial during video compression. Another problem that periodically crops up is the visual aliasing that tends to be associated with wavelets at lower bitrates [67,68]. Decimated wavelet transform

is not shift invariant and, as a result, it scales up the coefficients badly which leads to suppression of wavelet coefficients. In signal compression, the high frequency sub-band coefficients are not exactly reconstructed and introduces cyclo-stationarity into the image. JPEG2000 is one of the classic example of wavelet failure, despite having more advanced entropy coding, being designed much later than JPEG, being much more computationally intensive, and having much better PSNR, comparisons have consistently shown it to be visually worse than JPEG at same file sizes. [69,70].

1.6 Aim and objectives of the research

a. *Problem statement*

The idea of the present investigation is to develop new compression technique by using TFR tool that includes wavelet transform and fractional Fourier transforms for digital signal/image data. However, coding of low frequency wavelet coefficients for compression encoding is challenging part in present signal compression technology. By the combination of formal wavelet compression techniques with other compression techniques significantly improves the compression performance.

b. *Objectives*

An attempt has been made

1. To analyze the TFR of signals using wavelet transform.
2. To develop a new lossy compression algorithm for a two-dimensional signal.
3. To develop an improved wavelet-based lossy compression algorithm.
4. To develop new lossless hybrid wavelet compression.

c. Solutions

The solutions for the problem statements are obtained by following way:

1. Time-frequency responses and filter implementation for mother wavelets are studied.
2. A new lossy compression algorithm using neigh shrink in DWT-DCT is developed.
3. An improved lossy compression using modified singular value decomposition and wavelet-based progressive image compression methods are developed.
4. A novel lossy and lossless compression algorithm is developed by hybridizing the wavelet transform with fractional Fourier transforms.

d. Results and discussion

Combination of existed wavelet transform algorithm with optimal threshold coder provides good digital signal representation with fewer bit rate transmission, with good compression performance without compromise in image quality. Significant improvement of hybridization of wavelet with fractional transforms creates a new development in image compression.

This thesis is prepared as follows

The **Chapter 1**, presents the outline of the thesis with introduction to digital signal analysis in time frequency plane, followed by signal compression techniques. An introduction to wavelet transform for digital signal analysis in time frequency plane and its role in compression process is discussed in this chapter. Lastly, objectives and contributions of proposed research work are exhibited.

Chapter 2, presents the mathematical background of wavelet transform as a time-frequency based signal analysis. This chapter gives prior knowledge about a multiresolution property of wavelets and quadrature mirror filter design used to code the digital signals. The TFR of digital signals using Fourier transforms (FT), continuous wavelet transform (CWT) and discrete wavelet transform (DWT) are briefly emphasized.

Chapter 3, introduces the standards of two-dimensional signals and role of wavelet transform in signal compression. Description for a traditional procedure of two-dimensional signal compression using wavelet transform is given. A new compression algorithm with an improved neighbor shrink in DWT-DCT for grey scale image is discussed. Results are compared with standard compression technique JPEG2000.

Chapter 4, extends hybridization scheme proposed in Chapter 3. This chapter introduces another new lossless compression scheme by the combination of wavelet with fractional Fourier transforms for grey scale image. Wavelet decomposition is well known for spectrum characterization of image signals, it partitions the image signal into four different frequency subclasses. Whereas coding of low frequency is challenging part of image compression. In this chapter, these low-frequency wavelet coefficients are coded by using well-known signal coders discrete fractional cosine transform (DFrCT) and discrete fractional Fourier transforms (DFrFT). The results, discussions and comparative studies show the enhancement in quality of reconstruction and compression percentage.

Chapter 5, introduces a new hybridization scheme for progressive image compression using modified singular value decomposition (SVD) to improve the compression performance. A new lossy compression scheme segmented rank one updated SVD is introduced.

This modified SVD is applied as the pre-processing step for three wavelet-based progressive image compression algorithms embedded zero tree wavelet (EZTW), adaptive set partition hierarchical tree(ASPIHT), and binary tree coding. The results show some significant improvement in compression performance in terms of PSNR and compression percentage.

Chapter 6, encapsulate the core efforts of this thesis and puts forward ideas for future work.

Chapter 2

Digital signal analysis using wavelets

2.1 History of wavelets

In early 1700s the harmonic series data are measured by using the tables of astronomical positions called '*ephemerides*' [71]. The classical concepts of epicycles in astronomy were analogous to Fourier series. Several modifications were made by 'Alexis Clairaut' in 1754 to compute orbit function by the use of cosine series referred as discrete cosine transform (DCT). In 1759 'Joseph Louis Lagrange' developed a trigonometric series to characterize the vibration of a string by using sine series called as discrete sine transform (DST). In 1807 a French mathematician 'Joseph Fourier' discovered a trigonometric series to analyze the behaviour of heat [72,73] and stated the Fourier series as a '*periodic function, which can be expressed as a sum of sine and cosine functions*'. The features of wavelet transform can be traced out by Fourier transform, hence it is more appropriate to begin with Fourier transform

2.1.1 Fourier transform

Time and frequency are the two most commonly used parameters in analyzing the signal in the field of science and technology. Naturally occurring phenomena are represented by *oscillations or waves* as function of time or frequency. According to Fourier, the transformation of any periodic function from its time domain to frequency domain is very easy [74-76]. The term *Fourier series* (FS) is defined as:

$$x(t) = \frac{1}{2}a_0 + \sum_{p=1}^{\infty} a_n p \cos \omega t + \sum_{p=1}^{\infty} b_n p \sin \omega t \quad (2.1.1)$$

For non-periodic function, it can be represented as linear combination of complex exponentials, which are infinitesimally close in frequency. So FS can be represented as weighted integrals of complex sinusoids which are harmonically not related [77].

It can be derived from FS as,

$$x(t) = \sum_{p=1}^{\infty} c_n e^{jp\omega t} \quad (2.1.2)$$

the fundamental frequency $\omega = \frac{2\pi}{T}$. In the Fourier series representation, as the period increases the fundamental frequency decreases and the harmonically related components become closer in frequency. As the period becomes infinite, the frequency components form a continuous and the Fourier series becomes an integral [78]. And hence equation 2.1.2 is rewritten as,

$$X(f) = \frac{1}{2\pi} \int_{-\infty}^{\infty} x(t) e^{-ja\phi\omega t} dt \quad (2.1.3)$$

where, inverse continuous Fourier transform (ICFT) is given as:

$$x(t) = \frac{1}{2\pi} \int_{-\infty}^{\infty} X(f) e^{ja\phi\omega t} df \quad (2.1.4)$$

By the application of Fourier transform, one can easily transform the periodic or non periodic functions from its time domain to frequency domain [79].

The main drawback of Fourier representation is that, it fails to describe the status of each frequency component of signal at a specific point of time [80]. Fourier transform (FT) characterizes the frequency information of complete signal, but fail to describe the frequency information at a given time interval. Infinite duration integration over a time scale and complementary nature in time and frequency representation of FT creates loses in time locality [81].

2.1.2 Short time Fourier transform

Short-time Fourier transform is termed as '*Windowed Fourier Transform*' reproduced by 'Dennis Gober' to overcome the problem of temporal locality in FT. He modifies the FT by dividing the signals into the small section and then computes the FT for each section. It represent the signal as a two-dimensional function of time and frequency. $STFT(\tau, x)$ for a signal $x(t)$ at time t and frequency x is defined as,

$$STFT(\tau, x) = \sum_{k=0}^{N-1} x(t)h^*(t - \tau)e^{-j\omega t} \quad (2.1.5)$$

where, $h^*(t - \tau)$ is a window function (* denotes complex conjugates). STFT computes, a time-varying spectra by sliding a window along the signal $x(t)$. Each time, the window moves, its FT is computed by the product $x(t)h^*(t - \tau)$. Figure 2.1. shows the computational procedure of STFT by varying the window function ($\tau = -6, 0, 6$).

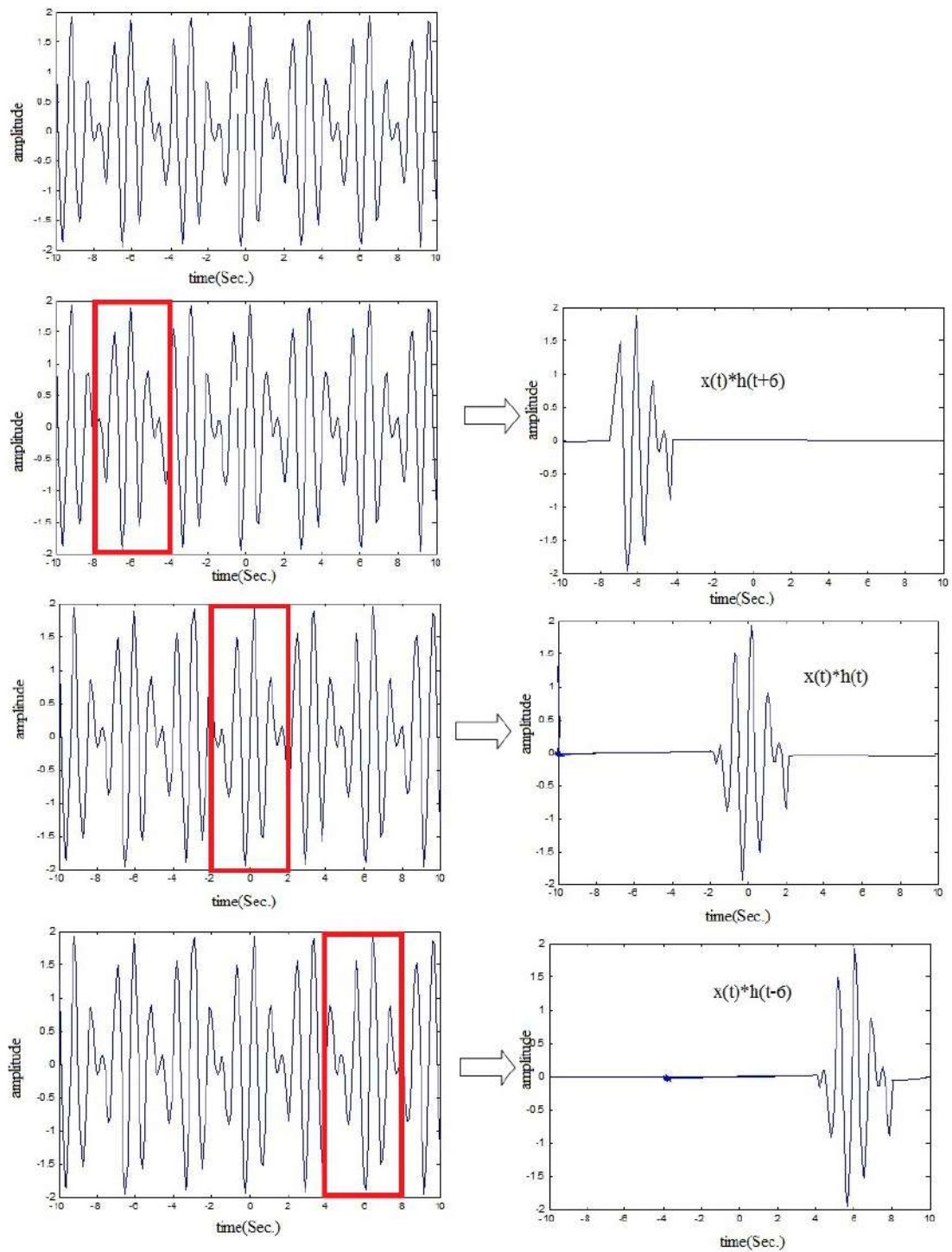


Figure 2.1: STFT computations by sliding a window

Limitation of STFT is that, it has fixed window size for overall process. Better time locality can be observed in small window size, but it provides poor frequency resolution.

However, the use of rectangular window function gives better frequency resolution but it creates 'Gibbs ripple' [82]. In order to avoid Gibbs ripple, window functions are replaced with hanning or hamming window with slight compromise in frequency resolution. This frequency resolution can also be enhanced by increasing the window length excluding at the rate of time resolution [83]. Squaring the magnitude of STFT in equation 2.1.5 is also increases frequency resolution, and is given as

$$\hat{X}_{STFT}(\tau, x) = \frac{1}{N} \left| \sum_{k=0}^{N-1} x(t) h^*(t - \tau) e^{-j\omega t} \right|^2 \quad (2.1.6)$$

However, use of STFT always results in trade-off between time and frequency resolution.

2.2 Continuous wavelet transform

CWT is an improved version of STFT and computational procedure of CWT is similar to that of STFT in time domain [84]. From the figure 2.2, we can observe that the sine wave is smoother and infinite in length, on the other hand the wavelet is very compact and irregular in shape.

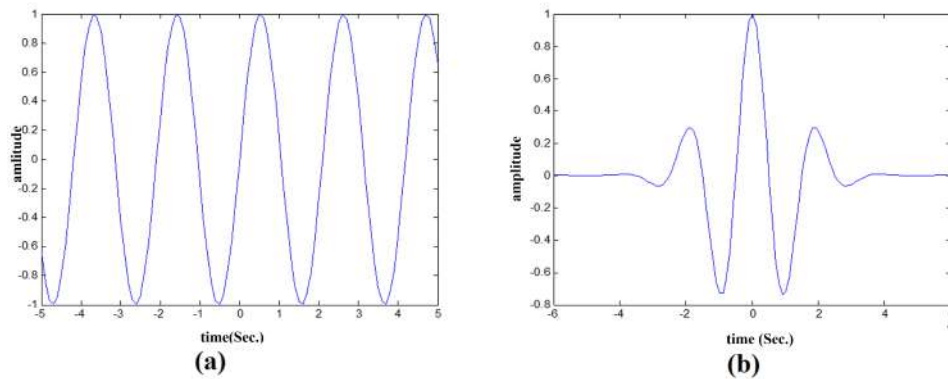


Figure 2.2: (a) sine wave; (b) mother wavelet (debauches)

Shape irregularity of mother wavelet helps in analyzing the non-stationary signals and its compactness supports for temporal localization of signal features. The mother wavelet

uses shifting and scaling operation to analyse any non stationary signal in time-frequency plane.

Shifting and scaling operations in wavelets

To overcome the time locality problem in FT, wavelet transforms use shifting operation for time domain analysis and scaling operation for frequency domain analysis of any signal [85]. Shifting and scaling operations are explained with the help of an exponentially sudden decaying signal. Consider, the signal $Y(t)$ where, $Y(t) = \cos 5te^{-x^2}$ is subjected to wavelet transform by performing shifting and scaling operation. Shifting operation is realized by subtracting the variable t with shifting factor τ , is $Y(t - \tau)$ It shifts the function by units,

$$i.e. \quad Y(t - \tau) = \cos(5t - \tau)e^{-x^2} \quad (2.2.1)$$

after shifting operation, the scaling process begins by dividing the variable by scaling factor λ and which compress the function as:

$$i.e. \quad Y\left(\frac{(t - \tau)}{\lambda}\right) = \cos\left(\frac{(5t - \tau)}{\lambda}\right)e^{-x^2} \quad (2.2.2)$$

A function shifted by unit 2 and scaled by factor 0.4 is plotted in figure 2.3.

The shifting and scaling operation in wavelet decomposition process generates a set of wavelet coefficients.

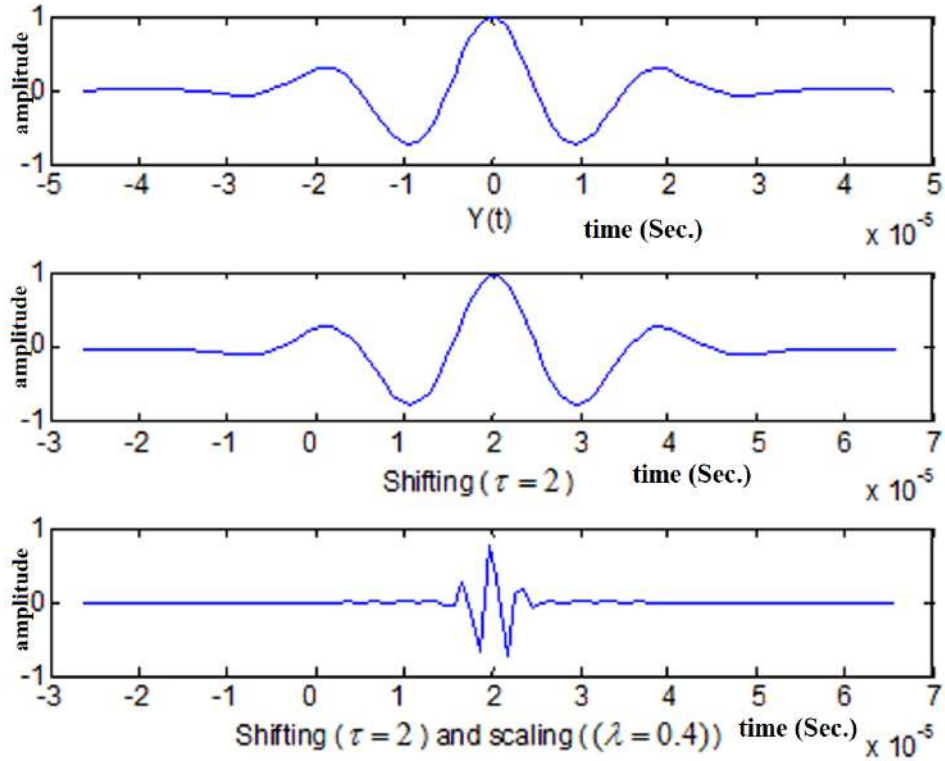


Figure 2.3 Wavelet decomposition of function $Y(t)$ by shifting ($\tau = 2$) and scaling ($\lambda = 0.4$) operations

For any function $\psi(t)$, is said to be a 'mother wavelet', it must satisfy the following two property [86],

1. Integral of the function is zero

$$\int_{-\infty}^{\infty} x(t)\psi(t)dt = 0 \quad (2.2.3)$$

2. Squared integral of function has finite energy

$$\left| \int_{-\infty}^{\infty} x(t)\psi(t) \right|^2 dt < \infty \quad (2.2.4)$$

CWT of a function $Y(t)$ with respect to $\psi(t)$ is termed as,

$$X_y(\tau, \lambda) \cong \int_{-\infty}^{\infty} Y(t) \frac{1}{\sqrt{|\lambda|}} \psi * \left(\frac{t - \tau}{\lambda} \right) dt \quad (2.2.5)$$

where, τ and λ are shifting and scaling variables respectively and $\psi * \left(\frac{t-\tau}{\lambda}\right)$ is a mother wavelet function ($*$ indicates complex conjugation). $\frac{1}{\sqrt{|\lambda|}}$ is the normalizing factor, which represents the energy of shifting and scaling variables. The wavelet transform is a function of two real variables τ and λ . The function of wavelet can be redefined as,

$$\psi_{\tau,\lambda} = \frac{1}{\sqrt{|\lambda|}} \psi * \left(\frac{t-\tau}{\lambda}\right) \quad (2.2.6)$$

By combination of equation 2.2.5 and 2.2.6, we can rewrite the CWT as,

$$X_y(\tau, \lambda) \cong \int_{-\infty}^{\infty} Y(t) \psi_{\tau,\lambda} * (t) dt \quad (2.2.7)$$

Similarly, inverse CWT is written as,

$$Y(t) \cong \frac{1}{C} \int_{-\infty}^{\infty} \int_{-\infty}^{\infty} \frac{1}{\sqrt{|\lambda|}} X_y(\tau, \lambda) \psi_{\tau,\lambda} * (t) d\tau d\lambda \quad (2.2.8)$$

where, the $\eta(\omega)$ is a Fourier transform of $\psi(\omega)$

$$\eta(\omega) = \int_{-\infty}^{\infty} \psi(t) e^{-j\omega t} dt \quad (2.2.9)$$

hence C is defined as,

$$C = \int_{-\infty}^{\infty} \frac{|\eta(\omega)|^2}{|\omega|} d\omega \quad (2.2.10)$$

Inverse CWT exists, if 'C' is positive and finite. The computation of CWT is nothing but the inner product of function $Y(t)$ with the wavelet function $\psi_{\tau,\lambda}$. It finds out the correlation of the signal $Y(t)$ with a shifted and scaled wavelet function $\psi_{\tau,\lambda}$.

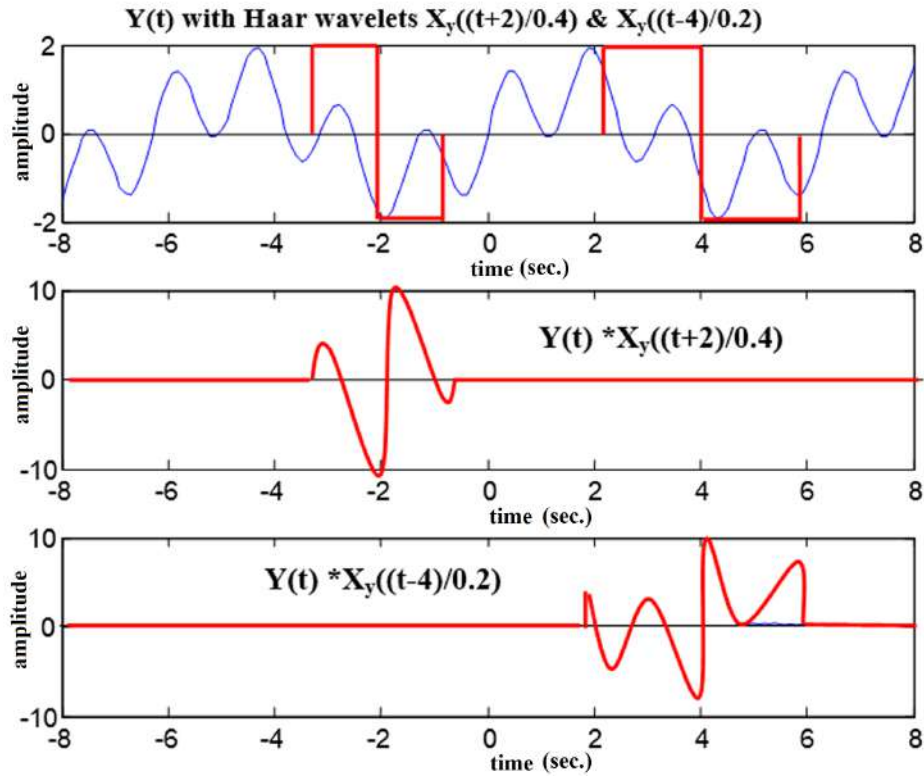


Figure 2.4 CWT of the function using 'Haar' wavelet

Figure 2.4 demonstrate that, the function $Y(t)$ as a sum of two sine waves which are used to compute CWT $X_y\left(\frac{t-\tau}{\lambda}\right)$ by using Haar mother wavelet with two different shifting and scaling factors $\tau = 2, 4$ and $\lambda = 0.4, 0.2$ respectively.

2.3 Discrete wavelet transform

Lack of phase information and rigorous computation procedure in CWT creates too much redundancy and imperfect signal reconstruction [87]. In order to tune the problem, CWT is sampled in dyadic grid, $\tau = k2^{-j}$ and $\lambda = 2^{-j}$ are substituted in equation 2.2.5, so that,

$$X_y(k2^{-j}, 2^{-j}) = \int_{-\infty}^{\infty} Y(t) \frac{1}{\sqrt{|2^{-j}|}} \psi * \left(\frac{t - k2^{-j}}{2^{-j}} \right) dt \quad (2.3.1)$$

$$= \int_{-\infty}^{\infty} Y(t) \sqrt{|2^{-j}|} \psi * (2^{jt} - k) \quad (2.3.2)$$

$$= \int_{-\infty}^{\infty} Y(t) \sqrt{2^j} \psi_{j,k}(t) = w_k^j \quad (2.3.3)$$

where, $\psi_{j,k}(t)$ is shifted and scaled form of mother wavelet $\psi(t)$ and is given by

$$\psi_{j,k}(t) = 2^{j/2} \psi(2^{jt} - k) \quad (2.3.4)$$

hence, the original signal can be reconstructed by sampling the CWT.

$$DWT_x(t) = \sum_j \sum_k w_k^j \psi_{j,k}(t) \quad (2.3.5)$$

where, w_k^j is a discrete wavelet coefficients of function $X(t)$ and are obtained by an inner product

$$w_k^j = \langle Y(t), \psi_{j,k}(t) \rangle = \int_{-\infty}^{\infty} Y(t) \psi_{j,k}(t) dt \quad (2.3.6)$$

Wavelets are orthogonal in nature since its inner product is zero

$$\langle \psi_a(t), \psi_b(t) \rangle = \int_{-\infty}^{\infty} \psi_a(t) * \psi_b(t) dt = 0 \quad (2.3.7)$$

2.4 Multiresolution analysis in wavelets

Ability of wavelets to decompose any function at different scaled levels is called as MRA and MRA involves 'layered sequence' [88]. It became popular mathematical tool for TFR as is often used in signal compression techniques. MRA uses mother wavelet and scaling function to analyze any signal

a. Scaling function

Consider $\phi_k(t)$ is a scaling function and is also an element of functional space $L^2(t)$

$$\phi_k(t) = \phi(t - k) \forall k \in I, \phi \in L^2$$

where, ' I ' is a set of all integers. The $L^2(\mathbb{R})$ is most commonly using functional space in signal processing applications, which contain finite and distinct integrals of squares. The set of functions from scaling functions generates a subspace of $L^2(\mathbb{R})$, and is given by

$$Z^0 = \text{Span}(\bar{\phi}_k(t)) = \sum_k w_k \phi_k$$

The basic scaling function spans set of two-dimensional functions by shifting and scaling operations and is defined as

$$\phi_{j,k}(t) = 2^{\frac{j}{2}} \phi(2^j t - k) \quad (2.4.1)$$

By changing the time scale in scaling function one can span a larger sub space $L^2(\mathbb{R})$.

Spanning of subspace is termed as:

$$V^s = \text{Span}(\bar{\phi}_k(2^j)) = \text{Span}(\bar{\phi}_k(t))$$

Since, $Y(t) \in V^j$ then the function can state as

$$Y(t) = w_k \phi(2^j t - k)$$

Where, $j < 0$, $\phi_{j,k}$ is narrow and covers larger span, leads to a scaling function representation with finer details. If $j > 0$, $\phi_{j,k}$ is wider and shifted into larger steps to represent with crude sequence [89].

The function $Y(t)$ is a linear combination of scaling $\phi(t)$ by a factor 2^j and shifted in terms of k . However, is compressed by j units and shifted by k units.

$$\text{Compressed} : \phi_o^j = \phi(2^j t) \quad \text{Shifted} : \phi_k^o = \phi(t - k)$$

In MRA, the functional space is decomposed into small sub spaces. If function $Y(t)$ is decomposed, each parts in the function $Y(t)$ is occupies each sub spaces and creates the

nest of spanned subspaces:

$$0 \subset \dots V^{-2} \subset V^{-1} \subset V^0 \subset V^1 \subset V^1 \subset \dots \subset V^j \subset V^{j+1} \subset \dots \subset L$$

Where V^0 is a center of space, V^j is the common subspace contained in all subsequent subspaces. Each subspaces V^j is spanned by scaling function $\phi(2^j t - k)$ if $\phi(t) \in V^1$. Hence $\phi(t)$ weighted sum of shifted $\phi(2t)$, is given as

$$\phi(t) = \sum_n h(n) 2^{1/2} \phi(2t - n) \quad n \in I$$

where $h(n)$ is the coefficient of scaling function and $2^{1/2}$ is used to normalize the scaling function with scale of 2.

b. Wavelet function

In general, wavelet equation can be written as

$$\psi(t) = \sum_l h(l) 2^{1/2} \phi(2t - l) \quad l \in I \quad (2.4.2)$$

where, ' I ' is a set of integers, $\psi(t)$ is a weighted sum of shifted and scaled function $\phi(2t)$. Equation 15 produces the wavelet function that exists in space, is obtained by scaling function $\phi(t)$. By using wavelet function, we can generate mother wavelet, and is given as:

$$\psi_{j,k}(t) = 2^{j/2} \psi(2^j t - l) \quad j, l \in I \quad (2.4.3)$$

A set of function $\psi_{j,k}(t)$ differentiates the spaces created by dissimilar time scales of scaling functions. Which also represent as detailed space W^j and these spaces are orthogonal to each other [90].

If at level ' j ' is denoted by $Y^j(t)$, then $Y^j(t) \in V^j$.

Basically, resolution information at level ' j ' is essentially included in the high-resolution information, which contains V^{j+1} :

$$V^j \subset V^{j+1}$$

This function, implies that

$$Y^{j+1}(t) \in V^{j+1}$$

In space, V^j must satisfy the scaling condition

$$Y(t) \in V^j \cong Y(2t) \in V^{j+1}$$

It describes that the variables in a space are the scaled version of the variable in the next space. The decomposition of subspace is given as:

$$V^{j+1} \in V^j \oplus W^j$$

whereas, set of elements $v^j + w^j$ in V^j and W^j are orthogonal, since the inner product of V^j and W^j is zero [19]. Hence $Y^j(t) \in V^j, G^j(t) \in W^j$ and are given by

$$Y^j(t) = \sum_{-\infty}^{\infty} w_{j,k} \phi(2^j t - k) = \sum_{-\infty}^{\infty} w_{j,k} \phi_{j,k}(t) \quad (2.4.4)$$

$$G^j(t) = \sum_{-\infty}^{\infty} z_{j,l} \psi(2^j t - l) = \sum_{-\infty}^{\infty} z_{j,l} \psi_{j,l}(t) \quad (2.4.5)$$

$w_{j,k}(t)_{k,l \in I}$ and $z_{j,k}(t)_{k,l \in I}$ coefficients belongs to $L^2(R)$.

For, any function $Y(t)$ in a functional space $L^2(R)$, $V^{-2} \subset V^{-1} \subset V^0 \subset V^1 \subset V^1 \subset \dots L^2$ belongs to a subspace $(V^j)_j^\infty = -\infty$,

1. *Density*: The union of a sequence $\cup_{j \in I} V^j$ is highly dense in the real squared integrals function.

$$\cup_{j \in I} V^j = L^2(-\infty, \infty) \quad (2.4.6)$$

It describes that the union of the sequence of members is approximated by its squared integrals in a vector space.

2. *Separation*: Intersection of any sequence is a null set:

$$\bigcap_{j \in I} V^j = \{0\} \quad (2.4.7)$$

3. *Scaling*: $Y(t) \in V^j \forall Y\left(\frac{t}{2^j}\right) \in V^0$ shows that scaling by a dyadic scale, one can move from one nested sequence to other.

4. *Orthonormal basis*: the set of the scaling function $\{\phi(t - k)\}_{k \in I}$ is an orthonormal if only if

$$\int_{-\infty}^{\infty} \phi(t - k)\phi(t - k^1)dt = f(x) = \begin{cases} 0, & \text{if } k \neq k^1. \\ 1, & \text{otherwise.} \end{cases} \quad (2.4.8)$$

Any scaling function of mother wavelet, that meet the above four properties performs efficient MRA [91].

c. Wavelet family

The wavelet transforms basically operated by using basic functions called as 'mother wavelet'. Different scaling and shifting functions are used by mother wavelets to characterize the wavelet transform. The family of wavelet basis functions are derived by scaling and shifting the mother wavelet with respect to their family. The inner product computation, between input signal and with different mother wavelet yields wavelet coefficients. Figure 2.5 demonstrates few wavelet functions which are common in use. Early 1909, first wavelet basis function '*Haar*' was introduced by Alfred Haar [92]. It was a unit step function supported for few signals. '*Daubechies*' is a popular wavelet function widely used in signal processing applications because of flexibility in selecting its order [93]. '*Symlet*' and

'*coiflet*' are also a class of wavelet functions having better frequency response with maximum flatness at zero to R frequencies and is advantageous during signal reconstruction [94]. The Haar, Daubechies, Symlet and Coiflet are densely sustained at orthogonality. Apart from these, several wavelet families like Mayer, Morlett, Mexican hat are shape based biorthogonal wavelets, efficiently serving in many applications [95-97].

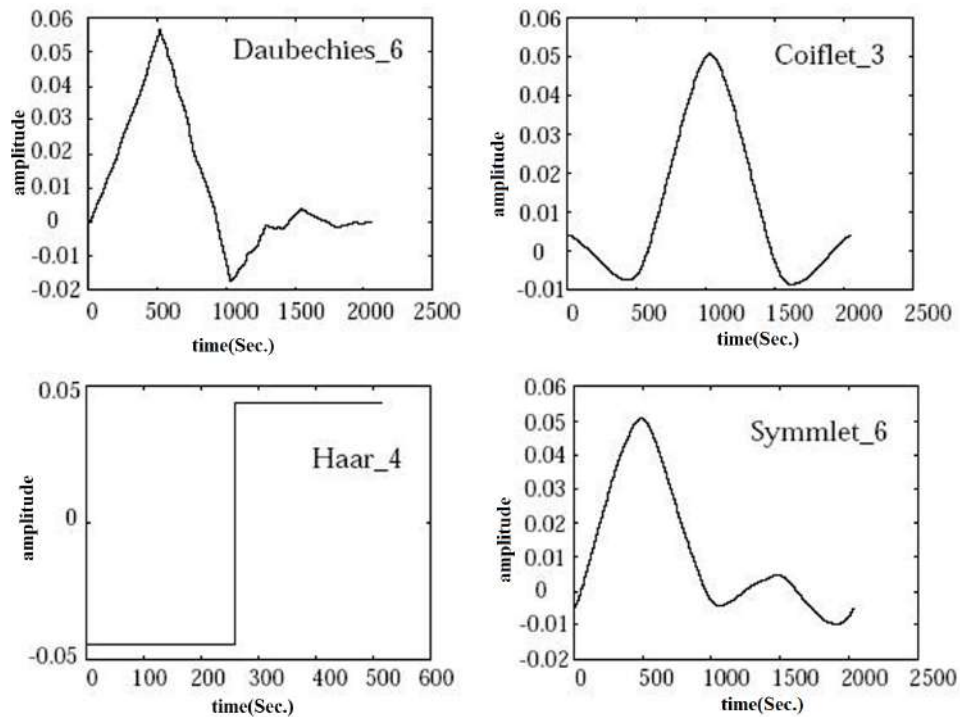


Figure 2.5 Different families of wavelets

2.5 Wavelet decomposition

The idea of decomposition is often used in signal processing for estimation of signal spectrum in time domain. The decomposition is also known as analysis process, which engages in partitioning of signals into its frequency components for further process. For

our discussion point of view, the equations 2.4.4 and 2.4.5 are rewritten respectively as,

$$Y^j(t) = \sum_{-\infty}^{\infty} w_{j,k} \phi(2^j t - k) = \sum_{-\infty}^{\infty} w_{j,k} \phi_{j,k}(t) \quad (2.5.1)$$

$$G^j(t) = \sum_{-\infty}^{\infty} z_{j,l} \psi(2^j t - l) = \sum_{-\infty}^{\infty} z_{j,l} \psi_{j,l}(t) \quad (2.5.2)$$

MRA for a functional space is given by

$$V^{j+1} = V^j + W^j$$

$$Y^{j+1}(t) = Y^j t + G^j t$$

$$= \sum_k w_{j,k} \phi_{j,k}(t) + \sum_l z_{j,l} \psi_{j,l}(t)$$

where, $\psi_{j,k}(t) = 2^{j/2} \psi(2^j t - l)$ and $\phi_{j,k}(t) = 2^{j/2} \phi(2^j t - k)$ The 2^j is a unitary function, hence scaling factor is given as,

$$\phi(t) = \sum_l h(l) 2^{1/2} \phi(2t - l) \quad (2.5.3)$$

shifting and scaling of time variable 't' is represented as

$$\begin{aligned} \phi(2^j t - k) &= \sum_l h(l) 2^{1/2} \phi(2(2^j t - k) - l) \\ &= \sum_l h(l) 2^{1/2} \phi(2^{j+1} t - 2k - l) \end{aligned}$$

where, $m = 2k + l$

$$\phi(2^j t - k) = \sum_m h(m - 2k) 2^{1/2} \phi(2^{j+1} t - m) \quad (2.5.4)$$

Therefore,

$$V^j = \text{Span} \{2^{j/2}\phi(2^j t - k)\} \quad (2.5.5)$$

$$Y(t) \in V^{j+1} = \sum_k w_{j+1,k}(t) 2^{(j+1)/2} \phi(2^{j+1}t - k) \quad (2.5.6)$$

In equation 2.5.6, scale $j+1$ is used as a scaling function and neglected wavelet function. Since at low-resolution representation, wavelet functions are not so necessary to regain *details* [98].

If the $\phi_{j,k}(t)$ and $\psi_{j,k}(t)$ are orthonormal then scaling coefficients are also computed by inner product,

$$w_{j,k}(t) = \int_{-\infty}^{\infty} Y(t) 2^{j/2} \phi_{j,k}(2^j t - k) dt = \langle Y(t) \phi_{j,k}(t) \rangle \quad (2.5.7)$$

By using equation 2.5.4, equation 2.5.7 is reduced as:

$$w_{j,k}(t) = \int_{-\infty}^{\infty} Y(t) 2^{j/2} \sum_m h(m - 2k) 2^j \phi_{j,k}(2^{j+1}t - m) dt \quad (2.5.8)$$

by interchanging the sum and integral of equation 2.5.8

$$w_{j,k}(t) = \sum_m h(m - 2k) 2^j \int_{-\infty}^{\infty} Y(t) 2^{j/2} \phi_{j,k}(2^{j+1}t - m) dt$$

where,

$$\int_{-\infty}^{\infty} Y(t) 2^{(j+1)/2} \phi_{j,k}(2^{j+1}t - m) dt = w_{j+1,k}(m)$$

$$w_{j,k}(t) = \sum_m h(m - 2k) w_{j+1,k}(m) \quad (2.5.9)$$

and hence the related wavelet coefficients are given by

$$q_{j,k}(t) = \sum_m h_1(m - 2k) w_{j+1,k}(m) \quad (2.5.10)$$

2.6 Wavelet reconstruction

The reconstruction process uses same scaling function and wavelet function (that are used to decompose the signal) to reconstruct the signal. Consider the signal with scaling functional space $Y(t) \in V^{j+1}$, and the function is given as,

$$Y(t) = \sum_k w_{j+1,k}(t) 2^{(j+1)/2} \phi(2^{j+1}t - k) \quad (2.6.1)$$

for next scale,

$$Y(t) = \sum_k p_{j+1,k}(t) 2^{(j+1)/2} \phi(2^{j+1}t - k) + \sum_k q_{j+1,k}(t) 2^{(j+1)/2} \phi(2^{j+1}t - k) \quad (2.6.2)$$

where,

$$\psi(t) = \sum_l h(l) 2^{1/2} \phi(2t - l) \quad (2.6.3)$$

From equation 2.5.4, 2.6.1 and 2.6.2,

$$\begin{aligned} Y(t) &= \sum_k w_{j,k}(t) \sum_l h(l) 2^{(j+1)/2} \phi(2^{j+1}t - 2k - l) + \\ &.. + \sum_k q_{j,k}(t) \sum_l h(l) 2^{(j+1)/2} \phi(2^{j+1}t - 2k - l) \end{aligned} \quad (2.6.4)$$

multiply the term $2^{(j+1)/2} \phi(2^{j+1}t - k)$ with equation 2.6.4 and then integrate to regenerate coefficients

$$w_{j+1,k}(k) = \sum_m w_j(m) h_0(k - 2m) + \sum_m q_j(m) h_1(k - 2m) \quad (2.6.5)$$

2.7 Interpretation of wavelet filter

In general, the digital systems are operated by using a set of digital filters, like low pass or high pass filters. Wavelet transform also uses a combination of low pass and high

pass filter banks termed as quadrature mirror filters (QMF) for signal decomposition and reconstruction [99]. In wavelet decomposition process, equation 2.5.9 and 2.5.10 uses the coefficients $w_{j+1,k}(m)$ to perform convolution for time reversal recursive coefficients $h_0(m)$ and $h_1(m)$. However, it was followed by down sampling process to generate a set of approximate and detailed coefficients [30]. Down sampling, is a filtering process which avoids the sampling of insignificant components in the signal.

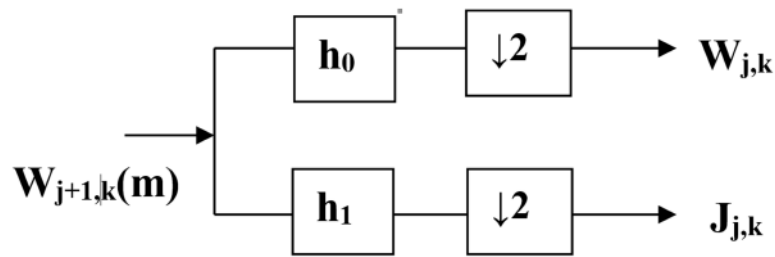


Figure 2.6 First level decomposition filter bank

Figure 2.6 shows the implementation of level one, wavelet decomposition using equation 2.5.9 and 2.5.10, where $h_0(m)$ and $h_1(m)$ are set of low pass and high pass finite impulse response (FIR) filters respectively. The filtered signal is down sampled by a factor two, which reproduce the set of scaling and wavelet coefficients for further decomposition levels. This decimation process is repeated for level one approximate coefficients to obtain second level decomposition as shown in figure 2.7.

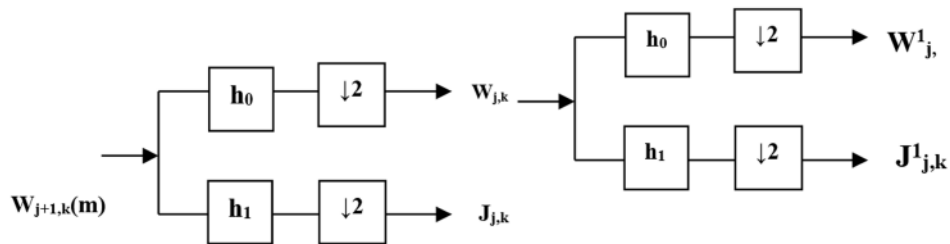


Figure 2.7 Second level decomposition filter bank

For reconstruction purpose, same FIR filter banks $g_0(m)$ and $g_1(m)$ are used to recombine

the approximate and detail coefficients by using equation 2.6.5, as shown in figure 2.8.

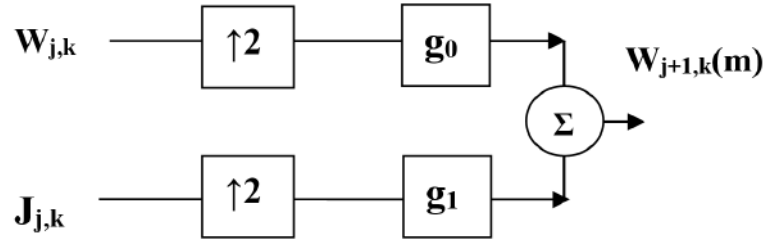


Figure 2.8 First level reconstruction filter bank

The combination of decomposition filters and reconstruction filters with scaling and wavelet function is shown in figure 2.9.

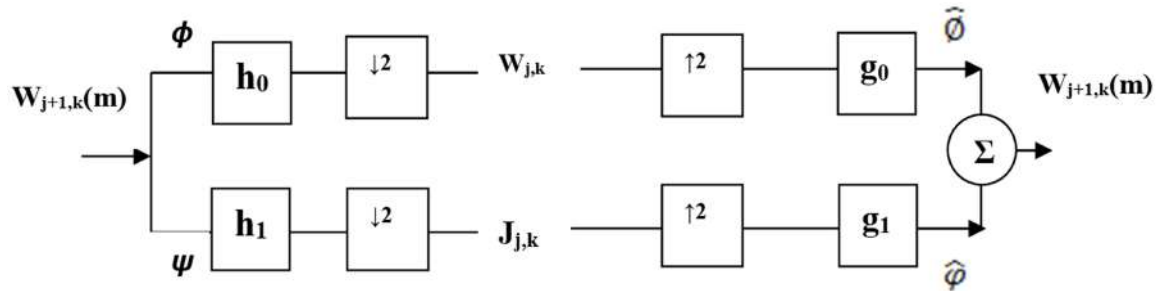


Figure 2.9 Combination of decomposition and reconstruction filter banks

For orthogonal property in wavelet transform shows,

$$\phi = \hat{\phi}, \psi = |\hat{\psi}$$

and $h_0(m) = g_0(m), h_1(m) = g_1(m)$. Similarly, for bi-orthogonal wavelet transform, the scaling and wavelet function are given as:

$$\phi(k) = \sqrt{2} \sum_m h_0(m) \phi(k - 2m) \quad \hat{\phi} = \sqrt{2} \sum_m g_0(m) \hat{\phi}(k - 2m) \quad (2.7.1)$$

$$\psi(k) = \sqrt{2} \sum_m h_1(m) \psi(k - 2m) \quad \hat{\psi} = \sqrt{2} \sum_m g_1(m) \hat{\psi}(k - 2m) \quad (2.7.2)$$

2.8 Summary

The chapter begins with the brief history of evolution of wavelet transform from time-frequency based signal analysis transforms. Drawbacks of FT and STFT are discussed in section 2.1, which explicate the need of wavelet transform in signal analysis. The scaling and shifting operations in CWT to analyze continuous signal are discussed in section 2.2. Reduction of CWT from its continuous time to discrete time as DWT by using scaling and wavelet function is discussed in section 2.3. In section 2.4 the mathematical interpretation for MRA, in extraction of a series of approximations using scaling function and details of the signal from wavelet functions is elaborated. The section ends with a small description on wavelet family. The explanation of wavelet decomposition and reconstruction of signal using MRA is illustrated in section 2.5 and 2.6 respectively. The chapter ends with section 2.7, with discussion on digital filter banks for decomposition and reconstruction at different levels.

Chapter 3

Two-dimensional signal (Image) compression using wavelets

3.1 Fundamentals of digital image

A human can visualize the surrounding system because of reflection property of matter. Reflected signals from the matter are continuous in nature, which are captured by using camera sensors. These continuous signals are converted into the digital signal by using sampling and A/D converters. Digital images are structured with irregular intensities in a two-dimensional space. The smallest unit of digital image is called as '*image pixel*'.

3.1.1 Digital image

The image is a two dimensional signals with two spatial coordinates (m, n) as independent variables and intensity as dependent variable. Consider $I(m, n)$ is an image with pixel position variation $(n = 1, 2, 3, \dots, M; m = 1, 2, 3, \dots, N)$ along m^{th} row and n^{th} column as shown in figure.3.1.

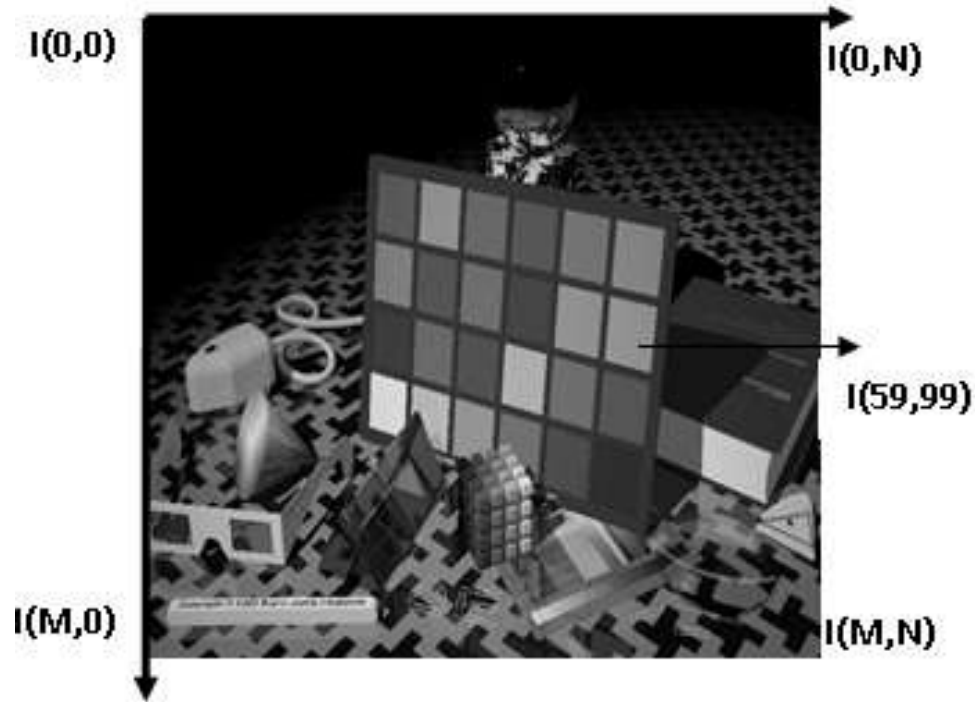


Figure 3.1: Digital image with $M \times N$ dimension

The quality of an image is defined by its resolution and is specified in terms of three parameters:

- *Spatial resolution*: it defines, the number of pixels occupied spatial positions in a captured image (i.e. it defines a dimension of an image). It can be represented as $column(c) \times rows(r)$ (Example: 256×256 , 512×512etc.).
- *Temporal resolution*: capturing the multiple images with respect to the time period is defined by 'frame'. Each captured image is considered as frame and number of frames per unit time is termed as frames per second (FPS). (Example: visual perception in TV surveillance is at 25-30 FPS).
- *Bit resolution*: it defines the gray level intensity value of pixels in a captured image. It is also related to quantization process, i.e. the number of bits required to store

the image in a given quantization level (Monochromatic image with two gray levels needs 2 bit representation, gray scale image with 256 different gray level needs 8 bit representation and colored image with 768 gray levels and needs 24-bits representation). Bit resolution is also referred as a dynamic range of an image [100, 101].

3.1.2 Types of image

In order to process image data, a prior knowledge of image data type is necessary. In general, images are classified[102] as,

- *Monochromatic image*: each pixel in an image is represented by one bit, either white or black called monochrome.
- *Grayscale image*: an image in which, the pixel has single numerical value, varies from 0 to $n - 1$ (one of 2^n shades of gray level). It has a number of bit planes (n might be a multiple of 4 or 8) with most significant bit plane consists of most significant bits of all pixels in an image.
- *Continuous tone image*: in this type of image, gray level correlations between adjacent pixels are nearly one. Small differences are hard to notice by human eyes, and hence a pixel of an image can be symbolized by a single big number. Color image has 3 vectored arrays, which allocate a numerical value to each pixel. Each array has its individual channels of red, green and blue and they are ordered subsequently. (Example: Natural image captured by digital camera)

- *Discrete tone image*: image has either indistinguishable gray levels or they may vary from one-pixel position to another pixel position. These images have a more number of redundancies, because pixel values occur repeatedly in image. (Example: Graphical images generated by the computer)
- *Cartoon-like image*: : image with a homogeneous gray level area. Each area has identical pixel value but neighboring area pixel values are entirely different.

3.1.3 Image formats

The digital computer needs to display, store and communicate the image data in the form of binary bits. For effective storage and communication of image data, it was standardized into different image file formats. Table 3.1 shows some of the image file formats used frequently and their properties.

These image formats store any image data by adapting its own compression scheme and header information. Based on user requirement, different image file formats are available in online sources. In general, to store image with more number of detailed/gray levels, JPEG/TIFF image file format is appropriate. However, to store image with fewer details/gray levels, GIF/PNG are better.

Table 3.1 Image file formats used frequently and their properties [103].

Img. formats	Expansion	Properties
GIF	Graphical interchange file	Limited gray levels; lossless compression.
JPEG	Joint Photographic Experts Group	Flexible, less complex, speed; both lossy and lossless compression.
BMP	Bit map pictures	Less flexible; both lossy and lossless compression.
TIFF/TIF	Tagged image file format	flexible, adaptive and detail in nature.

3.2 Image compression using DWT

An image is two dimensional signals, with a set of pixels arranged in a matrix form composed by low and high frequency bands [104]. Hence it is important to separate the low and high-frequency information from an image. Wavelet transform, explicitly classify the frequency bands into high and low frequency sub bands in terms of approximate and detailed coefficients [105]. Figure 3.2 shows the general block diagram of wavelet-based image compression

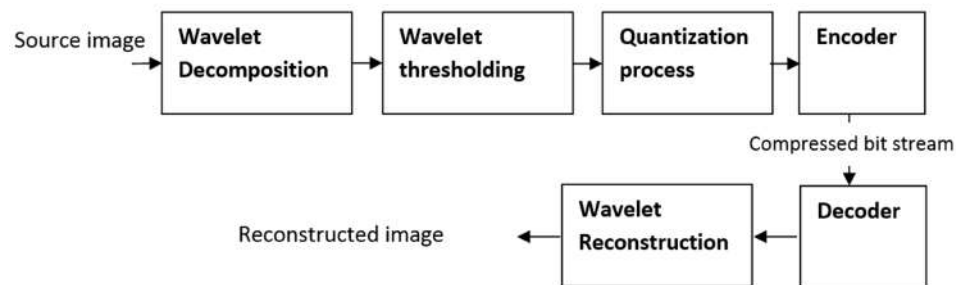


Figure 3.2 General block diagram of wavelet compression and decompression process

3.2.1 Wavelet decomposition using filter banks

Wavelet based subband coding is an efficient encoding technique, which takes an advantage of human perceptual visual system to code the two-dimensional signal. Basically, it saves the bandwidth of signal by discarding the unwanted sub-band at encoding stage. A split band quantization method introduced in [106] uses pulse code modulation to code high and low-frequency sub bands. Later on, a Laplacian pyramid decomposition is introduced in [107-108] to generate approximate and detailed frequency coefficients. For a given digital filter H_k [109], its QMF H_g is defined as,

$$H_g(\omega) = H_k\left(\frac{\omega_j}{2} - \omega\right) \quad (3.2.1)$$

$$\lambda_g(\omega) = \lambda_k(\omega) \pm \left(\frac{pi}{2}\right) \quad (3.2.2)$$

where, $H_g(\omega)e^{j\lambda_k(\omega_j)}$ is complex frequency response of a filter H_k , and $\omega_j = e\pi f_j$ is sampling rate.

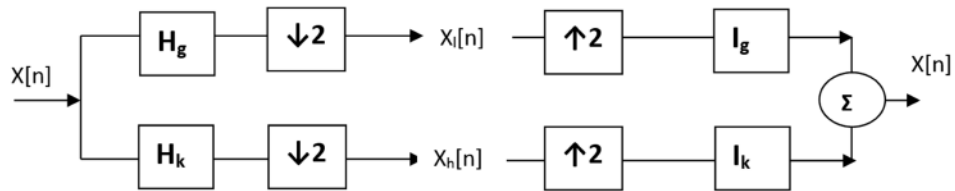


Figure 3.3 Two channel QMF

From figure 3.3, the input signal $X[n]$ is filtered by analysis filters (H_k is high pass filter and H_g is low pass filter), where, $x_l(n)$ and $x_h(n)$ are low frequency and high-frequency sub bands, which are down sampled by factor two to satisfy 'nyquist criteria' [110]. At receiver side $x_l(n)$ and $x_h(n)$ are up sampled by factor two and to bypass through synthesis filter I_g and I_k respectively.

Implementation of QMF design for image sub-band coding and development of multiresolution signal analysis lead to a new approach for wavelet based sub-band coding system [111, 112].

Pyramid decomposition for a source image S by use of QMF [113] is shown in figure.3.4

(a).

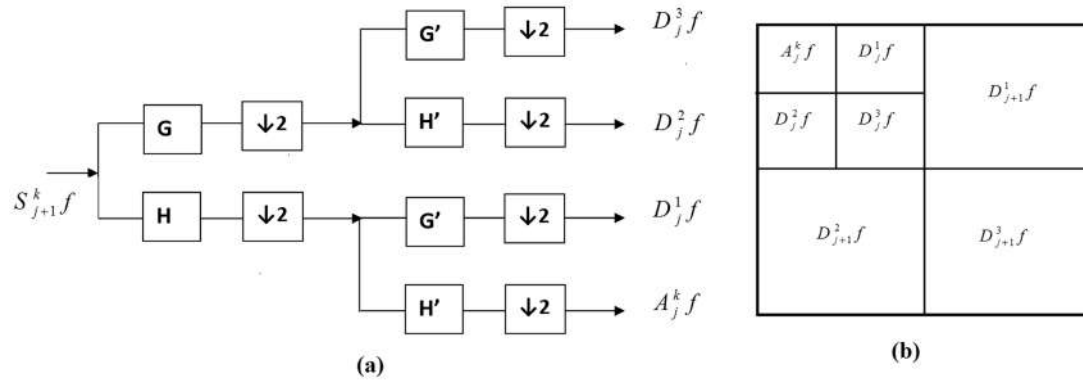


Figure 3.4 Level two wavelet decompositions

The rows and columns of the source image are convolved with one-dimensional wavelet filters \mathbf{H} and \mathbf{G} respectively. This filtering process generates A_j^k , low frequency sub-band (approximate coefficients) and D_j^1, D_j^2 and D_j^3 are , vertical, horizontal and diagonal high-frequency sub bands (detailed coefficients) at the resolution as shown in figure3.4 (b). Similarly in the reconstruction process, which adds zero in between every two rows and two columns and then convolves with same one-dimensional filter bank that is used for decomposition process as shown in figure 3.5,

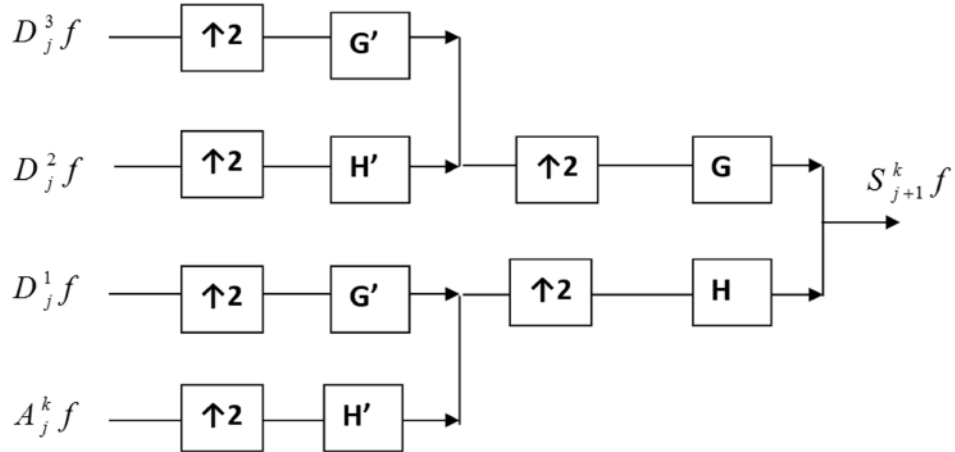


Figure 3.5 Level two wavelet reconstructions

3.2.2 Wavelet threshold for image compression

Thresholding is a significant feature in wavelet-based image compression, since it truncates the unwanted frequency components in a signal by selecting suitable threshold value [114]. Wavelet decomposition process convert the source signal into a fine frequency subbands. From section 3.2.1, we know that the low-frequency subband has significant image information but less signal energy than the high-frequency subband. Hence thresholding process suits for detailed wavelet coefficients and limited for approximate coefficients [115].

The key endeavor of thresholding process is to kill the detailed coefficient to achieve better compression. Application of threshold increases the number of zeroes in the subband and is the key for compression [116].

Wavelet compression method exploits the decomposition process of an image into wavelet basis by using shrink method [117]. But in shrinkage process, selection of optimum threshold is challenging task. However selection of small threshold value leads to less compression ratio and high threshold value increases the compression ratio but at the

cost of signal quality. Hence various soft thresholding techniques like bayes shrink [118], visu shrink [119] and sure shrink [120] along with normal shrink [121], are well-known methods to find optimal wavelet threshold.

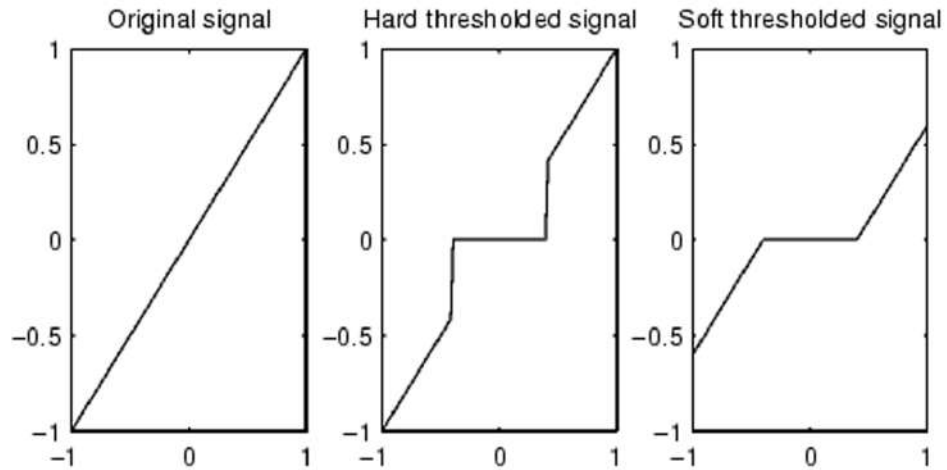


Figure 3.6 The hard and soft threshold in wavelet

After selection of optimal threshold value, there are two choices in wavelet threshold, hard and soft thresholding. In hard threshold, the coefficients above the optimal threshold are made zero or killed. Whereas, in soft threshold, the coefficients value above the optimal threshold are shrunk to its absolute value. From the figure 3.6, we can observe the smoothness in soft wavelet threshold as compare to hard threshold.

The hard threshold:

$$T_h(X, \lambda) = \begin{cases} X = X, & \text{if } |X| \geq \lambda. \\ X = 0, & \text{otherwise.} \end{cases} \quad (3.2.3)$$

Similarly, for soft threshold:

$$T_s(X, \lambda) = \text{sign}(X) \max(0, |X| - \lambda) \quad (3.2.4)$$

Hard threshold method creates a discontinuity in the reconstructed signal, which is not found in soft threshold (found signal smoothing).

3.2.3 Wavelet-based encoders for progressive image compression

The wavelet-based progressive image compression techniques evolution is started with,

a. Embedded zero tree wavelet (EZTW)

It was the first progressive transmission algorithm introduced by 'J. Shapiro' in [122], which embeds the signal with bit stream by truncating of zero's in prioritized order. The concept of 'zero trees' states that, after each thresholding step, algorithm searches the insignificant wavelet coefficients and make them zero. If, descendant coefficients are zero, then are called as 'zero nodes' or 'zero roots' . Hence this method of compression is called as embedded zero tree wavelet (EZTW) coder. It uses parent-child relations in decomposed wavelet coefficients and creates a new data structure to encode the symbols. It classifies the decomposed coefficients into parent, child, and descendant.

The initial threshold of EZTW is calculated by using the formula

$$T_0 = [\log_2(\max(I))]^2 \quad (3.2.5)$$

where I is an image matrix, the significance test is performed on each wavelet coefficient and a wavelet coefficient 'z' is considered to be significant, if $|z| > T_0$, otherwise coefficients considered as insignificant. Based on significance test and status, the symbols are classified into zero tree root (ZR), isolated zero (IZR), positive significant (PS) and negative significant (NS). After completion of first iteration, the threshold will become $T_1 = T_0/2$ and process repeats until required bit rate is achieved. These symbols are encoded by Huffman encoder, finally, a lengthy compressed bit stream is obtained.

b. Set partitioning hierarchical tree(SPIHT)

The successive algorithm of EZTW is known as SPIHT with best compression performance. After wavelet decomposition process, the wavelet coefficients are ordered based on most significant bit (MSB). The significance of coefficients is determined by,

$$|C(i, j)| \geq 2^n \quad (3.2.6)$$

where, $n = n_0, n_0 - 1, n_0 - 2, \dots, k$ and i, j are the set of coordinates. Sorting process divides the entire set of coefficients into a sub set T and then compute the magnitude of coefficients.

$$\max(i, j) \in T |C(i, j)| \geq 2^n \quad (3.2.7)$$

The subset T, that satisfies the above condition become significant set, and it undergoes partition and creates new subset and the procedure is repeated for the new subset. The execution of encoder algorithm is imitated by the decoder, using an inverse operation of the encoder. The function to identify the significance bit of an encoder is given by,

$$S(\tau) = 1, \max(i, j) \in T |C(i, j)| \geq 2^n, \text{ otherwise} \quad (3.2.8)$$

From the figure 3.7, image pixels are divided into four adjacent pixels called node of a hierarchical tree. Each node has either no offspring or four offspring. A pixel in the highest level is called root of the tree with its offspring. Sorting process divides the clustered pixels into a subset.

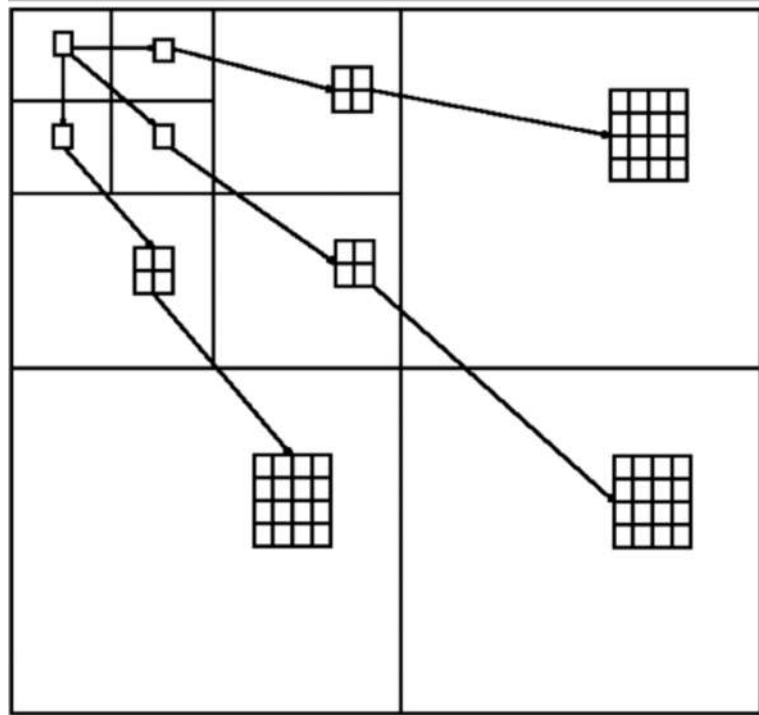


Figure 3.7 Root to descendent's dependency in a spatial domain

SPIHT algorithm uses two major passing operations on decomposed wavelet coefficients by using three subsets. After the application of threshold, wavelet coefficients are classified as list of an insignificant set (LIS), list of significant pixel (LSP), and list of insignificant pixel (LIP) by using sorting pass and refinement pass operations. For first iteration, initial threshold is calculated by using equation 3.2.5. Sorting pass is performed, by loading LIS by all decomposed wavelet coefficients using Morton scanning [123]. In refinement pass, the coefficients whose values are greater than threshold values are keep stored in LSP and remaining coefficients are loaded to LIP. This process is repeated for next iteration, up to defined bit rate, by halving its threshold value. LSP is also loaded with the sign of the significant pixels. In the end, reduced numbers of significant pixels are encoded by using different encoding techniques (Huffman encoder is commonly used in practice). Efficiency can be increased by using entropy-coders but at the cost of increased

complexity [124].

c. Set partitioned embedded block coder(SPECK)

This algorithm follows progressive bit-plane coding scheme to encode the wavelet coefficients. In significance test, if the wavelet coefficient is found significant, it outputs the sign of code and its position is stored in LIS. Refinement pass, produces the successive approximation of already known significant bit. After completion of each iteration level, threshold value will become half and the process repeats for next bit plane.

The scanning mode in SPIHT, performs unnecessary significance test on individual sub bands even though they are insignificant and the procedure needs more time. To overcome this situation and improve the efficiency, two partition schemes are used in SPECK, quad tree partition and octave tree partition as shown in figures 3.9 and.3.10.

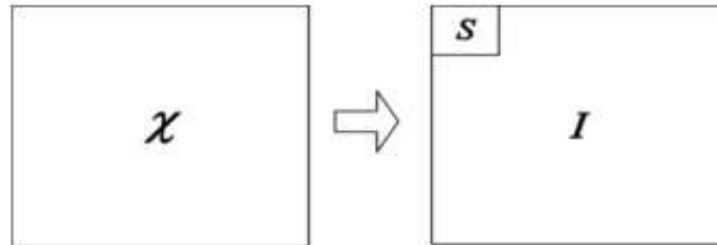


Figure 3.8 Transformation of an image ' x ' to set ' S ' and ' I '

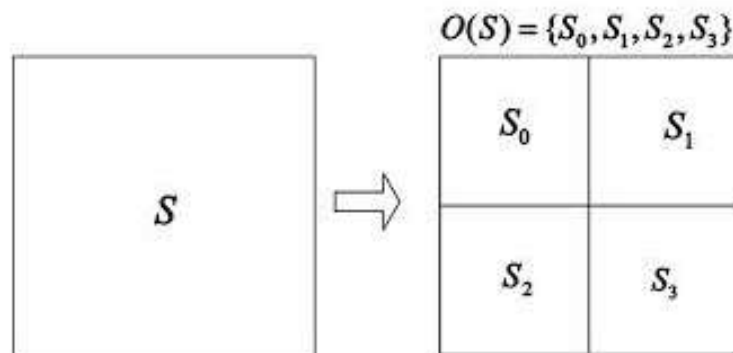


Figure 3.9 Quad tree partition of set ' S '

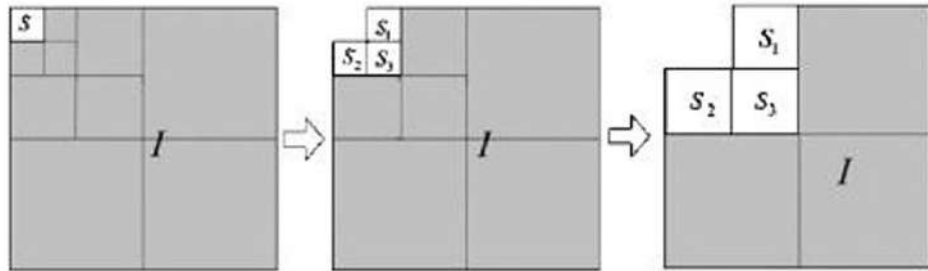


Figure 3.10 Octave partition of a set 'I'

Quad tree partitioning, concentrates on zooming the only area with high energy, in set S' and codes them. It codes the significance map with quad-tree, a well-known method of spatial partition. In quad-tree partitioning, the significance state of an entire block of coefficients is tested and coded, the block is subdivided into four sub-blocks of approximately equal size, and the significance-coding process is repeated recursively on each of the sub-blocks. In octave, it exploits hierarchical pyramid structure of the sub-band decomposition, where it is more likely that, more energy is concentrated at the topmost levels of the pyramid and as, one goes down the pyramid, energy content decreases gradually. In octave tree partitioning, a set I has group of pixels, in which some significant information is clustered at certain region. After decomposition, significant pixels get accumulated in set S , and this significant set undergoes sorting process. The large set created with insignificant bits, undergoes partition into four offspring.

The decoder receives significant test results from coded bit stream by following the same execution path of an encoder. As with SPIHT, the SPECK algorithm stores significant coefficients set, in an implicitly sorted list. Insignificant coefficients are placed in a list of insignificant sets (LIS). During the sorting pass, each insignificant set in an LIS is tested for significance against the current threshold. If the set becomes significant,

it is split into four subsets according to the quad-tree decomposition structure described above. The four new sets are placed into an LIS, recursively tested for significance, and split again if needed. SPECK maintains multiple LIS lists in order to implicitly process sets according to their size. During the sorting pass, each time, a set is split, the resulting subsets move to the next LIS. When a set is reduced in size to a single coefficient, and that coefficient becomes significant, then the singleton set is moved from its LIS to a list of significant pixels (LSP) for later processing in the refinement pass [125,126].

d. Wavelet difference reduction(WDR)

This algorithm follows SPIHT algorithm with improvement in locating the region of coefficients of interest. By the use of index coding in differenced reduction, it identifies the significant wavelet transform coefficients which are essential for resolution enhancement. As in SPIHT, it also uses three different sets to store the indexed positions of wavelet coefficients during encoding process. In sorting pass, instead of storing significant coefficient, it stores its position and is updated with its previously scanned significant coefficient during refinement pass, which leads to an effective preservation of edge information.

It offers good perceptual quality and compression ratio, edge correlation and preservation. It suits for a low-resolution medical image at low BPP rate[127].

e. Adaptive scanned wavelet difference reduction(ASWDR)

The performance of WDR shows that, it has some room for improvement. The adaptive algorithm ASWDR was introduced by walker which modifies the scanning order to predict the location of new significant values. If any coefficient is significant for threshold,

then succeeded significant coefficients are predicted by adaptive scanning. This scanning order of ASWDR dynamically adapts the locations of edge details in an image, and this enhances the resolution of compressed images[128]

3.2.4 Error metrics

There are several error metrics available to evaluate the quality of a reconstructed image, some of the most commonly used evaluation parameters are:

a. *Mean square error(MSE)*: Consider $I_o(m, n)$ in an original image and $I_r(m, n)$ is compressed image with dimension $M \times N$.

$$MSE = \frac{1}{MN} \sum_{i,j=1}^{M,N} I_o(m, n) - I_r(m, n) \quad (3.2.9)$$

b. *Peak signal to noise ratio(PSNR)*:

$$PSNR = 10 \log_{10}(Q^2/MSE) \quad (3.2.10)$$

where, Q is 255 for gray scale image.

c. *Structural similarity index mode(SSIM)*: Variation of brightness in reconstructed image amplifies the PSNR values. Measuring only PSNR is not the best choice to evaluate the image quality, therefore the use of SSIM as the improved version of PSNR clears the inconsistency in human visual perception. It is defined as,

$$SSIM(x, y) = \frac{(2\mu_x\mu_y + C_1)(2\sigma_{xy} + C_2)}{(\mu_x^2 + \mu_y^2 + C_1)(\sigma_x^2 + \sigma_y^2 + C_2)} \quad (3.2.11)$$

Here, x and y correspond to two image blocks need to be measured, μ_x, μ_y are average and σ_x, σ_y are the variance of x, y respectively. Is covariance of x and y . are variables

for stabilization factor. L =dynamic range, $K_1 = 0.01$, $K_2 = 0.03$, measures the similarity index of the reconstructed image with respect to original image.

d. *Compression ratio(CR)*: The key metric for measuring the image compression performance is compression ratio. It is defined as,

$$\text{Compression ratio} = \frac{\text{size of uncompressed image}}{\text{size of compressed image}} \quad (3.2.12)$$

Compression percentage (CP) is also given by [129],

$$CP = \frac{(\text{Size of original image} - \text{Size of compressed image})}{\text{Size of original image}} \times 100 \quad (3.2.13)$$

e. *Bit per pixel(BPP)*: Alternative measure of compression performance is by computing BPP.

$$BPP = \frac{\text{No. of bits}}{\text{No. of pixels}} = \frac{8 \times \text{No. of bytes}}{\text{Size of the image}} \quad (3.2.14)$$

f. *Percentage root mean square difference(PRD)*: The measure of fractional variations in signal compression during the application of fractional transform is given as,

$$PRD = \frac{1}{MN} \sqrt{\frac{\sum_{i,j=1}^{M,N} [I_o(m, n) - I_r(m, n)]^2}{\sum_{i,j=1}^{M,N} [I_o(m, n)]^2}} \quad (3.2.15)$$

3.3 Implementation of an improved neigh shrink in a hybrid wavelet transform for grayscale image compression

3.3.1 Previous work

Wavelet-based compression suits well for image compression applications because of its multiresolution property. Wavelet-based lossy image compression methods like EZTW, SPIHT, WDR are commonly used in some multimedia image compression, which yields embedded bit-stream of wavelet coefficients with declining threshold values to encode the most significant pixels or lists of pixels for reconstruction. But single basis function in wavelet does not meet all these properties and hence multi-wavelets with more than one scaling and wavelet functions are preferable [130]. A hybrid compression algorithm proposed in [131] achieves high compression ratio with moderate image quality for large size image data. Here the compression is achieved by ignoring high-frequency sub bands at level one. The high-frequency subbands at level two are encoded directly by eliminate zero and store data (EZSD). The LL subbands are compressed by DCT and encoded by arithmetic coding fallowed by run length encoder (RLE). An efficient hybrid compression algorithm is proposed in this section by using an improved neigh shrink for selection of optimal threshold for high-frequency subband at level two and three.

3.3.2 Proposed hybrid compression technique

a. Use of wavelet decomposition:

The wavelets give the best choice for image analysis due to its multi resolution property. Here decomposition is done by passing source image through a set of low pass and high pass filters to get approximate and detailed coefficients [132]. For each level decomposition of source image produces four sub-bands (LL, LH, HL, and HH). As source image undergoes decomposition, low-frequency subbands shift towards left corner by becoming more significant. At the same time, high-frequency sub-band shift towards the right bottom corner as insignificant. Hence, by ignoring this insignificant information in high-frequency sub-bands more compression can be achieved [133].

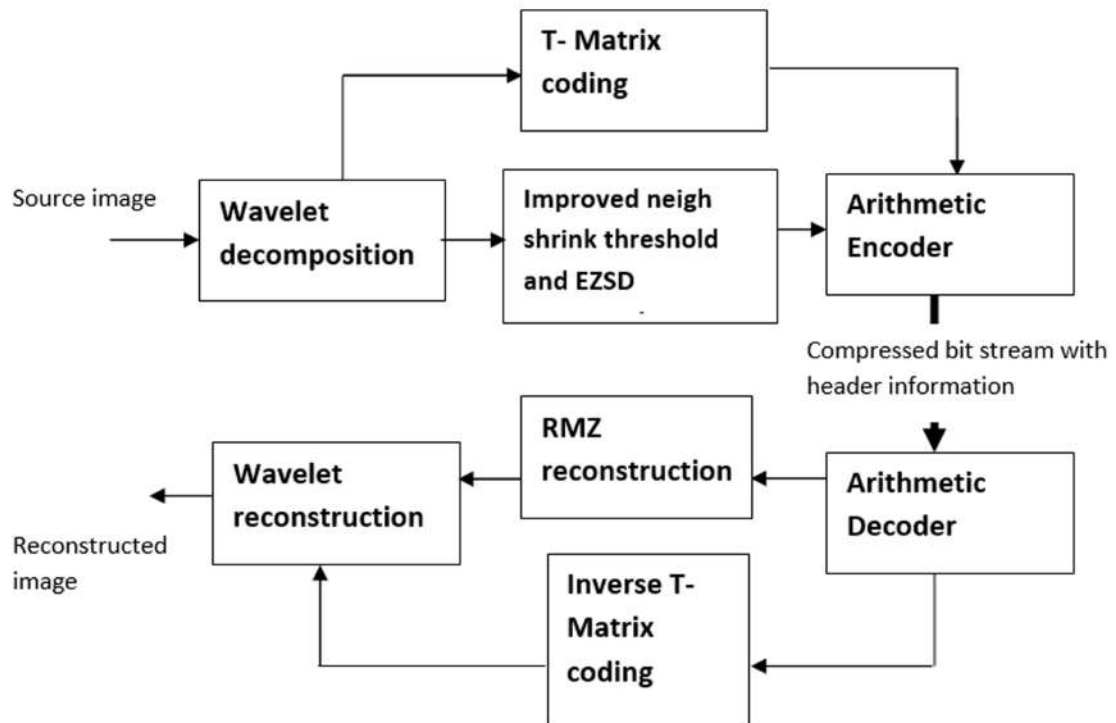


Figure 3.11 A block diagram of the proposed hybrid image compression

In this modified approach, the image is subjected to three-level wavelet decomposition. The high-frequency sub-band at first level contains less significant information, and hence it is ignored. While level two and three, high-frequency sub-bands contain some significant information, the direct encoding or ignoring of these sub-bands result in reduced image quality, hence the application of an optimal threshold is the key to improving the quality of the reconstructed image.

b. Quantization:

This step is lossy approach and it requires two levels of quantization. The level1 quantization reduces the size of LL_m by, ratio of maximum value of LL_m and Quality factor, as shown below,

$$Q_1 = \text{Quality factor} \times \max(LL_m) \quad (3.3.1)$$

$$LL_m = \text{round} \frac{LL_m}{Q_1} \quad (3.3.2)$$

The quality factor in equation 3.13 indicates the quality of the image and is obtained by the maximum value in LL2 divided by all the values in LL2. The process helps LL2 subband coefficients to be more convergent (Quality ranges from 0.005 to 0.01) to get required compression rate. Level2 Quantization is performed on LL2 sub-band after DCT and then divide the matrix by Q_2 . This eliminates the insignificant coefficients by inserting zeros.

$$Q_2(m, n) = \begin{cases} 1, & \text{if } m = 1, n = 1. \\ -m + n + R, & \text{if } m \leq 1, n \leq 1. \end{cases} \quad (3.3.3)$$

c. Coding of low-frequency sub-band using T-matrix coding:

The DCT uses a small set of values to reconstruct the original signal and also round up the very small values to zero during encoding. Hence it high-quality reconstruction is possible in the compression process.

The decomposed LL2 subband has high energy and more correlated information and DCT is used to compresses the sub-band. The one-dimensional forward and inverse DCT are illustrated as,

$$J_k = S_k \sqrt{\frac{2}{N} \sum_{i=0}^{N-1} G_i \cos \frac{\pi}{N} K(i + \frac{1}{2})} \quad (3.3.4)$$

where,

$$S_k = \frac{1}{\sqrt{2}}, \text{ if } k = 0 \text{ to } N - 1, 1, \text{ otherwise} \quad (3.3.5)$$

The normalization factors $\sqrt{\frac{2}{N}}$ and $\sqrt{\frac{1}{N}}$ makes DCT matrix orthogonal.

Because of the high degree of correlation, the LL2 subband coefficients are difficult to encode directly by arithmetic coding [134]. Therefore, the subband is divided into number of parts and each part is processed by one-dimensional DCT and is quantized by using formula,

$$Q(n) = Q(n - 1) + 2 \quad (3.3.6)$$

The transformed values are stored in a row matrix called as a transformed matrix (T-matrix). This process increases the significance of coefficients and de-correlation. Each row of T-matrix has DC values and AC coefficient stream, T-matrix is scanned column by column for converting it into a one-dimensional array and is compressed by RLE and arithmetic code. The RLE reduces the length of repeated data, and arithmetic code converts reduced data set into bit streams [135].

d. Coding of high-frequency subband using improved neigh shrink and EZSD:

After the level two and level three wavelet decomposition, redundancy shifted towards in high-frequency sub-bands. Hence application of improved neigh shrink with stein unbiased risk estimator (SURE) as optimal threshold possibly increases the compression quality.

For given detailed sub-band, select the wavelet coefficient need to be shrinking and place a neighboring window $C_{i,j}$ at center.

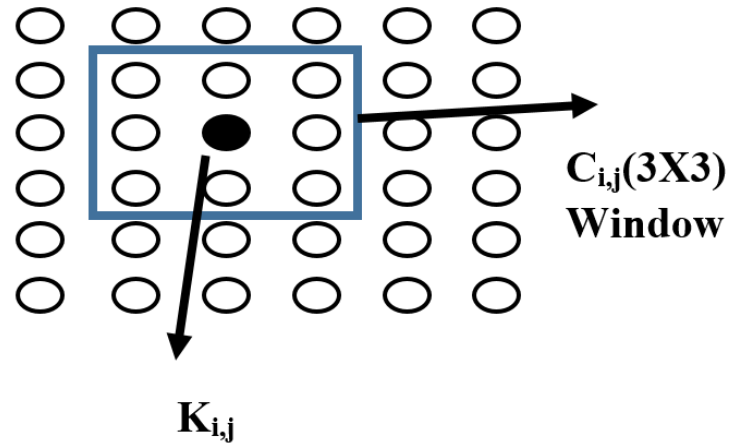


Figure 3.12 A graphical representation of improved method to shrink wavelet coefficient

Let,

$$S_{i,j}^2 = \sum_{i,j \in B_{i,j}} K_{i,j}^2 \quad (3.3.7)$$

where $S_{i,j}^2$ summation has the pixel indices out of the wavelet sub-band range then corresponding term in the summation is to be ignored [136]. The neigh shrink is given by,

$$K_{i,j} = K_{i,j} C_{i,j} \quad (3.3.8)$$

Shrink factor is given by,

$$K_{i,j} = \frac{1 - \lambda^2}{K_{i,j}^2} \quad (3.3.9)$$

here, the optimal threshold λ and window length L are calculated by *SURE* for wavelet coefficients of any sub-band $w_{i,j} = k_{i,j} : i, j$.

$$(\lambda^s, L_s) = \arg_{\lambda, L} \min \text{SURE}(w_k, \lambda, L) \quad (3.3.10)$$

Whereas in denoising application noise level is defined with suitable values but in compression, we keep the value of noise level as one. Thresholded and quantized (quality_i=0.01) high-frequency sub-bands have a rich number of zeroes, and unnecessary coding of these zeroes make the algorithm assy. Therefore, EZSD is used to eliminate blocks of these zeroes and to store the blocks of non-zero data. It begins with splitting high-frequency sub-bands into non-overlapped blocks (8X8, 16X16) and searches for non-zero blocks. If a non-zero block is found, it will be stored in a reduced array and its position is stored in position array, else it jumps to a next block. The reduced array may contain some more zeroes because some blocks contain more zeroes as compared to the data in them. Therefore, the use of EZSD results in a compact form of the reduced array, which helps in the encoding process.

Arithmetic coding is used to compress a stream of data sequence into one-dimensional length code word. The run-length encoding helps to avoid coding of repeated coefficients, which reduces the length of the code word. Hence, the arithmetic coding technique converts code word into bit streams.

e. Return zero matrix (RZM) algorithm

During reconstruction, this process is used as converse for EZSD method. The reduced array of decoded high-frequency sub-bands is expanded by searching zeros followed by a number of them; the repeated zeros in a new array are counted. The data in an array is replaced by blocks of the matrix and the method applied to all high-frequency sub-bands.

3.3.3 Results and discussions

The proposed method tested with 8-bit gray scale Boat, Lena, Gold-hill, peppers and artificial images figure 3.13. The table 3.2 shows the PSNR and Structural Similarity Index Mode (SSIM) and comparison of the proposed method with SPIHT, WDR and JPEG 2000 at a compression ratio of 80:1. The PSNR and SSIM values of JPEG2000 obtained from [137] and for consistency, same test images are used in the simulation. The figure 3.14 shows that boat image is compressed by SPIHT, WDR, JPEG2000 and proposed method at a compression ratio of 80:1.

The results tabulated in table 3.2, shows that PSNR and SSIM value of the proposed method for boat image are 3.9db and 0.1 are higher than the JPEG2000. But in artificial images, the PSNR and SSIM are lesser in the proposed method, this due to the rich significant edge information in images and are not in standard dimension. The quality factor is used to obtain the required compression ratio has some limitation ($0.005 \leq Q \text{ factor} \leq 0.5$) and it depends on the use of wavelet family (preferred debauchees) and encoded array. From the results, we observe that the image quality of proposed method is significantly improved by use of an optimal threshold for the second level high-frequency sub band.

Table 3.2 Comparison of the proposed method with other methods

<i>Images</i>	<i>CR</i>	<i>SPIHT</i>		<i>WDR</i>		<i>JPEG2000</i>		<i>Proposed</i>	
		PSNR	SSIM	PSNR	SSIM	PSNR	SSIM	PSNR	SSIM
Boat	80:1	26.20	0.668	26.96	0.710	26.76	0.740	30.71	0.842
Lena	80:1	29.32	0.803	29.71	0.770	29.62	0.670	31.92	0.902
Goldhill	80:1	27.17	0.660	27.72	0.625	27.69	0.670	27.59	0.672
Peppers	80:1	29.36	0.753	28.93	0.740	29.54	0.783	29.66	0.804
Artificial	80:1	25.25	0.678	23.82	0.620	25.69	0.767	22.02	0.604



Figure 3.13 Input test images (a)boat; (b)Lena; (c)gold hill; (d)pepper

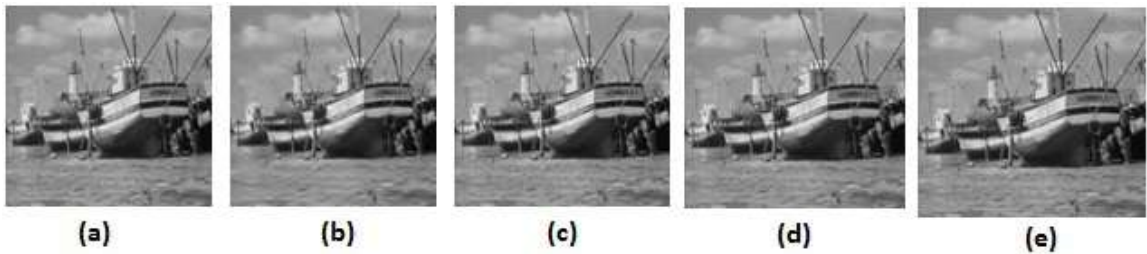


Figure 3.14 (a) Original boat image compressed at compression ratio of 80:1 using (b) SPIHT

(c)WDR; (d)JPEG2000[137]; (e)Proposed method(Q=0.006)

3.4 Summary

This chapter forms the base for image compression using DWT, from the image basics to existing progressive image compression technologies. It also includes, proposed, hybrid image compression method using improved neigh shrink wavelet threshold. Some early works, which are supportive for wavelet filters are also traced out in this chapter. Description of image fundamentals discussed in section 3.1 included with image resolutions, types of image and formats of the image, which helps in selection of data sets and compression techniques.

Wavelet filter bank implementation for wavelet decomposition and reconstruction process is discussed in section 3.2.1. The hard and soft thresholding techniques in wavelets for image compression are explained in section 3.2.2. A review of wavelet-based progressive image compression techniques like EZTW, SPIHT, SPECK, WDR, and ASWDR are given in section 3.2.3. Compression performance measuring metrics to evaluate the compression algorithm is explained in the section 3.2.4.

In section 3.3, a hybrid image compression algorithm by using improved neigh shrink in wavelet and T-matrix coding is discussed. After wavelet decomposition, one-dimensional discrete cosine transform is applied to decorrelate approximate coefficients and are stored as T-matrix. The detail coefficients are thresholded using improved neigh shrink', and EZSD algorithm is applied to eliminate redundancy in the coefficients and are stored as a reduced array. The compressed approximate and detailed coefficients are encoded by arithmetic coding. The simulated results show that proposed algorithm has significant improvement in image quality in terms of PSNR and SSIM, when compared with existing wavelet-based compression methods including JPEG 2000 at high compression rate.

Chapter 4

Image compression techniques using wavelet and fractional transforms

4.1 Introduction

Time-frequency based compression algorithms have property of multi-scale characterization, which produce high quality image during reconstruction [138-141]. Wavelet-based image compression methods, discussed in chapter 3, reveal that there is a possibility of coding low frequency subbands to increase compression ratio with limited decomposition levels. It is found that the increase in decomposition level leads to degradation of reconstructed image quality, due to aliasing effect [142,143]. However, discrete fractional transform is a simple coding technique which elucidate change in the characteristics of signals gradually, from a time domain to frequency domain.

4.2 Fractional transform in image compression

Rapid developments of signal compression technology in areas such as quantum mechanics, pattern recognition, image and video processing applications [144-147] attracted towards fractional transforms. Fractional transforms are generally termed as rotational

Fourier transform as they rotate signal in the time-frequency plane. The minimum mean square error of original image is estimated by using fractional domain filtering in fractional transform is a key for image compression [148]. The fractional parts in discrete fractional Fourier transform (DFRFT) and discrete fractional cosine transform (DFRCT) provides the extra degree of freedom in computations of coefficients. Also, they assist in a compact coding of information with reduced number of DFT coefficients [149].

This thesis is limited to the discussion of three types of fractional transforms, DFRST, DFRCT, and DFRFT.

a. Discrete fractional sine transform

The DFRST is related to DFT by operating on real part of the matrix. DFRST is equivalent to twice the length of an imaginary part of DFT, hence it has the close relation with DFT [150]. For any sequence of numbers $x(n)$, where N are a real numbers is given by,

$$Y(m) = \sqrt{\frac{2}{N}} \sum_{n=1}^{N-1} x(n) \sin\left(\frac{mn\pi}{N}\right) \quad \text{for, } 1 \leq n \leq N - 1 \quad (4.2.1)$$

whereas, inverse DFRST is given by:

$$x(n) = \sqrt{\frac{2}{N}} \sum_{m=1}^{N-1} Y(m) \sin\left(\frac{mn\pi}{N}\right) \quad \text{for } 1 \leq n \leq N - 1 \quad (4.2.2)$$

In this section, the ‘N’ point DFRST kernel is generated by using odd DFT Hermits eigenvector. It $V = [0, v_1, v_2, \dots, v_N, 0, -v_N, -v_{N-1}, \dots, -v_1]$ is odd eigenvectors of DFT kernel matrix $M_{2N+2}v = \phi v(\phi = -j, j)$, then $\hat{V} = [V_1, V_2, \dots, V_N]^T$ are the eigenvectors of N-point DST kernel matrix, and hence DFRST is

$$S_{N,\alpha} = j\phi \hat{V} \quad (4.2.3)$$

Table 4.1 Eigen values multiplied by DST kernel matrix to get DFRST

N	Multiplicity of 'j'	Multiplicity of ' - j'
Odd	$\frac{N+1}{2}$	$\frac{N-1}{2}$
Even	$\frac{N}{2}$	$\frac{N}{2}$

For DFRST kernel matrix, the Eigenvector \hat{V}_N given to Eigen values of $e^{-j(n-1)\alpha}$, where n is an odd integer. The N-point DFRST kernel is given as

$$S_{N,\alpha} = \hat{V}_N \hat{D}_N^{2\alpha/\pi} \hat{V}_N^t \tag{4.2.4}$$

$$= \hat{V}_N \begin{bmatrix} 1 & & & 0 \\ & e^{-2j\alpha} & & \\ & & \cdot & \\ & & & \cdot \\ 0 & & & e^{j2(N-1)\alpha} \end{bmatrix} \hat{V}_N^t \tag{4.2.5}$$

where $\hat{V}_N = [V_0 | V_2 | \dots | V_{2N-2}]$, \hat{V}_N is N^{th} order DFT Hermite eigen vectors, and α indicates the rotational angle of fractional transform in time-frequency plane.

b. Discrete fractional cosine transform

The DFRCT is the general version of discrete cosine transform (DCT) with an additional free parameter as a fractional order. Fractional order modulates the transform into DCT or conventional DCT. Hence DCT for a sequence $x(n)$ is given in [151] by using equations 4.2.6 and 4.2.7,

$$F(k) = \alpha(k) \sum_{n=0}^{N-1} x[n] \cos \left[\frac{(2n + 1)\pi k}{2N} \right], \quad for 0 \leq k \leq N - 1 \tag{4.2.6}$$

Where,

$$\alpha(k) = \begin{cases} \frac{1}{\sqrt{N}} for k = 0 \\ \sqrt{\frac{2}{N}} for 1 \leq k \leq N - 1 \end{cases} \tag{4.2.7}$$

for one-dimensional DCT kernel matrix given by equation 4.9.

$$M_{DCT}(k, n) = \begin{cases} \frac{1}{\sqrt{N}}, k = 0; 0 \leq n \leq N - 1 \\ \sqrt{\frac{2}{N}} \cos \left[\frac{(2n+1)\pi k}{2N} \right]; 1 \leq k \leq N - 1; 0 \leq n \leq N - 1 \end{cases} \quad (4.2.8)$$

Similarly, inverse DCT (IDCT) is given by equation 4.10

$$S(n) = \sum_{k=0}^{N-1} \alpha(k) F(k) \cos \left[\frac{(2n+1)\pi k}{2N} \right], 0 \leq n \leq N - 1 \quad (4.2.9)$$

In DCT, rich number of infinite eigenvectors generated from Hermite-Gauss eigenvectors of Fourier matrix [152]. For DFRCT kernel matrix the eigenvector \hat{V}_k has the Eigen values of $e^{-jk\alpha}$, where k is even ($\alpha = \pi/2$).

If $V = [0, v_1, v_2, \dots, v_N, 0, -v_N, -v_{N-1}, \dots, -v_1]$, are even eigenvectors of DFT kernel matrix $M_{2N-2}v = \phi v(\phi = 1, -1)$, then

$$\hat{V} = [V_0, \sqrt{2}V_1, \dots, \sqrt{2}V_{N-2}, V_{N-1}]^T \quad (4.2.10)$$

are the eigenvectors of N-point DCT kernel matrix, and hence DFRST is

$$C_{N,\alpha} = \phi \hat{V} \quad (4.2.11)$$

ϕ corresponds to eigen values.

Table 4.2 Eigen value's multipliable to DCT kernel matrix to get DFRCT

N	Multiplicity of 'j'	Multiplicity of ' - j'
Odd	$\frac{N+1}{2}$	$\frac{N-1}{2}$
Even	$\frac{N}{2}$	$\frac{N}{2}$

Hence DFRCT kernel for N point is given as,

$$C_{N,\alpha} = \hat{V}_N \hat{D}_N^{2\alpha/\pi} \hat{V}_N^t \quad (4.2.12)$$

$$= \hat{V}_N \begin{bmatrix} 1 & & & 0 \\ & e^{-2j\alpha} & & \\ & & \cdot & \\ & & & \cdot \\ 0 & & & e^{j2(N-1)\alpha} \end{bmatrix} \hat{V}_N^t \tag{4.2.13}$$

where $\hat{V}_N = [\hat{V}_0 | \hat{V}_2 | \dots | \hat{V}_{2N-2}]$, \hat{V}_N is an eigenvector of DCT derived from the N^{th} order DFT Hermite eigenvectors by equation 4.2.13.

c. Discrete fractional Fourier transform

Development of continuous fractional Fourier transform (CFRFT) for signal analysis made many researchers develop the discrete contradictory part of it. The rotational property of DFRFT is quite similar to the CFRFT. There are several methods to compute the DFRFT matrix, but for time constraint eigenvector based computational method are preferable. It can be realized by using the fractional power of kernel matrix. The DFRFT defined in [153] uses a set of eigenvectors of DFT matrix as a counterpart to the ‘Hermit’s Gaussian’ function which resembles the CFRFT. The mathematical unitary definition of DFRFT matrix $S^\alpha[m, n]$ is given by

$$S^\alpha[m, n] = \sum_{K=0}^{N-1} Q_K[m] (\lambda_K)^\alpha Q_K[n] \tag{4.2.14}$$

where, $Q_K[m]$ are orthonormal eigenvectors set of the $N \times N$ DFT matrix and λ_K are coupled with Eigen values. S^α matrix is computed by using following steps. First, the matrix Z decomposes the arbitrary vector $x(n)$ into its even and odd parts. The P matrix maps even part of N -dimensional vector $x[n]$ into first $\lceil N/2 + 1 \rceil$ components and odd part to the remaining components [154]. Whereas the matrix Z is unitary and symmetry, that is $Z = Z^T = Z^{-1}$ and W is real symmetric with tri-diagonal structure.

Hence resultant similarity transform is given by diagonal elements of even and odd matrix with eigenvectors e_k, o_k ,

$$ZWZ^{-1} = \begin{bmatrix} E_v & 0 \\ 0 & O_d \end{bmatrix} \tag{4.2.15}$$

even though, an eigenvector of an above-transformed matrix is either even or odd vectors. The common set of eigenvectors of W and DFT matrix is determined irrespective of the dimension of W . Order the eigenvectors set by using zero crossing values of discrete Hermits Gaussians [155]. Where eigenvectors of E_v and O_d matrix with highest Eigen values doesn't have any zero crossing but second highest has one and so on. An even eigenvector of Z is calculated by $e = Z \left[\hat{e}_k^T | 0 \dots 0 \right]^T$ and $e = Z \left[0 \dots 0 | \hat{o}_k^T \right]^T$ through \hat{e}_k, \hat{o}_k , where k is zero crossing ($0 \leq k \leq [N/2]$) and ($0 \leq k \leq [(N - 3)/2]$) respectively. Finally equation 4.2.14 becomes,

$$S^\alpha[m, n] = \sum_{K=0, k \neq (N-1+N_2)}^{N-1} u_K[m] e^{-j\frac{\pi}{2}k\alpha} u_K[n] \tag{4.2.16}$$

whereas $u_k(n)$ is a discrete Hermits-Gaussian function at the k^{th} order, It is observable that if N is even or odd, there are no eigenvectors with $N-1$ or N zero crossings. Hence peculiar Eigen value multiplicity of DFT matrix to get DFRFT kernel matrix is given as,

Table 4.3 Eigen value's multipliable to DFT matrix to get DFRFT kernel matrix

N	1	-j	-1	J
4m	m+1	M	M	m-1
4m+1	m+1	M	M	M
4m+2	m+1	M	m+1	M
4m+3	m+1	m+1	m+1	M

4.3 Improved lossy image compression algorithm using DWT and DFRCT

4.3.1 Previous work

The lossy image compression is a technique which represents an image data with a reduced number of bits and in turn, reduces the storage space, but reconstructed image is quite different than original image [156]. The most common fractional transform used in image processing application is two dimensional DFRFT, which can preserves the rotational property and helps in analyzing the signal in time-frequency domain [157]. A lossy hybrid image compression technique using DFRFT-SPIHT proposed in [158,159] uses DFRFT for compression and SPIHT for encoding process. Based on these references, we developed a new lossy compression algorithm by coding the decomposed low frequency wavelet coefficients by using DFRCT. This has increased the compression performance of the algorithm significantly.

4.3.2 Flow of DWT_DFRCT algorithm

The wavelet transforms facilitate to analyze the signal in time-frequency domain by representing the source image into clusters of significant coefficients in four frequency spectrums. A compact time domain analysis in DFRCT helps us to code the more significant subbands with reduced size without reducing the signal quality. This combination becomes more efficient because it generates more de-correlated coefficients than spatial based compression algorithms. The following steps are used to explain the proposed compression algorithm (figure 4.1).

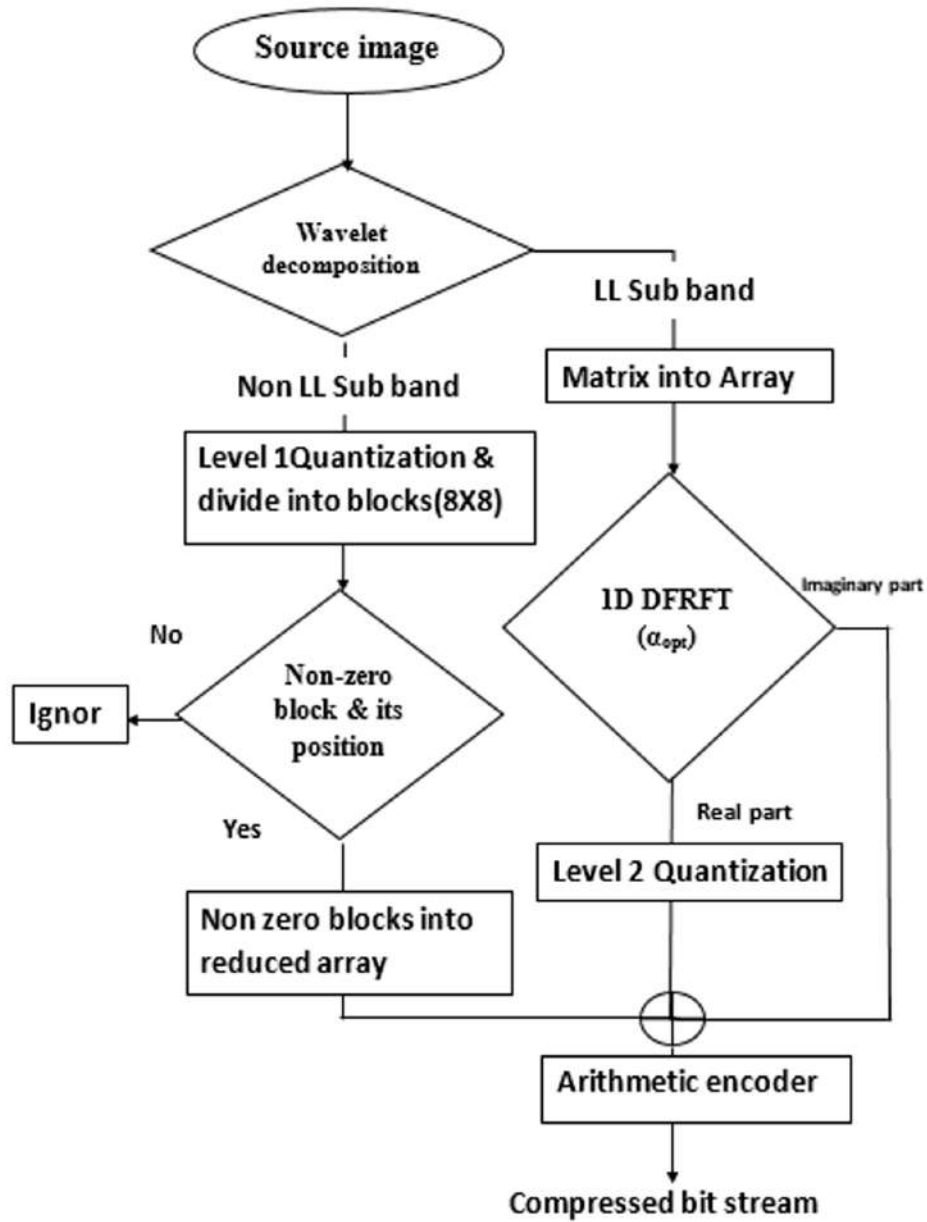


Figure 4.1 Pipelined view of a proposed lossy compression algorithm

Step 1:The image is subjected to wavelet decomposition with a sufficient number of levels, which splits the image into LL and non-LL subbands. First level non-LL subbands are neglected (zeroed).

Step 2: Remaining non LL subbands are segmented into blocks of defined size (8X8). Store the significant non-zero blocks and its position except these remaining blocks are

zeroed. Apply quantization by using equations 3.3.2 and 3.3.3 then encode them by arithmetic coding.

Step 3: Create the quantization matrix, then for each column of LL subband apply one-dimensional DFRCT and quantization. Specify the optimal fractional order for different test images for good compression performance and store them as a reduced array followed by the arithmetic encoder with header tags.

Step 4: This is orthogonal process hence the decompression is quite converse to the compression method. IDFRCT is applied to decoded LL subband and decoded blocks of nonzero non-LL subbands are restored to their original position remaining all blocks are padded by zero. Finally, IDWT is applied for both the sub-bands to reconstruct high-quality source image.

4.3.3 Results and discussion

The strength of proposed compression algorithm is evaluated by numerical simulations. The original test images Lena, Barbara, cameraman, rice, and IC dimension 512×512 are used to analyze the compression techniques. The table.4.4 evaluates the proposed compression algorithm at compression ratios 20%, 40, 50, 60, 70, 80 and 85% by varying the wavelet decomposition levels, optimum quantization factors and fractional orders are used. Here we observed that the 20% of compression is achieved by wavelet decomposition at level one and remaining process uses level three decomposition, to increase the compression ratio. At the same time, the quantization factors for non-LL sub-band varies from 0.001 to 0.2 and for LL subband compression by using optimum fractional order varies from 0 to 1.

Table 4.4 MSE, PSNR at optimum wavelet decomposition level, quantization factor and (α_{opt})

of proposed method for chosen compression percentage for 'lena' image

Compression percentage	Wavelet decomposition level	Quantization factor for non LL	α_{opt} for LL	MSE	PSNR
20	1	0.001	0.93	18.745	36.23
40	3	0.002	0.90	20.189	35.29
50	3	0.006	0.84	20.221	35.19
60	3	0.01	0.99	20.175	35.08
70	3	0.03	0.98	21.194	34.86
80	3	0.08	0.97	26.154	33.95
85	3	0.16	0.98	37.956	32.33

The graph used in figure 4.2, analyzes the proposed method by plotting PSNR values versus compression percentage for different test images. Here the increase in compression percentage leads to reduced PSNR values.

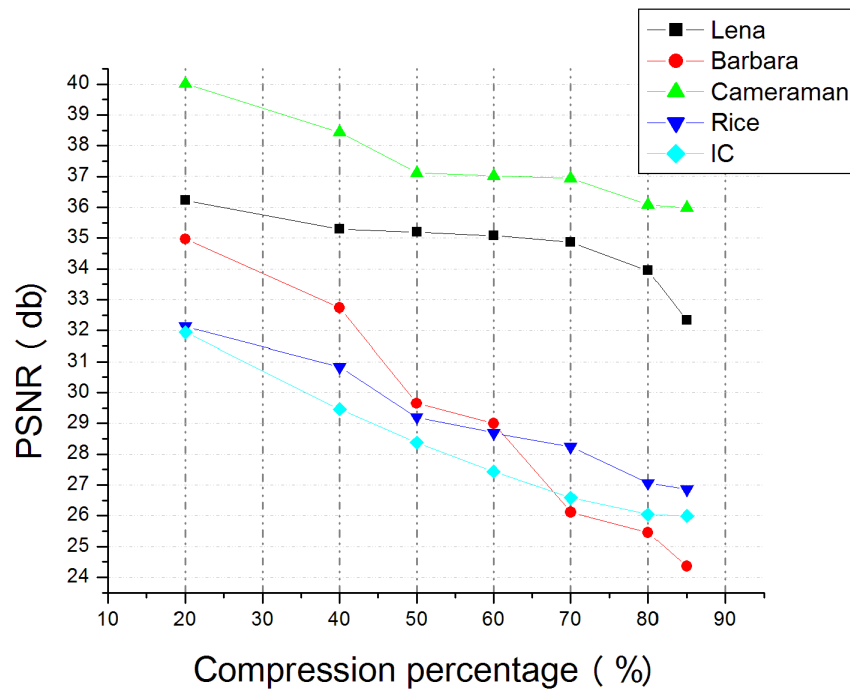


Figure 4.2 The graph for different test images using DWT-DFRCT



Figure 4.3 (a)Original lena image(512X512) compressed by using proposed method at (b)20% with PSNR 36.23db;(c)40% with PSNR 35.29db;(d)60% with PSNR 35.08db;(e)80% with PSNR 33.29db;(f)85% with PSNR32.33db;

Table 4.5 MSE, PSNR comparison of proposed method with DFRCT and DFRFT

Test im- ages	CP (%)	DFRCT[26]			DFRFT[26]			DWT-DFRCT (level 3)			
		α_{opt}	MSE	PSNR	α_{opt}	MSE	PSNR	Q	α_{opt}	MSE	PSNR
Lena	75	0.94	313.8	22.0	0.93	97.8	25.21	0.05	0.94	22.73	34.52
Barbara	75	0.99	543.04	19.6	0.91	339.7	20.91	0.04	0.98	172.8	25.73
Cameramen	75	0.99	464.30	20.37	0.97	180.7	24.40	0.02	0.96	14.28	36.54
Rice	75	0.92	161.52	24.95	0.92	122.2	24.57	0.3	0.98	121.4	27.28
IC	75	0.99	512.26	19.94	0.94	44.8	26.11	0.2	0.96	153.6	26.26

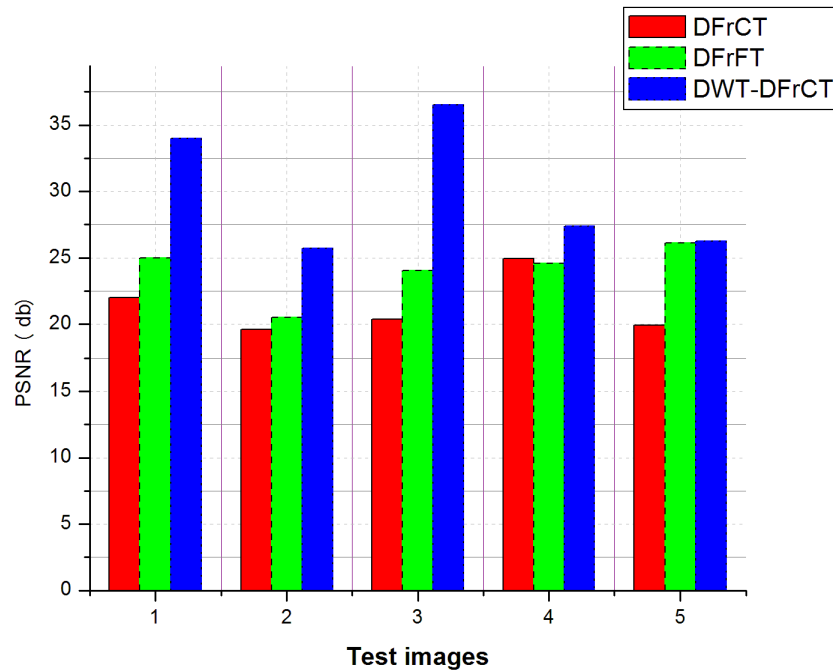


Figure 4.4 PSNR comparison of test images (1.Lena; 2.Barbara; 3.cameraman; 4.rice; 5.IC) using DFrCT,DFrFT and DWT-DFrCT

Figure 4.3 shows the reconstructed images by using proposed method for Lena image at fixed compression percentages of 20%,40%,60% and 85% respectively. Table.4.5 compares the proposed method with DFrFT and DFrCT[160] by tabulating PSNR, MSE values at fixed compression percentage 75%. Here we observed that the reconstruction quality of Lena and cameraman is better than the other methods. The images with less edge information are recovered better by proposed method with reduced error rate. Figure 4.4 shows the graphical PSNR comparison of the proposed method with DFrFT and DFrCT at compression percentage 75%.The results show that quality of reconstruction by proposed methods is significantly improved in terms of PSNR and MSE.

4.4 Lossless Image compression algorithm using DWT and DFRFT

4.4.1 Previous works

Maintaining quality of reconstruction at high compression rate is very difficult part in data compression. Several applications like medical imaging, defense and satellite image processing fields, use wavelet based lossless image compression algorithms. A lossy compression algorithm is proposed in section 4.3, loses quality of reconstruction due to coarse quantization process and reckless killing of less significant coefficients and ignorance of imaginary part in DFRCT during an encoding process. In order to overcome these limitations and to improve the image quality during reconstruction, an alternative method, hybrid wavelets with fractional Fourier transform is proposed, which can deliver high compression percentage.

4.4.2 Flow of DWT_DFRFT algorithm.

This algorithm uses advantages of both wavelet and fractional Fourier transforms to enhance the compression performance. The wavelet transform is used to extract the spectrum of a source image into low frequency (LL) and high frequency (non-LL) sub-bands. One dimensional DFRFT is applied for LL sub-band for compact encoding into a reduced array. The steps involved in the proposed method (figure 4.5) are as shown below,

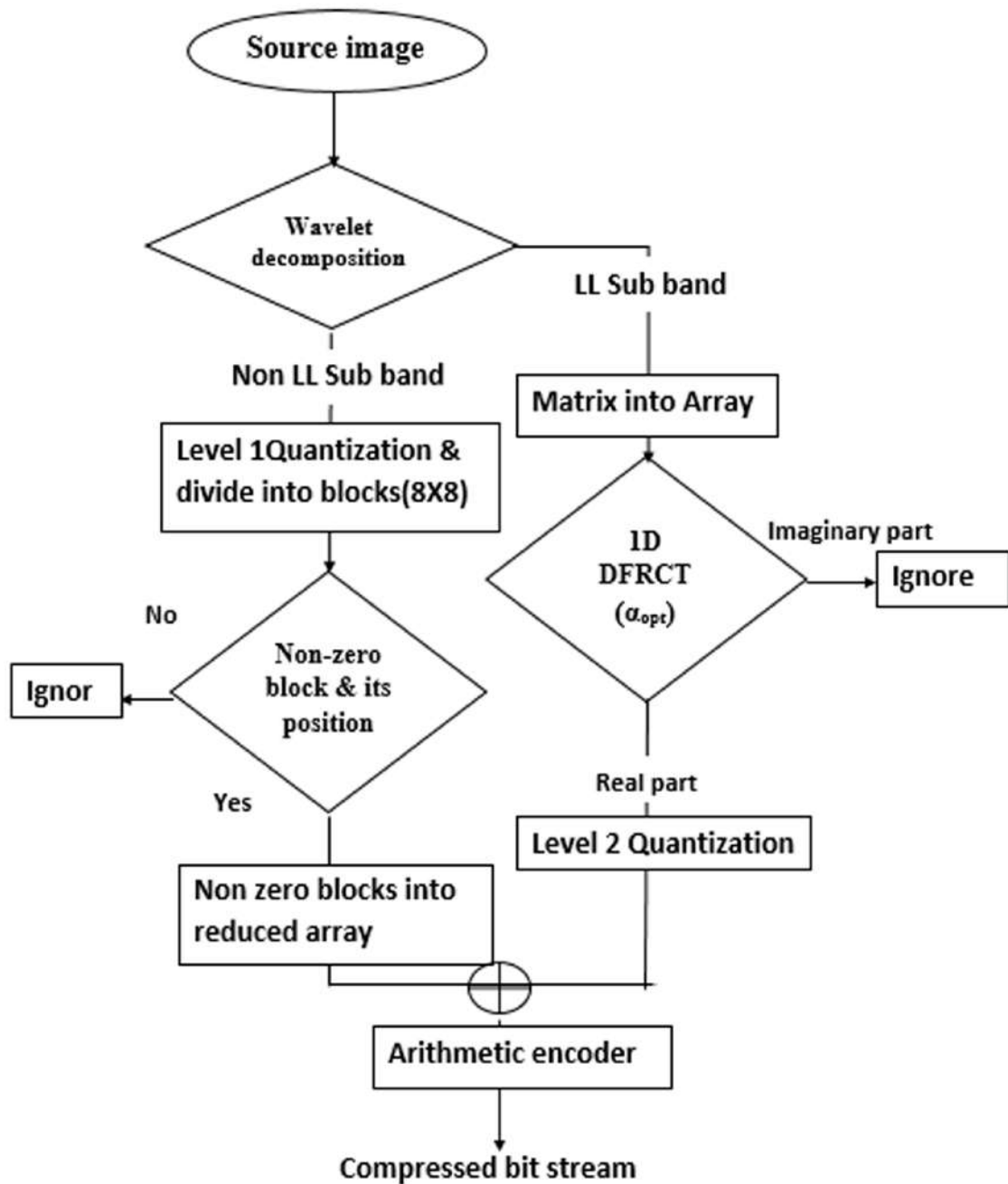


Figure 4.5 A block view of proposed method

Step 1: First, apply the two-dimensional discrete wavelets transform for decomposition (mother wavelet debouches of scale 5).The source image is split into LL and non-LL sub-bands.

Step 2: Apply level1 quantization for decomposed subbands to increase the correlation,

by multiplying quantization scale with the median value of the sub-bands. Then divide the sub-band by M1, as explained below

$$M1 = Quantization_Scale \times median(sub_band_A) \quad (4.4.1)$$

$$Sub_band_A = round(sub_band/M1) \quad (4.4.2)$$

Step 3: One dimensional DFRFT with the optimal fractional order(α_{opt}) is applied to each column of LL sub-band. Further, in level2 quantization transform is applied for the column by dividing the quantization matrix by using equation 4.20. And store the values in a reduced array and size of LL sub-band,

$$M2(m, n) = \begin{cases} 1, if(m = 1, n = 1) \\ m + n + R, if(m \neq 1, n \neq 1) \end{cases} \quad (4.4.3)$$

Step 4: Remaining non-LL sub-bands are partitioned into non-overlapped blocks of standard size 8×8 . Search for the block having nonzero values and then store them in the reduced array along with its position. Blocks with zeros are neglected and not included in a reduced array.

Step 5: All reduced arrays are encoded by an arithmetic encoder into a compressed bit stream. Since reduced array contain both positive and negative values and are encoded by the arithmetic encoder.

Step 6: The decompression process is the reverse of the compression process, where reduced arrays are decoded by the arithmetic decoder. The LL subbands recovered by inverse DFRFT with fractional order(α_{opt}) and by multiplying level2 Quantization factor M2. Similarly, non-LL subbands recovered to their original position and remaining blocks are padded by zero. Again multiply the quantization factor M1 for each non-LL sub-bands then apply an inverse discrete wavelet transform to reconstruct the original image.

4.4.3 Simulation results and discussions

Original test images Airplane, house, boat, Arial, peppers, Barbara, and mandrill are chosen to evaluate our compression algorithm. Table.4.6 tabulates percentage root mean square difference (PRD) and PSNR values of proposed method at a high compression percentage from 50%, 55,60,70 to 90% with optimal fractional orders(α_{opt}) for Barbara image. Fig.4.6 shows reconstructed 'barbara' image from proposed method at different compression percentage. Table.4.7 gives PRD, PSNR comparative tabulation of the proposed method with other combination of wavelet transform with DFRCT and DFRST at compression percentage (80%). From Table.4.7, we can observe that the PSNR values and compression percentage are inverse in relations, as we increase the compression percentage the PSNR values get decreased and vice-versa. PSNR value of the proposed method for boat image at 80% is 2db and 0.41db lesser than remaining two methods respectively. PRD also varied in the same manner, since of the proposed method is less efficient in reconstructing the images with a large number of edges.

Table 4.6 PRD and PSNR calculation of proposed method at different CP for Barbara image

Compression percentage	α_{opt}	PRD	PSNR
50	0.94	8.56	28.24
60	0.96	10.04	26.03
70	0.98	10.13	25.77
75	0.96	10.13	25.73
80	0.92	10.14	25.70
90	0.98	10.92	25.24



Figure 4.6 (a) Original Barbara image compressed using by DWT-DFRFT at CP (b)20% (c)40%;(d)60%;(e)70%;(e)80%;

Table 4.7 PRD and PSNR comparison of proposed method with DWT-DFRST and

Test Im- age	CP (%)	DWT-DFRCT								
		DWT-DFRST			DWT-DFRCT			DWT-DFRFT		
		α_{opt}	PRD	PSNR	α_{opt}	PRD	PSNR	α_{opt}	PRD	PSNR
Airplane	80	0.90	4.12	29.95	0.88	3.47	31.4	0.85	2.70	33.5
House	80	0.98	5.08	31.04	0.98	4.84	31.1	0.94	4.20	32.2
Boat	80	0.97	5.58	30.41	0.92	5.88	32.4	0.86	5.69	30.0
Aerial	80	0.96	8.76	25.65	0.90	8.42	26.3	0.90	7.92	26.7
Peppers	80	0.99	10.12	26.47	0.97	9.82	27.7	0.97	7.84	28.9
Barbara	80	0.94	11.43	24.48	0.92	10.32	25.64	0.91	10.02	25.7
Mandrill	80	0.96	9.21	25.50	0.94	8.86	26.42	0.94	8.64	26.8

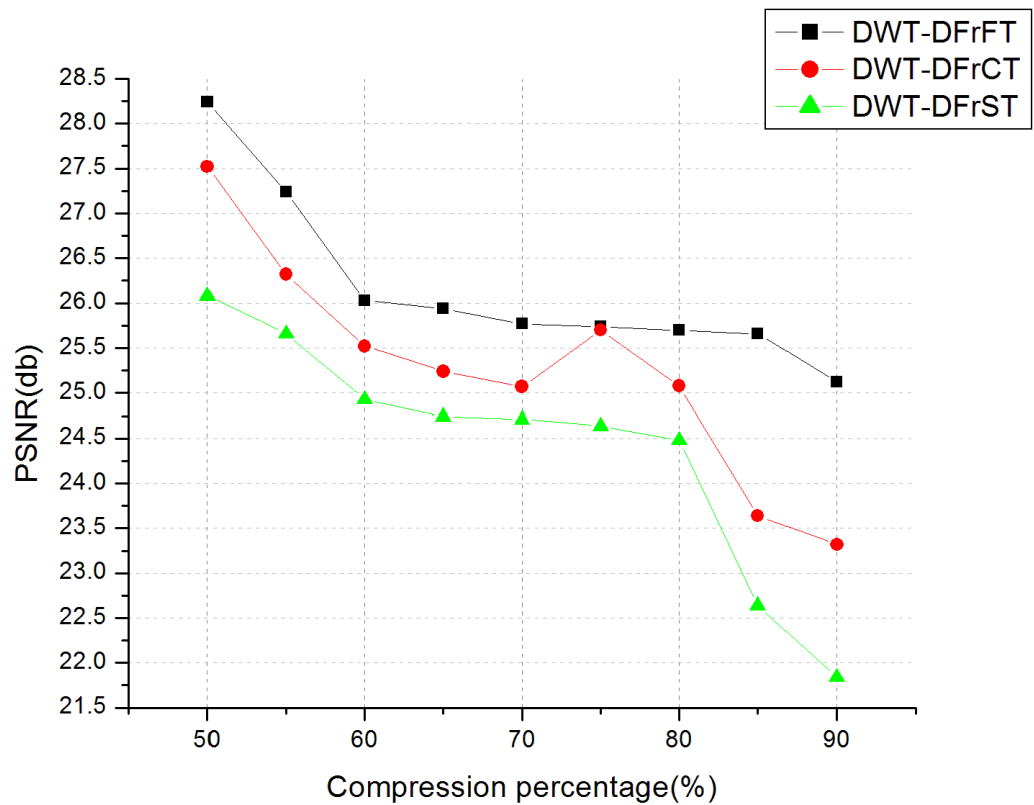


Figure 4.7 Comparison of the proposed method with DFrCT and DFrST for Barbara image at different CP (50% to 90%)

The Fig.4.7 is the graphical comparison of the proposed method with other methods. This graph indicates that the proposed method shows some significant improvement in the reconstruction process.

4.5 Medical image compression using hybrid DWT with block based DFRFT

4.5.1 Introduction

From the discussion of lossless compression algorithm proposed in the section 4.4, we found sensitive frequency components in the wavelet decomposed images are efficiently coded by using DFRFT. But, organization of two dimensional wavelet coefficients into one dimensional array during encoding stage creates complexity and image blurrier. Hence, In this section an improvement has been made by application of block based DFRFT to resolve the problem of blurring and is applied for specific medical image data.

4.5.2 Flow of proposed method

The proposed method block diagram is as shown in the figure 4.8 and it was described by following steps

Step 1: The source image is decomposed into LL and non LL sub bands by an application of Decimated wavelet transform using Debauchees family. Apply the level one quantization for all subbands using equation.4.18.

Step 2: Mean value of LL sub band is computed and stored, for each pixel of LL Sub band is subtracted by obtained mean value. Now a new reduced matrix is generated, segment it into a sub blocks of 8X8 size, then apply the one dimensional discrete fractional Fourier transform for each column of sub blocks. Second level quantization is applied for both real and imaginary part of matrix.

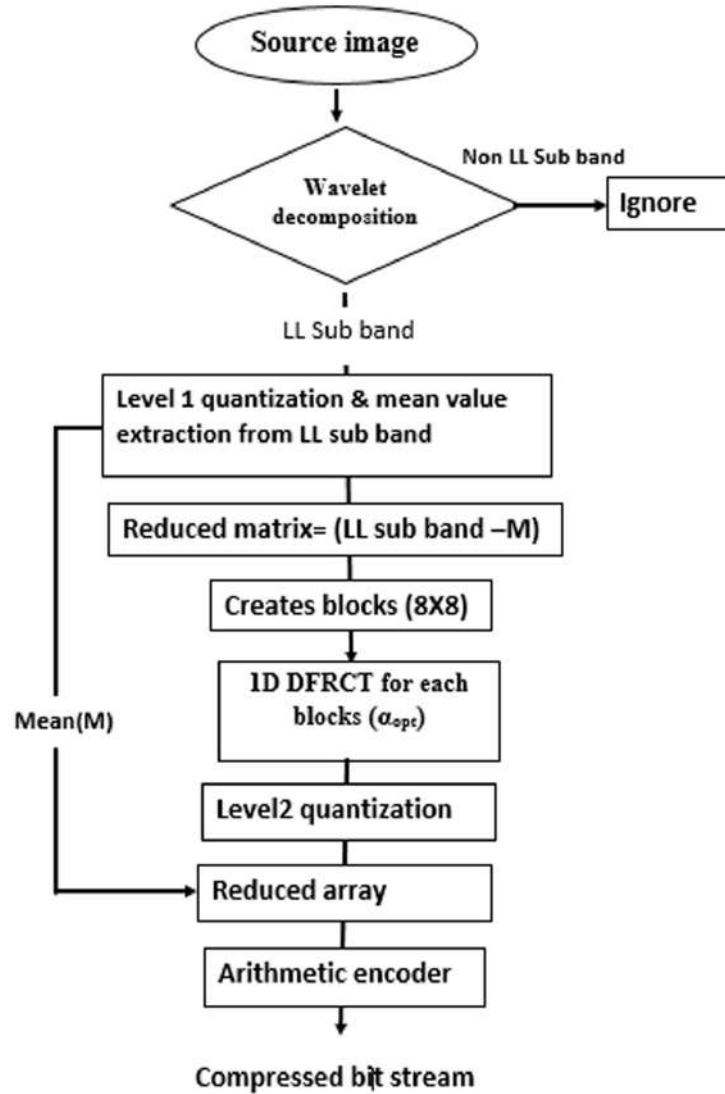


Figure 4.8 Pipeline view of proposed compression technique

Step 3: The non LL subbands are strictly neglected or made it as zero. Reduced matrix of LL sub bands are converted into single array and encoded by arithmetic encoder to obtain the compressed bit stream.

Step 4: Decompression process is converse to the compression. After decoding the reduced array of LL sub band, apply one dimensional inverse discrete fractional Fourier transform and level two de-quantization to reconstruct the blocks and then recombined it into reduced matrix.

Step 5: The reduced matrix is added with Computed mean value at encoder stage to reconstruct exact LL sub band.

Step 6: Apply the inverse discrete wavelet transform for both LL and non LL sub band to reconstruct source image.

4.5.3 Results and discussion

Some samples of medical data like X-ray, MRI, PET and Ultrasound images achieve from standard data base med-pix, Michigan University medical labs shown in Fig. 4.10 are chosen to evaluate our compression algorithm.

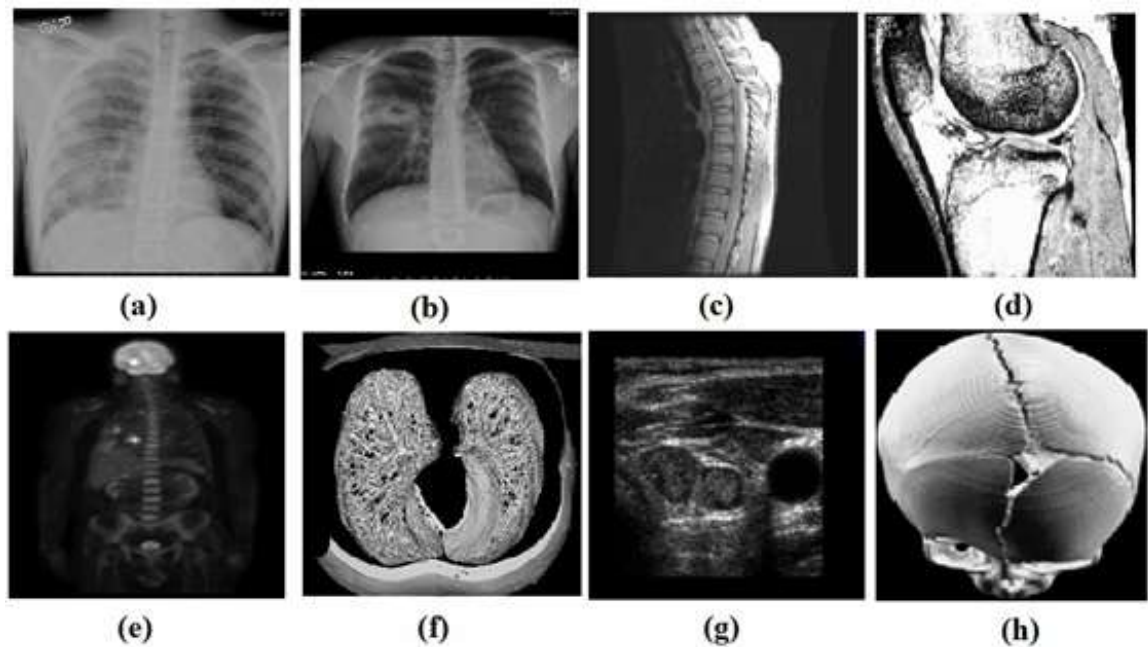
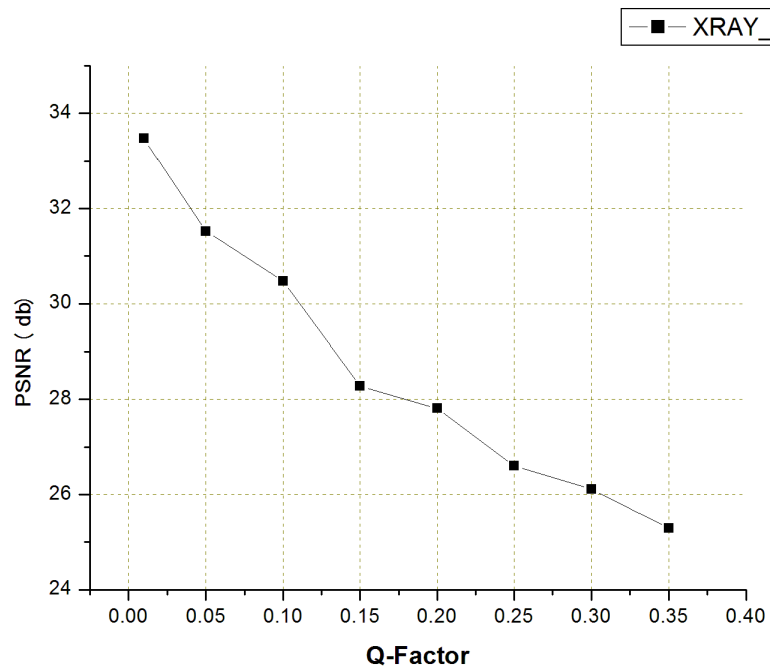


Figure 4.9 Original test images (a)Lung contusion(XRAY_1);(b)MRSA lungs abscess X-Ray(XRAY_2); (c)Pine_bone(MRI.1); (d) knee_uni (MRI.2); (e) PET_1; (f) Lung(ULTR.1); (g) Tharoid structure(ULTR.2); (h) Skull(ULTR.3);

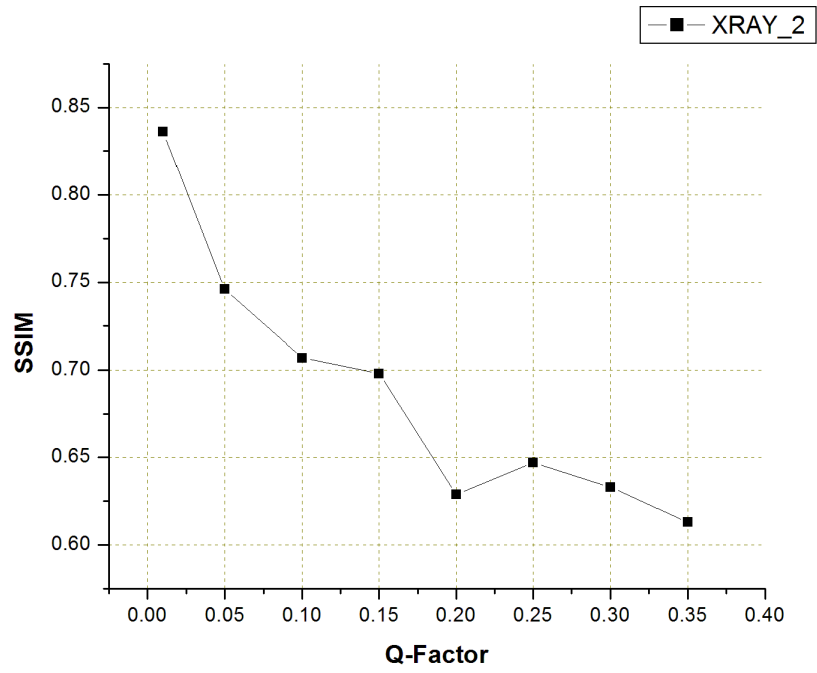
Table 4.8 PSNR and SSIM of proposed method at different CP for X-Ray images

Images	CP (%)	Q-factor	α_{opt}	PSNR	SSIM	Encoding time(Sec)
XRay_1	20	0.10	0.99	32.50	0.837	12.50
	40	0.13	0.98	31.31	0.821	10.32
	60	0.20	0.97	30.18	0.796	7.41
	80	0.40	0.99	26.88	0.754	4.31
XRay_2	20	0.07	0.96	31.47	0.712	16.6
	40	0.12	0.97	29.27	0.661	10.64
	60	0.2	0.97	28.19	0.612	8.66
	80	0.3	0.99	26.12	0.602	5.34



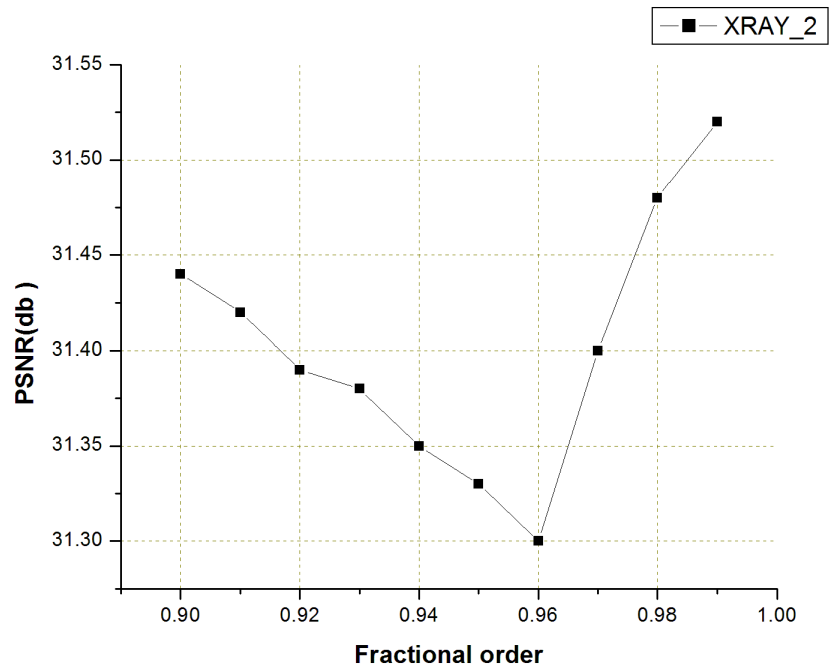
(a)

(4.5.1)



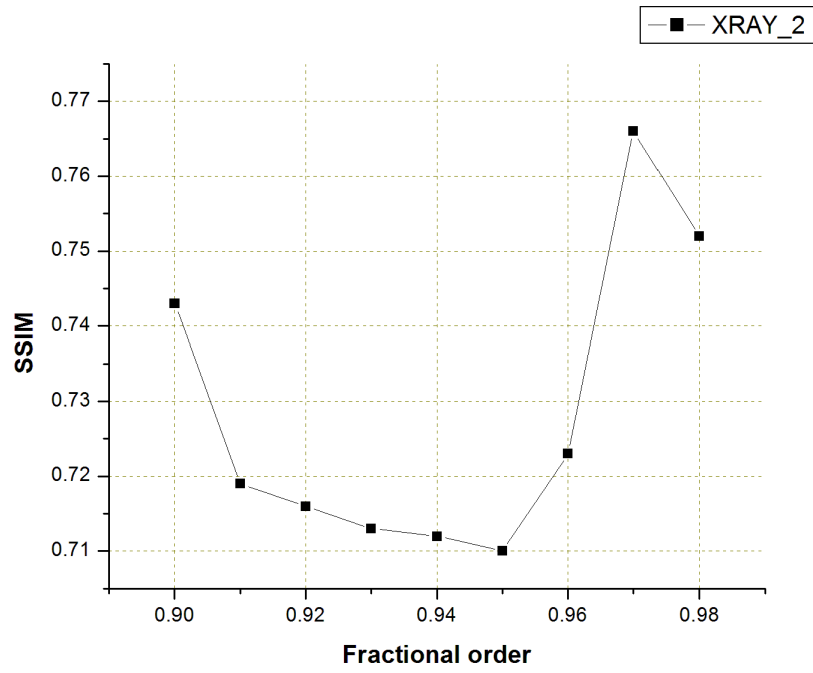
(b)

Figure 4.10 PSNR (a) and SSIM (b) varied along the Q-Factor



(a)

(4.5.2)



(b)

Figure 4.11 PSNR (a) and SSIM (b) varied along the Fractional order

X-ray image are rich in smoothness, so to conserve all significant information is not so necessary. In Table 4.8 high Q-factor is applied to achieve good PSNR and SSIM.

Table 4.9 PSNR and SSIM of proposed method at different CP for MRI and PET images

Test images	CP(%)	Q-factor	α_{opt}	PSNR	SSIM	Encoding time(sec)
MRI_1	20	0.01	0.99	35.64	0.901	32.4
	40	0.03	0.96	35.34	0.896	24.8
	60	0.04	0.96	34.32	0.856	18.3
	80	0.10	0.99	31.68	0.839	10.2
MRI_2	20	0.07	0.99	27.78	0.695	28.4
	40	0.12	0.98	26.21	0.647	21.8
	60	0.20	0.99	23.53	0.533	14.5
	80	0.40	0.99	19.92	0.389	9.10
PET_1	20	0.005	0.97	39.89	0.924	36.7
	40	0.007	0.98	39.24	0.905	34.0
	60	0.01	0.99	38.78	0.890	30.4
	80	0.02	0.98	38.46	0.870	25.6

MRI images contain more significant information and hence less Q-factor is used in table 4.9 to achieve compression. Figure 4.10 and 4.11 are the evidence for graphical analysis for optimization of proposed compression algorithm by selecting suitable Q-factor and Fractional orders. Here we observe by figure 4.11, the optimal fractional order to maintain better quality is ranging from 0.98 to 0.99.

Table 4.10 PSNR and SSIM of proposed method at different CP for ultrasound images

Test images	CP(%)	Q-factor	α_{opt}	PSNR	SSIM	Encoding time(sec)
ULTR_1	20	0.001	0.98	25.45	0.797	92.3
	40	0.005	0.99	25.07	0.750	60.6
	60	0.01	0.98	24.87	0.724	54.8
	80	0.04	0.98	24.29	0.719	42.0
ULTR_2	20	0.001	0.97	39.45	0.889	120
	40	0.002	0.98	35.86	0.807	102
	60	0.005	0.95	33.72	0.783	98.6
	80	0.01	0.99	32.33	0.724	64.3
ULTR_3	20	0.001	0.69	31.06	0.821	120
	40	0.004	0.96	30.45	0.820	98.3
	60	0.008	0.90	30.14	0.848	74.2
	80	0.03	0.98	30.07	0.843	40.6

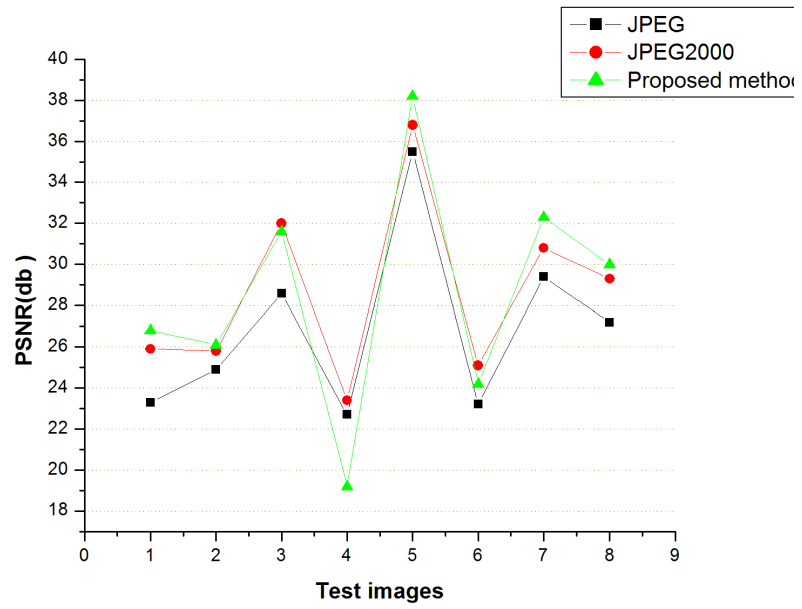
Table 4.10 tabulates the PSNR and SSIM values for some ultrasound images at different compression percentage with optimal Q-factor and fractional order. Ultrasound images are more sensitive medical images compared to other images, so less quantization factor is selected in our algorithm for compression.

Table 4.11 PSNR Comparison of proposed method with JPEG and JPEG2000 at CP 80

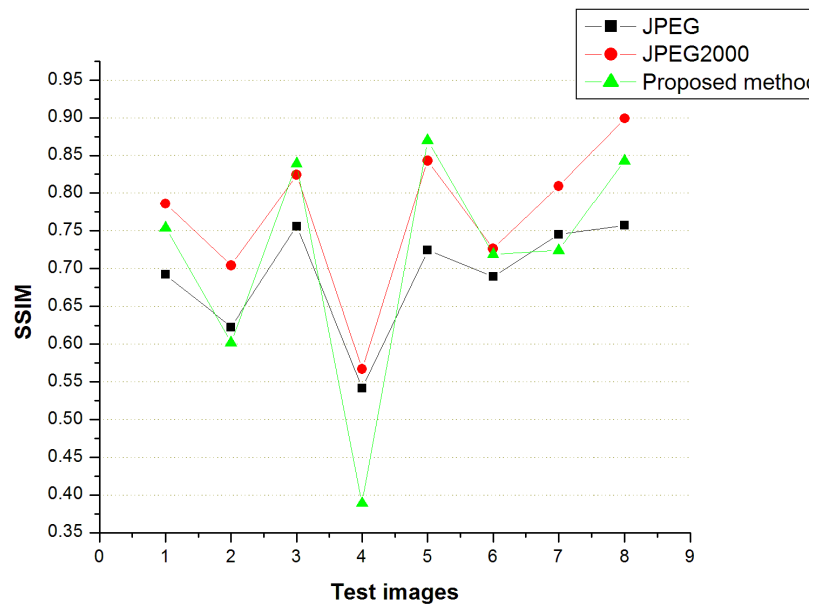
Images	CP	JPEG	JPEG2000	Proposed method		
	(%)	PSNR	PSNR	Q-Factor	α_{opt}	PSNR
XRAY_1	80	23.3	25.9	0.4	0.99	26.8
XRAY_2	80	24.9	25.8	0.3	0.99	26.1
MRI_1	80	28.6	32.0	0.1	0.99	31.6
MRI_2	80	22.7	23.4	0.4	0.99	19.2
PET_1	80	35.5	36.8	0.02	0.98	38.2
ULTR_1	80	23.2	25.1	0.02	0.98	24.2
ULTR_2	80	29.4	30.8	0.01	0.99	32.3
ULTR_3	80	27.2	29.3	0.03	0.98	30.0

Table 4.12 SSIM Comparison of proposed method with JPEG and JPEG2000 at CP 80

Images	CP	JPEG	JPEG2000	Proposed method		
	(%)	SSIM	SSIM	Q-Factor	α_{opt}	SSIM
XRAY_1	80	0.692	0.786	0.4	0.99	0.754
XRAY_2	80	0.623	0.704	0.3	0.99	0.602
MRI_1	80	0.756	0.824	0.1	0.99	0.839
MRI_2	80	0.542	0.567	0.4	0.99	0.389
PET_1	80	0.724	0.843	0.02	0.98	0.870
ULTR_1	80	0.689	0.726	0.02	0.98	0.719
ULTR_2	80	0.745	0.809	0.01	0.99	0.724
ULTR_3	80	0.757	0.820	0.03	0.98	0.843



(a)



(b)

Figure 4.12 PSNR(a) and SSIM(b) graphical comparison of proposed method with JPEG and JPEG2000

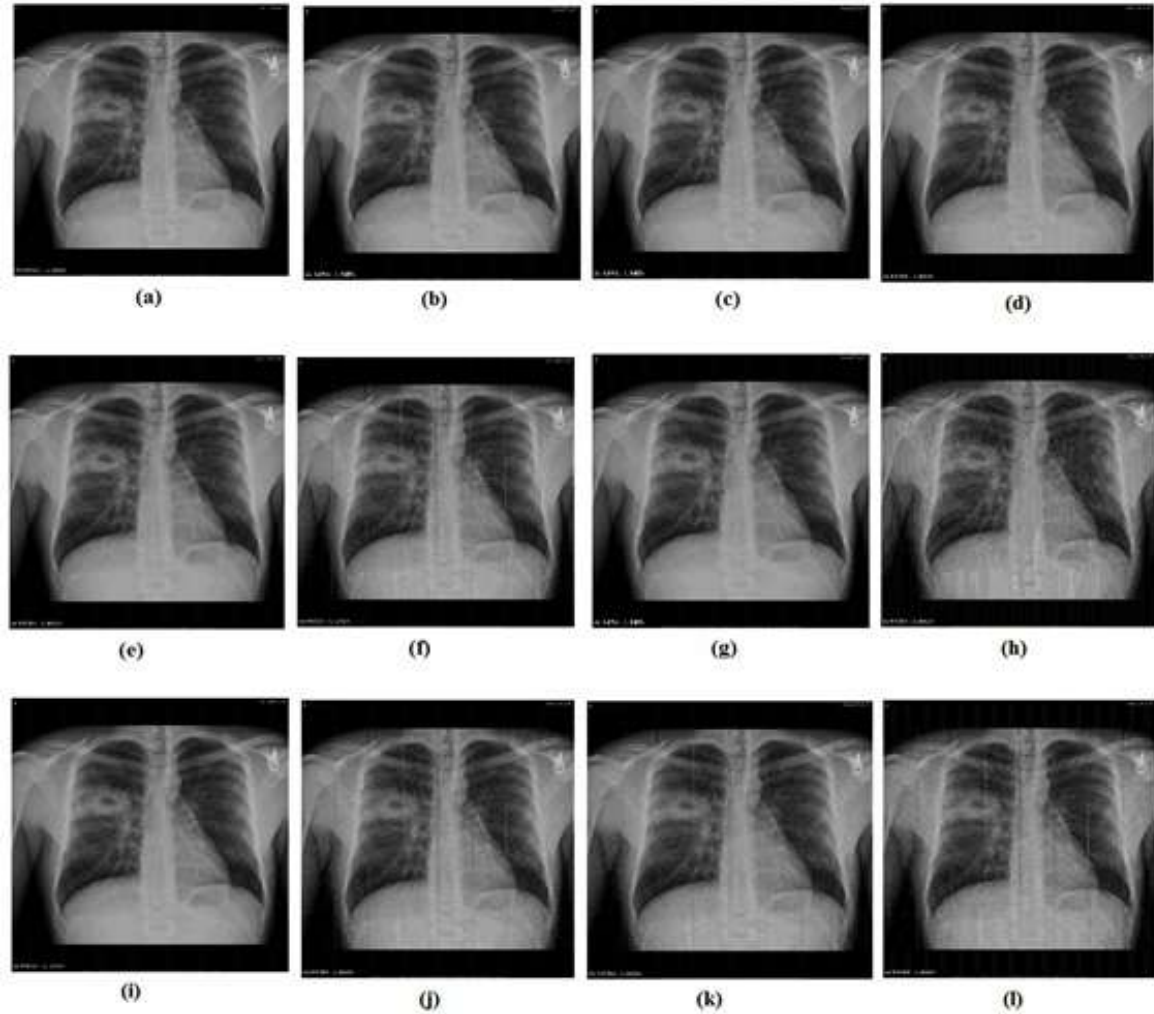


Figure 4.13 XRay_2 image compression using JPEG2000 at compression percentage (a)20%; (b)40%; (c)60%; (d)80%; compression using JPEG at (e)20%; (f)40%; (g)60%; (h)80%; and compression by proposed method at (i)20%; (j)40%; (k)60%; (l)80%;

The table 4.11 and table 4.12 illustrate a comparative simulation of proposed method with JPEG and JPEG2000 for same medical images at fixed compression percentage 80%. Figure 4.12 shows the graphical comparison of proposed method with art of work evidences that the proposed method can compete with art of work at high compression percentage. Figure 4.13 shows the simulated images by JPEG2000, JPEG and proposed method.

Above all studies includes that proposed method have significant improvement in compressing the medical image. This algorithm operates at high compression percentage without affecting image quality made it several advantages in applications like telemedicine.

4.6 Summary

In this chapter, fractional Fourier transforms such as DFRST, DFRCT and DFRFT are described in section 4.2. The DFRST and DFRCT are constructed by using Eigen values of DFT kernel. The operating capability of DFRCT on real values and compact coding of DFRFT with respect to fractional orders allows us to compress the signal efficiently.

In section 4.3 an improved lossy compression technique is proposed by using wavelet and DFRCT to achieve a high quality of reconstruction of an image at high compression rate. The algorithm uses wavelet transform to decompose an image into the frequency spectrum of low and high-frequency subbands. Two levels of quantization make this algorithm lossy but arithmetic coding used to encode the sub-bands overcomes some losses. In section 4.3.4 experimental results of the proposed method are discussed and compared with existing compression algorithms and some significant improvements can be observed in terms of peak signal to noise ratio and self-similarity index mode at high compression ratio.

A new lossless image compression algorithm is proposed in section 4.4, which uses both DWT and DFRFT for image compression. Wavelets are the best choice for feature extraction of the source image at different frequency resolution but the low-frequency subbands of wavelet decomposition are until the untouched part in compression method due to their sensitive nature. On the other hand, fractional Fourier transform is a convenient form of generalized Fourier transform, helps in the compact lossless coding of the source image with optimal fractional orders. Hence discrete fractional Fourier transform is used to compress those sensitive sub-bands carefully. The experimental results of the proposed algorithm with a different set of test images are compared with some of the existing image

compression algorithms. The result shown in section 4.4.3 reflects significant improvement in image reconstruction quality of the proposed method.

The block based in DFRFT is proposed in the section 4.5 is an improved version of DWT-DFRFT method explained in section 4.4. The low frequency wavelet coefficients are coded using block based DFRFT, increases the compression performance. The simulation results of proposed method using X-ray, MRI and ultrasound medical images presented in section 4.5.3, reveal that proposed algorithm is best suited for medical image compression.

Chapter 5

Hybrid compression schemes using modified singular value decomposition and wavelets

5.1 Background with previous work

Recently, developed compression algorithms like JPEG and JPEG2000, introduced by joint photographic experts group uses DCT and wavelet transform for image compression [161-165]. DCT based compression techniques suffered by blocking of an artifact, but multi-resolution and overlapping nature of wavelet alleviates the blocking artifact and creates superior energy compaction [166]. From the discussion of section 3.2.3, we found that, wavelet-based compression EZTW [122] produces unavoidable artifacts during low bit-rate transmission and is a complex process, which requires more storage space. Increasing the number of bits in the encoding bit stream and neglecting of few significant bits can also reduce the image quality in SPIHT compression. Prior scanning of significant coefficients before encoding confirms the gradual improvement in the progressive image compression[167].

Because of its high-quality reconstruction by using SVD made, it can be used as pre-processing step for many image compression algorithms [168, 169] . A hybrid method of SVD and EZTW for ECG signal compression is proposed [170] shows significant improvement in compression ratio and excellent quality of image reconstruction with fewer bitrates. But, it has drawback of computational complexity and cost effectiveness and it is limited for ECG signal only. Another lossy compression algorithm proposed by [137] using SVD and wavelet difference reduction (WDR) shows some improvement in quality. These two references signify that, the use of SVD as pre processing step for progressive image compression possibly improves the compression performance. In this chapter, new median based SVD is developed and used as a pre processing step for adaptive SPIHT and binary tree coding algorithm. With small improvement in MSVD by mean value computation is developed and used as pre processing step for EZTW.

5.2 Median based rank one updated singular value decomposition for image compression(MSVD)

An image is formed with a two-dimensional matrix of $m \times n$ pixels; each pixel represents its intensity value. The SVD is applied to the matrix representing an image to get $U \Sigma V^T$, where 'U' and 'V' are the orthogonal matrices of $m \times n$ and $n \times n$, respectively, Σ is a nonnegative and diagonal matrix of $m \times n$. The compression is achieved by selecting a much smaller number of ranks to approximate the original image during reconstruction.

Here, ranks are reduced in two stages, first by subtracting the image matrix by its median value before performing the SVD and then add the median value after reconstruction. Secondly, divide the image into sub-block to exploit the uneven complexity of the original image. Appropriate ranks have been selected adaptively for each sub-block by

specifying the percentage of the sum of singular values instead of a fixed value [171, 172].

For image ' I ', median-based rank one updated SVD process is given by,

Original Image(I):

$$I - \text{median}(I) = U\Sigma V^T \quad (5.2.1)$$

where U is m by n , V is n by m , and $\Sigma = \text{diag}(r_1, r_2, \dots, r_k, 0, \dots, 0)$

$$\text{Specifiedpercentage} = \frac{(r_1 + r_2 + r_3 + \dots + r_{k1})}{(r_1 + r_2 + r_3 + \dots + r_k)} \quad (5.2.2)$$

where $k1$ is rank for each sub-blocks of image

Reconstructed Image:

$$I_1 = U\Sigma_1 V^T + \text{median}(A) \quad (5.2.3)$$

where U is m by $k1$, V is $k1$ by n , and $\Sigma_1 = \text{diag}(r_1, r_2, r_3, \dots, r_{k1})$

Table 5.1 Percentage of ranks used for specified singular values for reconstruction of Lena

image (8X8 block)		
% sum of singular values used	Average ranks used	Average percentage of ranks used
85	2.110	0.264
70	1.022	0.127
55	1 .000	0.125
40	1 .000	0.125
25	1 .000	0.125

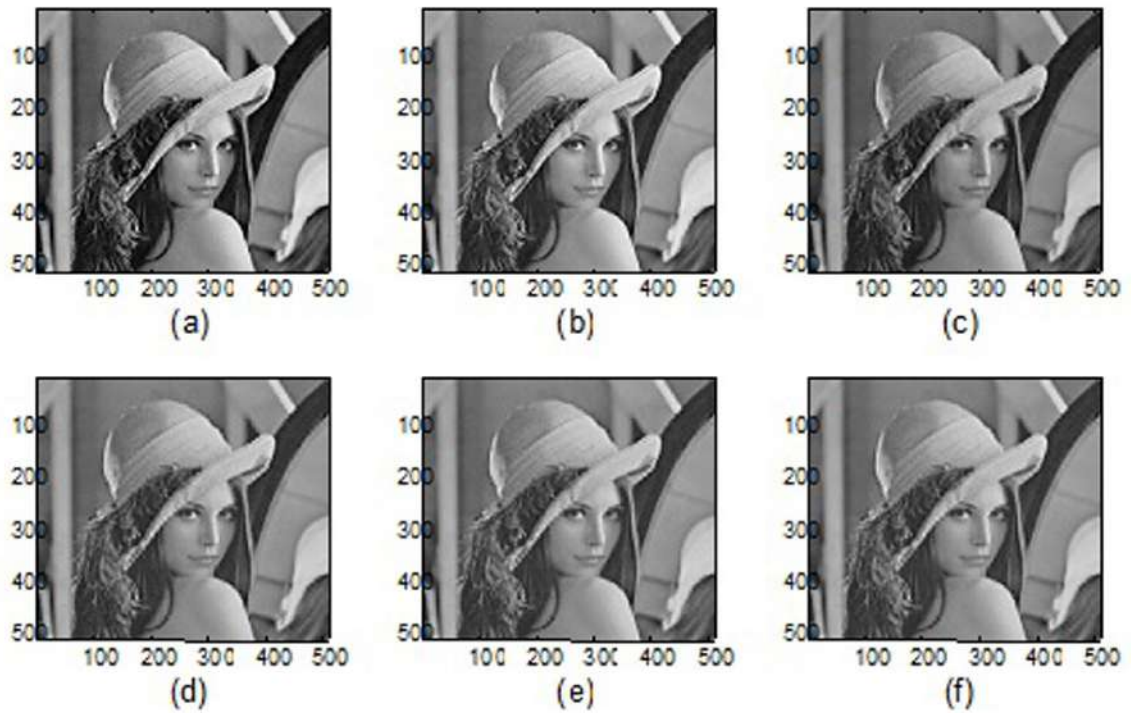


Figure 5.1 (a) Original lena (512X512) reconstructed with percentages of ranks (b) 85% of ranks,(c)65% of ranks,(d) 50% of ranks,(e)40%of ranks,(f)25% of ranks

This process condenses the allocation of singular values. When a sub-block has the complex image, its singular values are scattered than the one that contains a simple image. Table 5.1 show, the average ranks and the percentage of ranks used for the 8x8 block-size compression with the rank-one update from 25 to 85 percent of singular value sum. Notice that, from 25 to 70 percentages, only one rank is assigned to all sub-blocks and it achieves high compression without affecting the psycho-visual quality as shown in a figure.5.1

5.3 Hybrid gray scale image compression using MSVD and adaptive set partition hierarchical tree

5.3.1 SPIHT with adaptive coding order (ASPIHT)

ASPIHT algorithm is similar to conventional SPIHT algorithm except prior coding order during the initialization process of its insignificant lists. The wavelet coefficients on the edges are often more significant due to larger magnitudes and hence scanning the neighborhood of these significant coefficients is necessary [173, 174]. During the scanning process, the more priorities are given to the previously scanned significant neighborhoods than other regions and are encoded by SPIHT to achieve efficiency in the reconstruction of edges. In this method, the original image is decomposed and reconstructed by using cohen-daubechies-feauveau (CDF) 9/7-tap wavelet filter to improve the compression performance of SPIHT [175]. ASPIHT algorithm is applied to an image that follows a bit-plane encoding as shown in the figure 5.2. It is a three-step process; Initialization, sorting pass and refinement pass. It uses three lists: list of insignificant pixel (LIP), list of insignificant set (LIS) and list significant pixel (LSP) to perform the above three-step process. Initialization process begins with finding the maximum value in wavelet coefficient and calculates the initial threshold by equation 5.4 as follows,

$$T = \log_2(\max(\max(I_m))) \quad (5.3.1)$$

where, as the Initial threshold and I_m is the two-dimensional array (decomposed wavelet coefficients). The LIP is initialized with the list of nodes from low-frequency sub-bands of wavelet coefficients by Morton scanning order [176]. The LIS is initialized with lists of all offspring and descendants of nodes stored in LIP. Initially, the LSP is an empty list,

and during the sorting pass, it holds the list of significant coefficients along with the sign bit. In sorting pass, each coefficient in the LIP and LIS is compared with the defined threshold by performing significance test using formula as follows,

$$S_T(\tau) = \begin{cases} 1, \max_{(i,j) \in \tau} \{|C_{i,j}| \geq 2^T\} \\ 0, otherwise \end{cases} \quad (5.3.2)$$

If the coefficient identified as significant, then it is moved to LSP along with sign bit, otherwise to LIP. Similarly in LIS, if the set becomes significant it is partitioned the set into its offspring and descendants. Here each offspring undergo the significance test and if its coefficients are significant are moved to LSP otherwise to LIP. If these significant offspring have any descendants, the LIS is reloaded with a new set of offspring and check for significance test, under the same pass. Otherwise, a set is removed from the list. Adaptive coding is performed by scanning the neighbor coefficients of the previously scanned significant coefficient, which are moved first to LSP. The scan then proceeds to the next coefficient and their offspring of LIS as shown in example 1. Finally, at refinement pass, the threshold is divided into half of its initial value and repeats the process for same prior nodes by using the above passes. The whole process is repeated till the required bit rate is achieved.

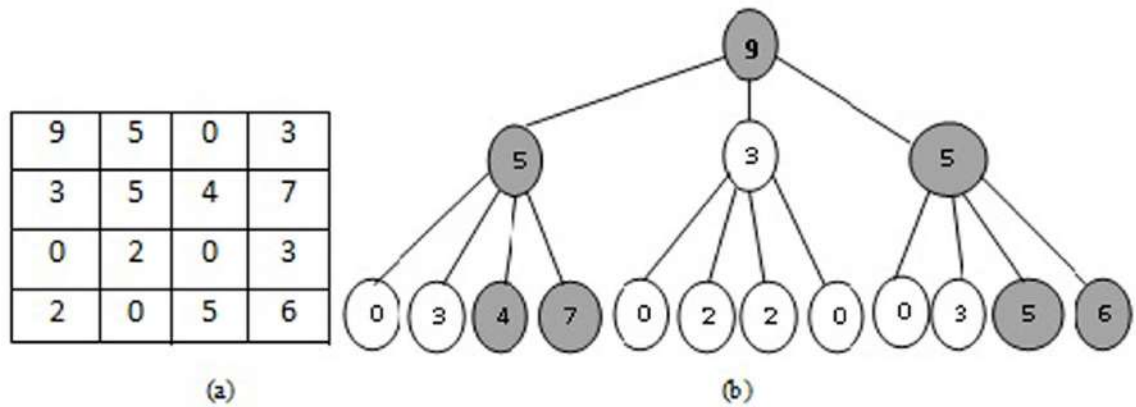


Figure 5.2(a) a block of wavelet coefficients processed by adaptive scanning ordered encode by SPIHT (b) Adaptive scanning order of the tree, where gray nodes are a significant node from the previous scanning

Example.1: Consider a simple block of wavelet coefficients shown in the figure 5.2 (a). For first pass the threshold $T_0 = \log_2 = 3, 2^3 = 8$, hence LSP is encoded by only 9 as a significant bit; For the second pass $T_1 = \frac{8}{2} = 4$ then two offspring with their descendants are significant hence, LSP encoded by 9, 5, 5, 4, 7, 5, 6. Now the parent and child relation is as shown in the figure 5.2(b). In the last pass, threshold becomes $T_2 = \frac{4}{2} = 2$, and here, the neighbor pixels of the significant parents and brothers need to be encoded. i.e. 3, 3 are encoded first then encode 3, 2, 2.

5.3.2 Realization of MSVD-ASPIHT

In this proposed method median based rank one updated SVD, described in section 5.2 is used as a pre-processing step for ASPIHT. The median value of its original image matrix is calculated and subtracts the original image matrix from that median value yields good image quality.

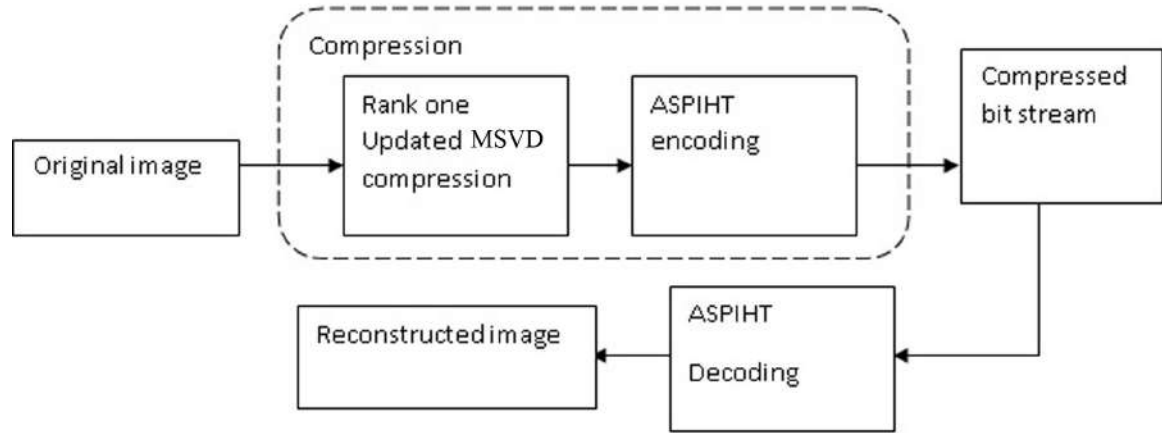


Figure 5.3 Generic representation of proposed MSVD-ASPIHT algorithm

Hence, by cascading of modified rank one updated SVD and ASPIHT, the proposed algorithm (figure 5.3) derive more benefits in achieving high PSNR at high compression ratio for specified bitrates.

1. First, the median value of original image matrix is extracted and the original image matrix is subtracted from that median value. Divide the complete image into 8×8 blocks and apply SVD for each block by using the equation 5.2.1.
2. Calculate the ranks of each sub-block by using its singular values. Then the average ranks and an average percentage of ranks is computed to reconstruct the image with specified percentage sum of singular values using equation 5.2.2.
3. Finally, an image is reconstructed using equation 5.2.3 and is added to the median value.
4. The resultant image is used as an input to the ASPIHT part of the proposed technique.

5. ASPIHT uses CDF 9/7-tap wavelet filter for decomposition and more significant wavelet coefficients are priority encoded into bit streams.
6. The decoder decodes bit stream and reconstructed by using CDF 9/7-tap wavelet reconstruction filters.

5.3.3 Results and discussions

The proposed compression algorithm was tested on 8-bit grayscale (512×512) Airfield, Artificial, Big-building, Boats, bridge, Deer, Fireworks, Goldhill, Lena, peppers images. Tables 5.2, 5.3 and 5.4 show the comparison between SPIHT, ASPIHT and JPEG2000 in terms of PSNR for 20:1, 40:1 and 80:1 compression ratios respectively.

Table 5.2 PSNR comparison for fixed compression ratio 20:1

Images	SPIHT	ASPIHT	JPEG2000	MSVD-ASPIHT
Artificial	31.64	31.96	32.36	33.34
Big_Building	28.24	28.51	29.01	31.71
Boats	31.57	31.68	33.18	35.52
Bridge	27.79	28.03	28.24	30.97
Deer	41.43	42.31	41.05	43.86
Fireworks	36.05	36.06	36.38	36.99
Goldhill	31.46	31.68	32.18	34.51
Lena	35.49	35.87	35.99	39.16
Peppers	33.39	33.65	35.07	36.36

Table 5.3 PSNR comparison for fixed compression ratio 40:1

Images	SPIHT	ASPIHT	JPEG2000	MSVD-ASPIHT
Artificial	28.04	28.34	28.54	30.16
Big_Building	25.85	26.08	26.54	29.38
Boats	28.50	28.65	29.75	32.82
Bridge	24.89	25.14	25.21	28.41
Deer	36.72	36.88	36.34	39.08
Fireworks	30.92	30.93	30.97	32.32
Goldhill	29.59	29.44	29.72	32.58
Lena	32.25	32.75	32.75	36.05
Peppers	31.79	32.06	32.40	34.87

Table 5.4 PSNR comparison for fixed compression ratio 80:1

Images	SPIHT	ASPIHT	JPEG2000	MSVD-ASPIHT
Artificial	25.25	25.55	25.69	27.83
Big_Building	23.74	23.95	24.33	27.95
Boats	26.20	26.42	26.76	30.52
Bridge	22.93	23.09	23.03	26.69
Deer	32.91	33.06	31.96	35.68
Fireworks	27.63	27.77	27.30	29.12
Goldhill	27.17	27.59	27.69	31.33
Lena	29.32	29.85	29.62	33.26
Peppers	29.36	29.79	29.54	32.57

Table 5.5 SSIM values for fixed compression ratio 20:1

Images	SPIHT	ASPIHT	JPEG2000	MSVD-ASPIHT
Artificial	0.890	0.903	0.897	0.917
Big_Building	0.769	0.776	0.786	0.772
Boats	0.832	0.835	0.898	0.835
Bridge	0.868	0.873	0.877	0.878
Deer	0.970	0.972	0.969	0.971
Fireworks	0.926	0.927	0.897	0.958
Goldhill	0.822	0.828	0.839	0.828
Lena	0.906	0.910	0.910	0.910
Peppers	0.832	0.834	0.875	0.834

Table 5.6 SSIM values for fixed compression ratio 40:1

Images	SPIHT	ASPIHT	JPEG2000	MSVD-ASPIHT
Artificial	0.791	0.825	0.737	0.848
Big_Building	0.668	0.674	0.707	0.676
Boats	0.750	0.755	0.828	0.756
Bridge	0.784	0.789	0.792	0.799
Deer	0.950	0.951	0.948	0.950
Fireworks	0.854	0.856	0.850	0.917
Goldhill	0.740	0.747	0.752	0.748
Lena	0.861	0.867	0.868	0.868
Peppers	0.799	0.803	0.832	0.804

Table 5.7 SSIM values for fixed compression ratio 80:1

Images	SPIHT	ASPIHT	JPEG2000	MSVD-ASPIHT
Artificial	0.678	0.724	0.767	0.769
Big_Building	0.572	0.576	0.596	0.580
Boats	0.668	0.670	0.740	0.671
Bridge	0.692	0.698	0.692	0.713
Deer	0.922	0.924	0.912	0.925
Fireworks	0.778	0.790	0.606	0.877
Goldhill	0.660	0.674	0.670	0.674
Lena	0.803	0.814	0.808	0.815
Peppers	0.757	0.759	0.783	0.761

Similarly, Structural Similarity Index Mode (SSIM) for the compression ratio of 20:1, 40:1 and 80:1 shown in tables 5.5, 5.6 and 5.7 respectively. From the tables 5.2, 5.3 and 5.4 we can observe that the PSNR quality of proposed technique for 'lena' is 3.12dB, 3.26dB, and 3.64dB higher than JPEG2000 for 20:1, 40:1 and 80:1 compression ratios. However, from tables 5.5, 5.6 and 5.7, SSIM are comparatively lesser than JPEG2000 compression method for artificial, boats, goldhill and peppers images.

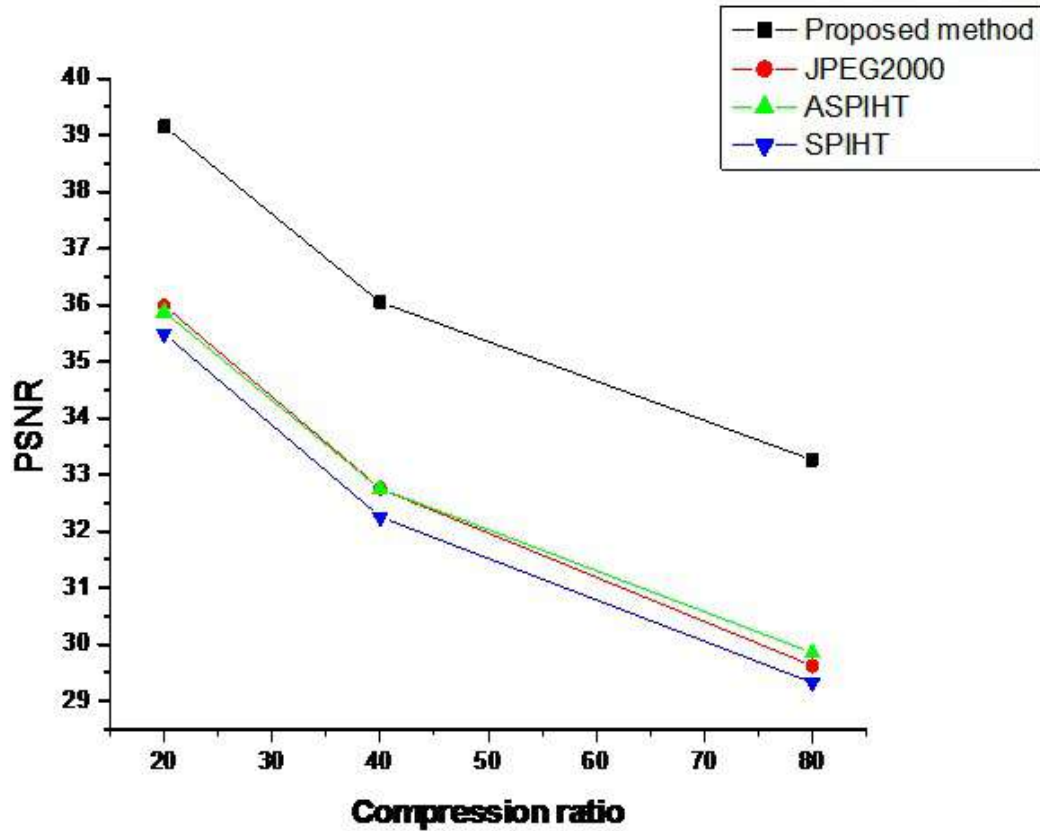


Figure 5.4 Compression performance of proposed method with other compression technique with respect to PSNR and compression ratio

Figure 5.4 illustrates compression performance of proposed method superior to other state-of-the-art techniques. It is shown in figure 5.5 the deer image is compressed by using JPEG2000, SPIHT, ASPIHT and proposed technique at the fixed compression ratio of 40:1.

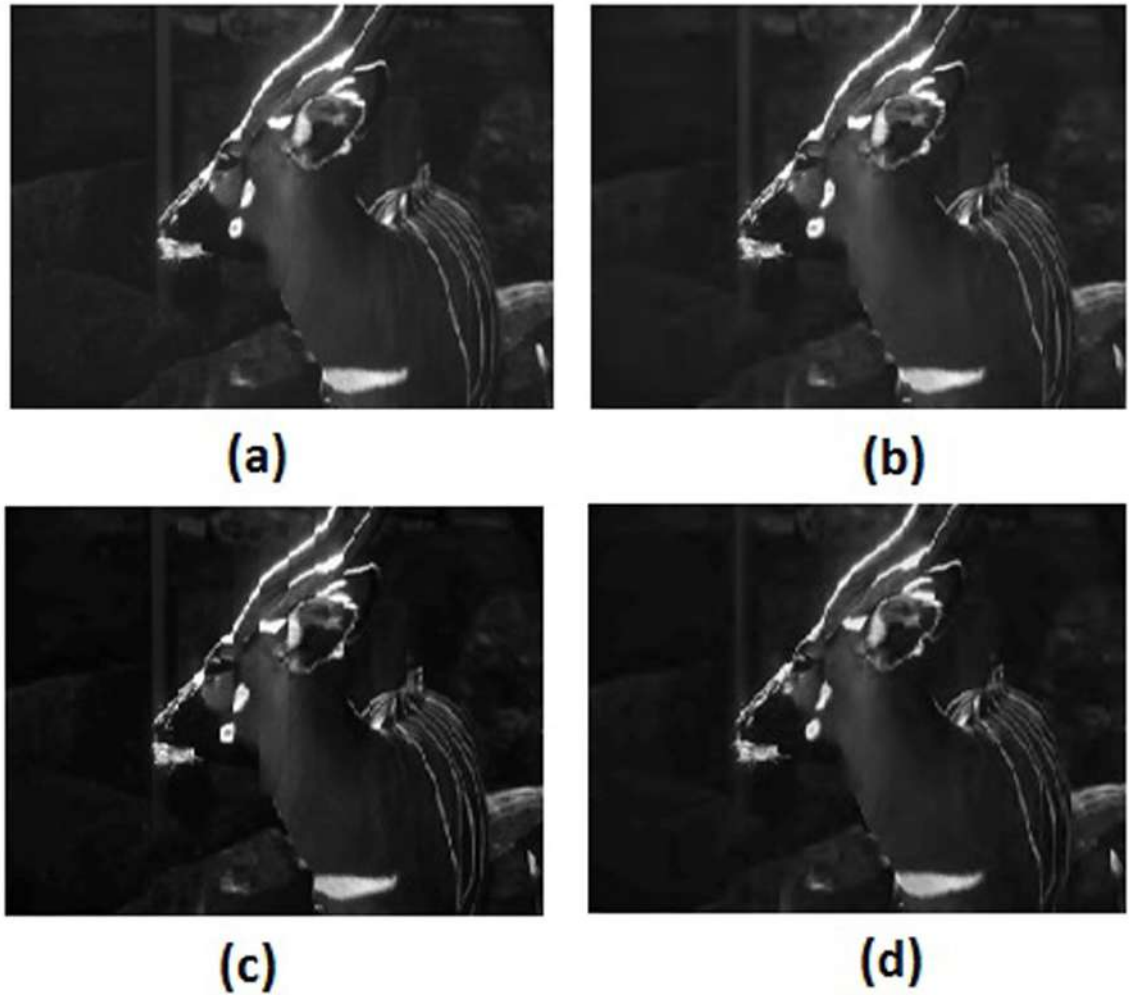


Figure 5.5 (a) Uncompressed 'deer' image (512X512) (b) compressed by ASPIHT (c) compressed by JPEG2000 [184], (D) compressed by proposed method at 40:1



Figure 5.6 (a) Original lena image (512X512) is compressed by compression ratios of (b) 20:1 ;

(c) 40:1; (d) 60:1 (e) 80:1 (f) 120:1 using proposed MSVD-ASPIHT method

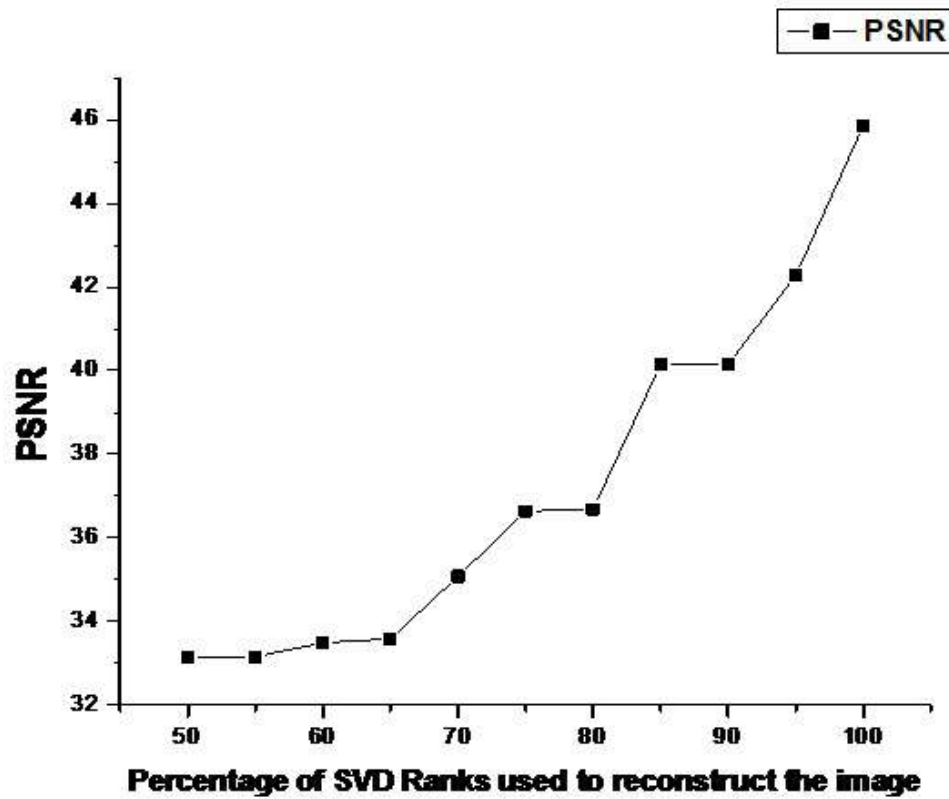


Figure 5.7 Performance evaluation of the proposed method for fixed compression (20:1) with respect to PSNR and percentage of SVD ranks for deer image

Figure 5.6 shows 'len' image, compressed at the different compression ratios using a proposed technique. Figure 5.7 illustrate the PSNR variation along the different percentage of SVD ranks used for reconstruction of 'lena' image (512×512) with fixed compression ratio at 20:1.

5.4 Improved binary tree coding for grey scale image compression by using MSVD

5.4.1 Binary tree coding

The wavelet decomposition distributes the energy of subband into clusters, hence coding of wavelet information becomes more important in image compression. In binary tree coding, the wavelet coefficients are divided into significant and insignificant sub-blocks (i.e code block) based on the threshold and assign them a binary bit for representations [177]. In binary tree coding algorithm, we consider a code block S of wavelet image with the size of $2^N \times 2^N$ and is converted into the one-dimensional indexed array using Morton scanning order [178]. Then the binary tree is constructed from bottom to top with node $\lambda(k)$ where $1 \leq k \leq 2 \times S$. The bottom level of the binary tree consists all wavelet coefficients of Morton scanning order. Upper levels of the tree are defined as follows.

$$\lambda(k) = \max \{ \lambda(2k), \lambda(2k + 1) \} \quad for 1 \leq k \leq S \quad (5.4.1)$$

$\lambda(2k)$ and $\lambda(2k + 1)$ are the offspring of $\lambda(k)$ and tree depth is $P=N+N+1$. After construction of binary tree for each code blocks, span the tree by depth, from top to bottom of the subtree in a bit plane. If tree node is insignificant it is coded with '0' otherwise with '1', and process is repeated for its two offspring. If the process reaches the bottom level and then corresponding coefficient become significant, then its sign is coded. It allows us to concentrate on areas of high energy even also codes the zero pixels compactly. The wavelet coefficients of edges are the treasure of significant coefficients with high magnitude, but they gradually change in natural images. Hence adaptive scanning of this significant coefficient along with it's a neighbors are effectively encodes edges and

improves the image quality [179].

5.4.2 Realization of MSVD-BTC

In this proposed algorithm entropy coding for encoded bit stream is avoided to speed up the execution process. The detailed steps of the proposed method (figure. 5.8) described in two parts with functions *Span-MSVD*, *Span-depth* and *Span-level*, where '*I*' is 8-bit grayscale image matrix. PR is the specified percentage of ranks used for reconstruction.

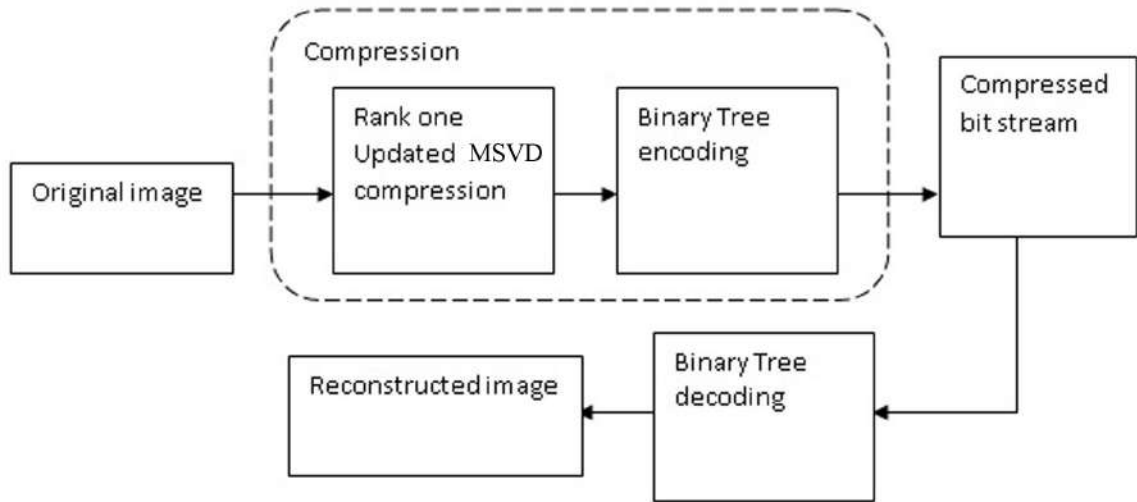


Figure 5.8 Pipelined view of proposed SVD-BTC image compression method

Part-1. The original image is pre-processed by Modified rank one updated SVD.

1. $FunctionCode = span - MSVD(L, Ep, Block, size)$

- Calculate the median m of I and $I_m = I - m$
- Divide the I_m into sub-blocks for defined block size 8×8 .
- Apply SVD for each block and calculate the average percentage of ranks (PR).

– if $PR \leq EP$

- * Ranks used for reconstruction.
- else
- * Neglect the ranks.
- Recombine the blocks into I_m .
- $I_m = I + m$

Part-2. After MSVD process reconstructed image Subjected to wavelet decomposition by CDF 9/7 tap wavelet filter. The wavelet coefficients are under Morton scanning order gives the indexed array for the binary tree. Where k is the index of the node of a binary tree, and T_b is the threshold, $T_0 = 2^{\lceil \log_2 \max(I) \rceil}$ and $T_b = \frac{T_0}{2}$

1. $FunctionCode = span_depth(\lambda, k, T_b)$

- if $\lambda(k)$ coded with significant with the large threshold value, $\lambda(k) \geq T_{k-1}$
- if $k \leq S$
 - $Jl = Span_depth(\lambda, 2k, T_b)$
 - $Jr = Span_depth(\lambda, 2k + 1, T_b)$
 - $code = Jl \cup Jr$
- else
 - $code = \{sign(V(k - s))\}$
- Else if $\lambda(k)$ has a significant parent and the neighbors of $\lambda(k)$ has just been coded with insignificant, namely, $k < 1$ and $tmod2 = 1\lambda(k - 1) < T_b$,
 - if $k < S$,

$$* J_l = \text{Span_depth}(\lambda, 2k, T_b)$$

$$* J_r = \text{Span_depth}(\lambda, 2k + 1, T_b)$$

$$* \text{code} = J_l \cup J_r$$

• *else*

$$- \text{code} = \{\text{sign}(V(k - s))\}$$

• *Else if $\lambda(k) \geq T_b$*

- if $k < S$,

$$* J_l = \text{Span_depth}(\lambda, 2k, T_b)$$

$$* J_r = \text{Span_depth}(\lambda, 2k + 1, T_b)$$

$$* \text{code} = \{1\} \cup J_l \cup J_r$$

- *else*

$$* \text{code} = \{1\} \cup \{\text{sign}(v(k - S))\}$$

* *else*

$$* \text{code} = \{0\}.$$

2. For Adaptive scanning, after Spanning the tree by depth with $\text{Span_depth}(\lambda, 1, T_0)$ the function we obtain the previously scanned significant nodes with the threshold $\{T_Z | Z \geq 0\}$. From bottom to top of the tree, find the brother of previously significant nodes.

For depth $n = N$, repeat up to $n > 1$

• *Function code = Span_Level(T_Z)*

$$- \text{For } K = \sum_{i=1}^{n-1} 2^i + 1 \text{ to } \sum_{i=0}^n 2^i$$

- $ck = \{.\}$.if $\lambda(k) \geq T_{k-1}$,
 - if $k \bmod 2 = 0$ and $\lambda(k+1) < T_{Z-1}$,
 - then $ck = \text{Span_depth}(\lambda, k+1, T_Z)$;
- else if $k \bmod 2 = 1$ and $\lambda(k-1) < T_{Z-1}$,
- then $ck = \text{Span_depth}(\lambda, k-1, T_{Z-1})$;
- $code = \{code, ck\}$
- $n = n - 1$.

The above function of Binary tree coding is the recursive function but for adaptive scanning order, we used the non recursive function to accelerate the process for each bit plane.

5.4.3 Results and discussions

The proposed compression algorithm was tested on 8-bit grayscale (512 X512) Barbara, Lena, Goldhill, Cameraman, Jet-plane, Peppers images. Tables 5.8-5.13 show the comparison of the proposed technique (decomposed at level 5) with SPIHT, BTC (without entropy coding), JPEG and JPEG2000 in terms of PSNR for the different bit per pixel (BPP) respectively. The PSNR values of SPIHT, JPEG, and JPEG2000 compression were obtained from [180] and same tested images are used for consistency check. For maximum compression in MSVD, we use 70 to 75 percentage ranks for reconstruction which boosts the image quality for binary tree coding. Hence the PSNR values of MSVD+BTC in tables are comparatively higher than BTC. Figure 5.9 shows the Lena image compressed by proposed technique at different bit rates.

Table 5.8 PSNR comparison for Barbara image at different BPP

BPP	SPIHT	BTC	JPEG	JPEG2000	MSVD-BTC
0.125	24.84	19.20	23.69	24.87	28.20
0.250	27.57	25.63	26.42	28.17	28.20
0.500	31.39	30.54	30.53	31.82	32.42
1.000	36.41	36.58	35.60	36.68	37.76
1.250	39.80	36.58	39.03	39.40	41.56

Table 5.9 PSNR comparison for Lena image at different BPP

BPP	SPIHT	BTC	JPEG	JPEG2000	MSVD-BTC
0.125	31.10	26.14	28.45	30.93	29.70
0.250	34.13	29.56	31.90	34.03	33.10
0.500	37.27	35.14	35.51	37.16	38.48
1.000	40.45	40.85	38.78	40.36	43.34
1.250	42.00	42.13	41.45	42.00	43.34

Table 5.10 PSNR comparison for Goldhill image at different BPP

BPP	SPIHT	BTC	JPEG	JPEG2000	MSVD-BTC
0.125	28.47	23.50	27.25	28.48	26.76
0.250	30.55	28.50	29.47	30.58	31.83
0.500	33.12	32.90	32.12	33.27	36.87
1.000	36.54	32.94	35.57	36.81	36.87
1.250	39.60	39.10	40.12	40.45	43.00

Table 5.11 PSNR comparison for Cameramen image at different BPP

BPP	SPIHT	BTC	JPEG	JPEG2000	MSVD-BTC
0.125	25.82	28.23	24.88	25.57	32.34
0.250	29.12	31.16	28.20	29.30	35.27
0.500	33.00	32.89	32.11	33.28	37.71
1.000	37.96	33.82	36.29	38.08	38.82
1.250	39.85	33.82	39.42	39.75	39.72

Table 5.12 PSNR comparison for Jet plan image at different BPP

BPP	SPIHT	BTC	JPEG	JPEG2000	MSVD-BTC
0.125	27.27	27.37	26.05	27.23	32.67
0.250	29.89	30.57	28.83	29.79	36.08
0.500	33.54	33.80	32.47	33.54	39.42
1.000	38.24	37.66	37.11	38.30	44.02
1.250	38.96	37.59	39.02	40.42	44.04

Table 5. 13 PSNR comparison for pepper image at different BPP

BPP	SPIHT	BTC	JPEG	JPEG2000	MSVD-BTC
0.125	34.24	28.06	29.45	33.83	31.26
0.250	35.44	31.35	31.58	36.03	34.95
0.500	38.86	35.57	35.83	39.96	39.33
1.000	41.45	40.78	38.75	42.36	43.90
1.250	42.15	40.98	39.95	42.87	43.91



Figure 5.9 (a) Original Lena uncompressed image (b) Compressed at 0.125 BPP ; (c) Compressed at 0.250 BPP; (d) Compressed at 0.500 BPP; (e) Compressed at 1.00BPP; (f) Compressed at 1.250 BPP using proposed method

5.5 Improved EZTW compression algorithm using mean based rank one updated SVD

5.5.1 Mean based rank one updated SVD(MNSVD)

Here we modify formal SVD proposed in section 5.2 by using two additional steps: In the first stage, complete image matrix is subtracted from its mean value before SVD decomposition and then add the mean value after SVD reconstruction. At second stage divide the mean extracted image matrix into sub-block to use the irregular density of the original image. Before SVD decomposition select the Suitable percentage of a sum of singular values instead of predetermined value. Consider for an image J , segmentation based rank one SVD process is given by,

1. A matrix S' is obtained by subtracting original image matrix ' J ' from its mean value.

$$S(m, n) = J(m, n) - \text{mean}(J) \quad (5.5.1)$$

2. Define the block size (32 x 32, 64 x 64, ...) for segmentation.
3. Apply the forward SVD for each sub-blocks of matrix ' S ' by using,

$$[Tu, T\alpha, Tv] = \text{svd}[B(m, n)] \quad (5.5.2)$$

Where Tu is m by n , Tv is n by n , and $\alpha = \text{diag}(r_1, r_2, \dots, r_k, 0, \dots, 0)$

4. The specific percentage of ranks is computed by using the equation 5.6

$$\text{Specifiedpercentage} = \frac{(r_1 + r_2 + r_3 + \dots + r_{k1})}{(r_1 + r_2 + r_3 + \dots + r_k)} \quad (5.5.3)$$

Where $k1$ is rank for each sub-blocks of an image.

5. Apply the Inverse SVD for reconstruction

$$B(m, n) = svd(Tu, T\alpha_{k1}, Tv) \quad (5.5.4)$$

Where Tu is m by n , Tv is $K1$ by n , and $\alpha_1 = \text{diag}(r_1, r_2, r_3, \dots, r_{k1})$

6. Recombine all sub-blocks to get $S(m, n)$, then add the mean value to reconstruct the original image.

$$J^{-1}(m, n) = S(m, n) + \text{mean}(J) \quad (5.5.5)$$

Block based rank one updated SVD is a lossy compression method, is used to compress the grayscale image at high PSNR with low compression ratio. Pre-processing of modified SVD to EZTW possibly improve compression performance in terms of PSNR and SSIM at specific bit rates.

5.5.2 Embedded zero tree wavelet (EZTW)

The wavelet transforms make easy to decompose and reconstruct the image by exercising on different mother wavelets. But low bit rate coding is still challenging part of wavelet-based progressive image compression somehow it is possible by designing of optimized encoders. Scalar quantization in lossy compression generates a sequence of zero and non zero symbols [180]. But the probability of zero's in overall symbols is high and so, low bit rate transmission is quite difficult. A new compression algorithm introduced in[122] shows the possible solution for progressive image compression. It uses parent-child relations in decomposed wavelet coefficients and creates a new data structure zero trees to encode the symbols. The source image is decomposed by using pyramid decomposition with

debauche's wavelet filters [112] at defined levels as shown in figure 5.10 (a). Scan the complete image by using Morton scanning order then classify the coefficients as

1. Parent: Coefficients at crude decomposed scale. (Each parent have four offspring)
2. Child: Coefficients corresponds to a same spatial location at the next bigger scale of parallel direction.
3. Descendent: Coefficients Childs offspring.

The initial threshold of EZTW is calculated by using the formula for decomposed wavelet coefficients $I(m,n)$,

$$T_0 = [\log_2(\max(I))]^2 \quad (5.5.6)$$

Significance mapping: If a wavelet coefficient 'z' is said to be significant if $|z| > T_0$, otherwise coefficient considered as insignificant. And also symbols are classified as shown in figure 5.2(b) based on its status as follows,

1. Zero tree roots: Coefficient and child are zero.
2. Isolated Zero: Coefficient is insignificant but has significant descendants.
3. Positive Significant: Coefficient values with positive sign greater than a threshold value.
4. Negative Significant: Coefficient values with negative sign greater than a threshold value.

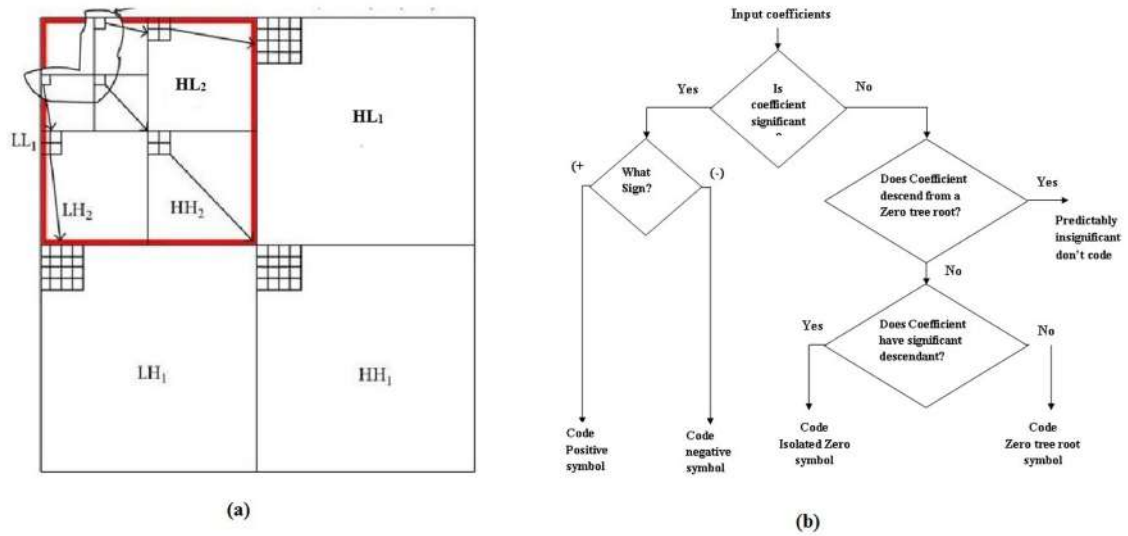


Figure 5.10 (a)Wavelet pyramid decomposition of sub band with parent child relation,(b) flow of Significant mapping for wavelet coefficients

For a First iteration rough structure of the original image is reconstructed. For further iterations, the threshold will become $T_1 = T_0 \setminus 2$ and carry out the significance test and repeat the process until required bit rate is achieved. These symbols are encoded by Huffman encoder, finally, a lengthy compressed bit stream is obtained [181].

5.5.3 Realization of MNSVD-EZTW

This method uses MNSVD to pre-process source image, then it is bypassed through EZTW encoder to get compressed bit stream. Hence, use of modified rank one updated SVD in EZTW (figure 5.11) gain more advantage in achieving high PSNR and SSIM at high compression ratio for defined bitrates.

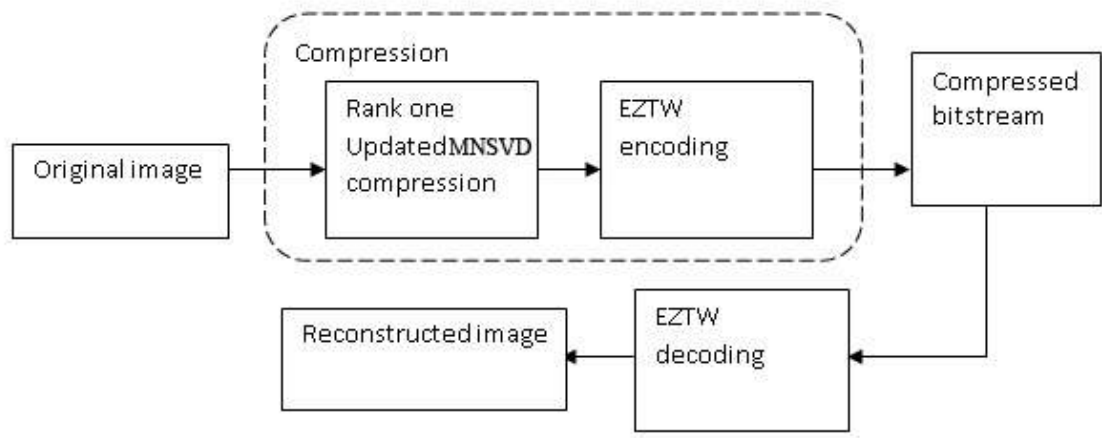


Figure 5.11 Channelized view of an MNSVD-EZTW method

It takes following steps,

1. Resize the original image for fixed standard size (256 x 256 or 512 x 512).
2. Extract the mean value from the resized image and subtract obtained mean value from the resized matrix itself to generate the high correlated matrix by using equation 5.5.1.
3. Apply segmentation with fixed block size and each block is subjected to SVD using equation 5.5.2.
4. A specific percentage of ranks is calculated by using sum singular values of each sub-blocks using equation 5.5.3.
5. Use inverse SVD for all sub-blocks using the equation 5.5.4 and add extracted mean value using equation 5.5.5.
6. Compute the signal to noise ratio and PSNR and bypass the resultant image as an input to EZTW part of a proposed method.

7. EZTW uses ‘Debauchees’ four tap wavelet filter for decomposition and applies specific threshold levels for compression then encode by using Huffman encoder.
8. Finally, a compressed bit stream is decoded by Huffman decoder followed by De-bouches 4-tap wavelet reconstruction filters.

5.5.4 Results and discussions

Standard 8-bit grayscale test images are used to test the proposed compression algorithm. Tables 5.14, 5.15 and 5.16 illustrates the comparative study of MNSVD-EZTW method with EZTW, SPIHT, and JPEG in terms of PSNR at compression ratio 30:1,70:1,90:1 respectively. Likewise, SSIM at the compression ratio of 30:1, 70:1 and 90:1 are tabulated in Tables 5.17, 5.18 and 5.19 respectively.

From the tables 5.14, 5.15 and 5.16 observations, the PSNR values of the MNSVD-EZTW method are improved from basic EZTW method. The PSNR value of the proposed technique for boat image is 0.8dB, 0.2dB and 2dB higher than JPEG compression technique at compression ratio 30:1, 70:1, and 90:1 respectively. Similarly from table 5.17,5.18 and 5.19 shows SSIM values of proposed compression scheme at compression rate 30:1 is much higher than JPEG technique except deer and Lena images.

Table 5.14 PSNR comparison for fixed compression ratio 30:1

Images	EZTW	SPIHT	JPEG	MNSVD-EZTW
Artificial	27.54	29.34	28.43	28.60
Big-Building	25.95	26.85	27.94	28.86
Boats	28.39	29.27	30.43	31.30
Bridge	27.33	26.35	27.79	28.13
Deer	31.78	38.32	39.45	32.07
Fireworks	34.02	33.29	34.24	35.09
Goldhill	28.88	30.20	31.09	32.13
Lena	29.26	33.24	34.77	32.38
Peppers	30.38	31.28	30.87	32.59

Table 5.15 PSNR comparison for fixed compression ratio 70:1

Images	EZTW	SPIHT	JPEG	MNSVD-EZTW
Artificial	22.51	25.61	26.42	24.22
Big-Building	21.84	24.02	25.06	24.41
Boats	23.21	26.44	26.59	26.70
Bridge	21.85	23.35	23.54	23.45
Deer	28.48	33.06	34.73	29.20
Fireworks	23.25	28.06	27.69	23.60
Goldhill	24.08	27.42	27.51	27.21
Lena	24.29	29.61	28.32	27.45
Peppers	24.28	29.66	28.99	27.34

Table 5.16 PSNR comparison for fixed compression ratio 90:1

Images	EZTW	SPIHT	JPEG	MNSVD-EZTW
Artificial	20.34	21.94	23.78	22.03
Big-Building	18.34	20.96	20.75	21.23
Boats	21.16	23.07	22.12	24.69
Bridge	19.14	20.45	20.34	21.23
Deer	24.18	27.46	25.09	25.13
Fireworks	19.44	24.39	22.14	19.61
Goldhill	21.85	24.24	24.32	24.99
Lena	21.24	24.94	24.98	24.75
Peppers	20.87	24.74	24.66	24.08

Table 5.17 SSIM values for fixed compression ratio 30:1

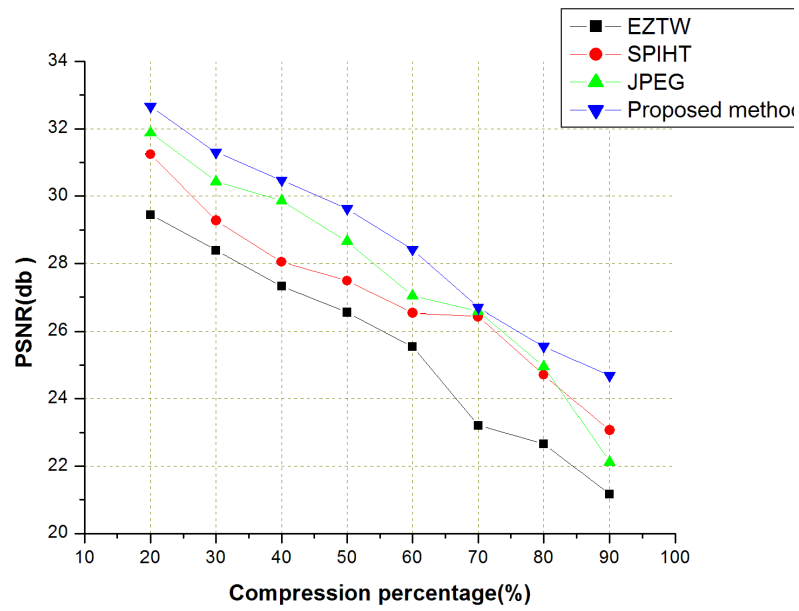
Images	EZTW	SPIHT	JPEG	MNSVD-EZTW
Artificial	0.845	0.818	0.819	0.846
Big-Building	0.768	0.712	0.733	0.767
Boats	0.802	0.789	0.763	0.806
Bridge	0.862	0.828	0.852	0.841
Deer	0.907	0.957	0.942	0.908
Fireworks	0.924	0.892	0.904	0.932
Goldhill	0.820	0.776	0.791	0.821
Lena	0.867	0.881	0.868	0.858
Peppers	0.893	0.785	0.799	0.880

Table 5.18 SSIM values for fixed compression ratio 70:1

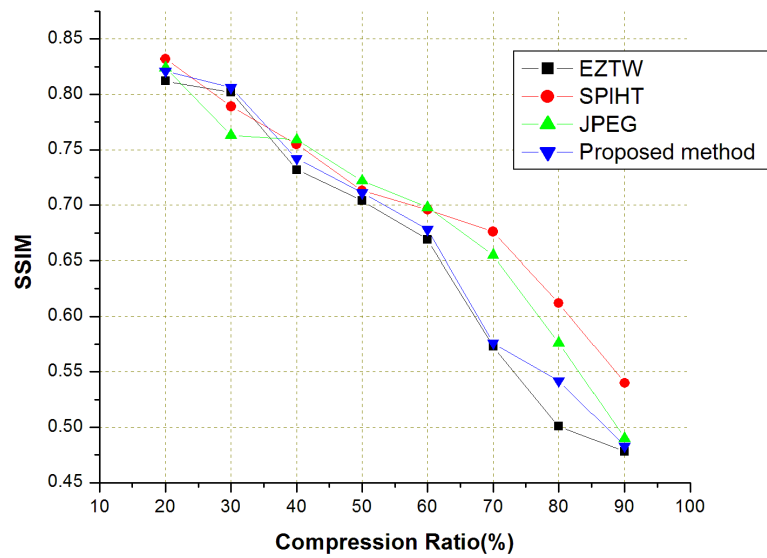
Images	EZTW	SPIHT	JPEG	MNSVD-EZTW
Artificial	0.519	0.690	0.664	0.621
Big-Building	0.522	0.577	0.594	0.525
Boats	0.573	0.676	0.655	0.576
Bridge	0.616	0.711	0.705	0.619
Deer	0.786	0.920	0.912	0.787
Fireworks	0.620	0.772	0.694	0.778
Goldhill	0.537	0.668	0.523	0.537
Lena	0.656	0.804	0.798	0.646
Peppers	0.695	0.753	0.656	0.695

Table 5.19 SSIM values for fixed compression ratio 90:1

Images	EZTW	SPIHT	JPEG	MNSVD-EZTW
Artificial	0.371	0.512	0.440	0.498
Big-Building	0.372	0.421	0.463	0.380
Boats	0.478	0.540	0.490	0.483
Bridge	0.491	0.548	0.498	0.510
Deer	0.734	0.842	0.759	0.745
Fireworks	0.545	0.671	0.643	0.742
Goldhill	0.447	0.544	0.581	0.450
Lena	0.565	0.682	0.564	0.568
Peppers	0.580	0.638	0.632	0.590



(a)



(b)

Figure 5.12 Performance evaluation graph of the proposed technique with another compression method with respect to PSNR(a),SSIM(b) v/s compression ratio

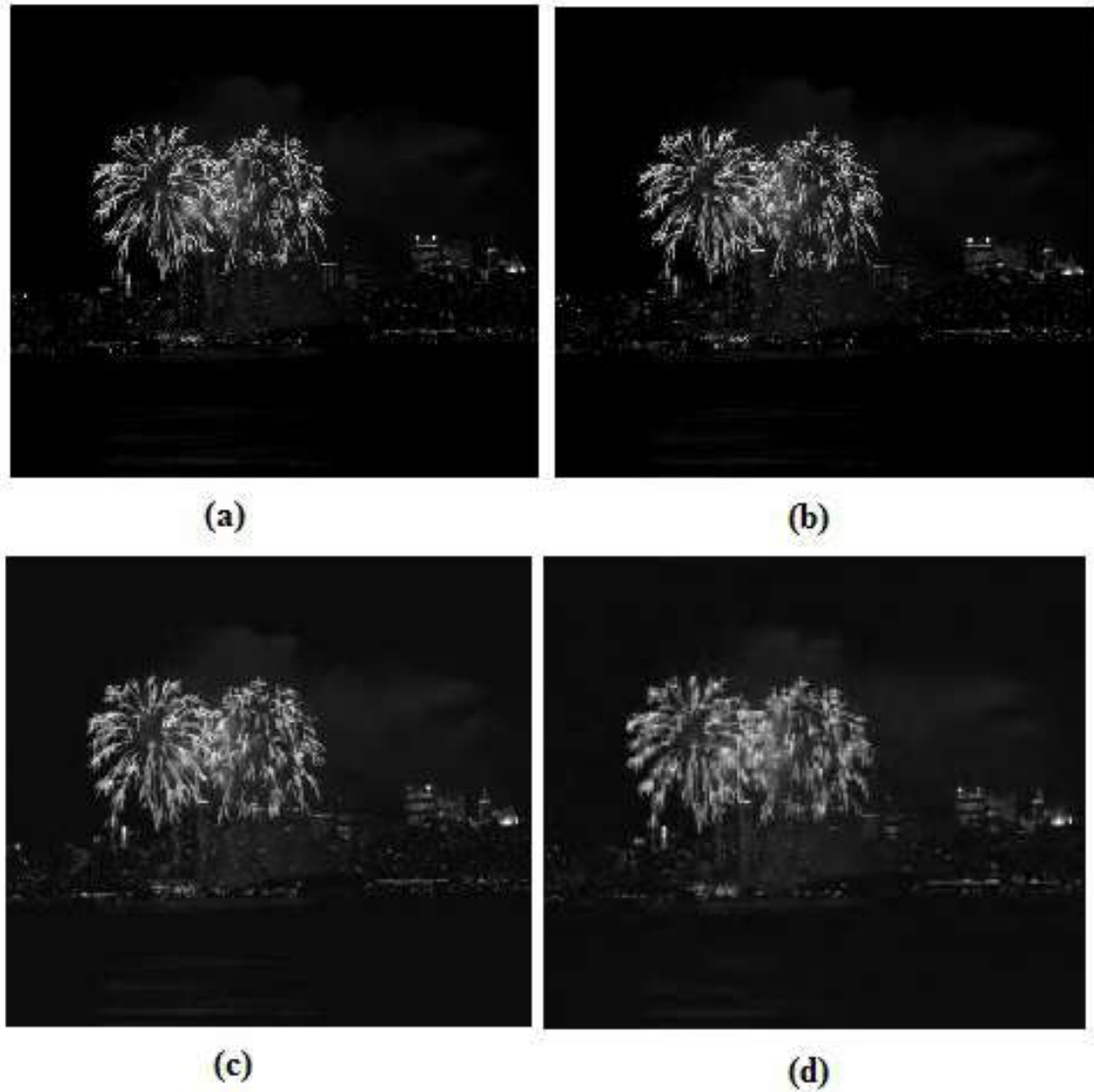


Figure 5.13 (a) Uncompressed fireworks image is compressed by compression ratios of (b) 30:1, (c) 70:1, (d) 90:1 using segmentation based rank one updated SVD-EZTW method

In figure 5.12(a) & 5.12(b), shows a graphical comparison by PSNR versus compression rate and SSIM versus compression rate of the proposed technique with another method for Boat image. From figure 5.12(a), we observe that the PSNR of the proposed technique is superior to another method, However, in figure 5.12(b), the SSIM of the proposed technique is enhanced little bit higher than EZTW and compete with the art of work.

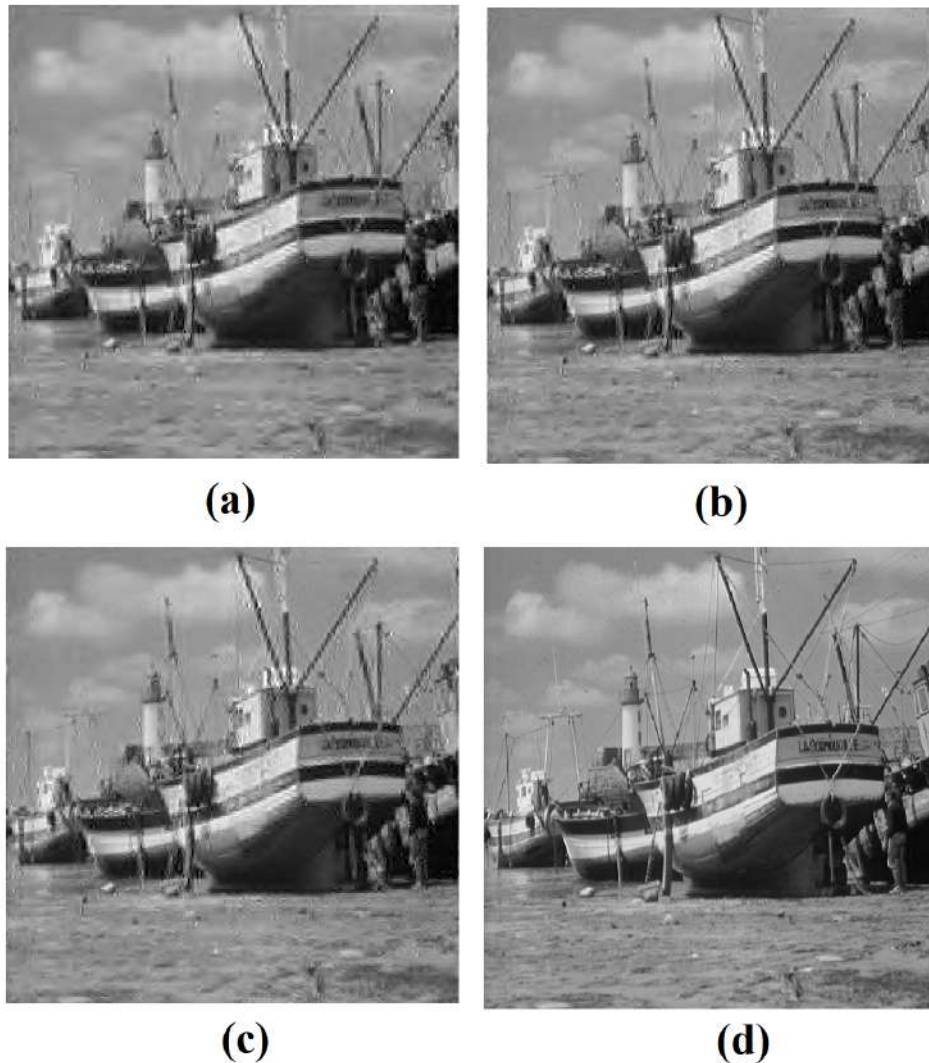


Figure 5.14 Original noisy-Boat image compressed by (a)EZTW (b) Basic SPIHT (c)JPEG (d)

MSVD at compression rate 50:1

It is shown in figure 5.13 the fireworks image is compressed by EZTW and JPEG and MNSVD-EZTW at fixed compression ratio 70:1. In figure 5.14, the noisy boat image is compressed using proposed technique at compression ratio 30:1, 70:1, and 90:1 respectively

5.6 Summary

In this chapter three compression algorithms implementation are described in section 5.3, 5.4 and 5.5 respectively. In section 5.3 the selection of optimized percentage of ranks in SVD and low bit rate coding in EZTW enhances the PSNR value of compression algorithm. SSIM values of some test images are degraded compared to JPEG and JPEG2000 at high compression ratio. Since in achieving high compression ratio compression algorithms neglects some significant information necessary for reconstruction. Similarly, selection of maximum percentage sum of singular values for reconstruction in SVD and adaptive encoding of prior significant pixels during reconstruction in ASPIHT and BTC process increases the PSNR value of compression algorithms described in section 5.4 and 5.5 respectively. However, in SVD-BTC compression algorithm, PSNR value for some test images are reduced since those test images have more number of edges leads to use of more number of significant bits. Apart from some small compromise in the processing of test images with rich edge information these compression algorithms are kept sustain and compete with another state of the art. From simulation results and discussions, the SVD-EZTW and SVD-ASPIHT are efficiently operated at high compression ratio and the significant improvement from its primitive EZTW and ASPIHT methods. However, SVD-BTC also has the high quality of reconstruction even at low BPP and shows significant improvement from BTC compression algorithm.

Chapter 6

Conclusion and Future scope of research work

This thesis begins with preface discussions of problems in representation of digital signals in time-frequency plane and then is extended to signal compression. This discussion identifies that, a significant progress has been made in representing signals in time-frequency domain and signal compression still have some room for development. This research work put effort in representing signal in time frequency plane and to develop compression techniques using wavelet

6.1 Time-frequency representation of signal in wavelet domain

Representation of signal in time-frequency plane encapsulate the signals into its subclasses of different frequencies existed in different time slots. This study notices that the definition of suitable mother wavelet and scales of wavelet filters are played a significant role in the representation of the signal in the time-frequency plane. The wavelet decomposition process splits the signal into most significant and least significant frequency sub-bands. This characterization of the signal in wavelet domain helps us to point out the internal redundancy of signal and in efficient encoding of signal.

6.2 Selection of wavelets for image compression

The wavelet decomposition process has a wide choice in selecting mother wavelet and decomposition levels required. No single basis function and particular levels fit for all types of image data, it may vary from image to image. As levels increase, source image gets decomposed into many subbands. Increase in levels leads to aliasing' effect during reconstruction of image and causes the reduction in image quality. Coarse quantization during compression process is also responsible for a loss of quality. Discussion on lossy and lossless image compression algorithms found that both has their own significance in the specific field of wide applications. Wavelet based signal analysis with wavelet filters, basis functions, and wavelet decomposition process reveal the use of QMF in extraction of wavelet coefficients for defined scale. The concept of wavelet threshold is a key feature of wavelet based image compression, which is effective in reducing the internal redundancy that exists inside the signal. Two major classes of thresholding techniques are discussed in this thesis and implementation of a soft threshold by calculating optimal threshold using improved neigh shrink to code detail coefficients is discussed and the developed algorithm shows significant improvement in the compression performance.

6.3 Image compression using hybrid wavelet transform

The thesis presents two category of compression schemes with focus on hybridization of wavelet algorithm, one catogory, uses combination of either of DCT, DFRCT, DFRFT with wavelet transform. Another one uses MSVD with wavelet transform.

6.3.1 Wavelets with fractional transforms

The first algorithm uses DWT and DCT with improved neigh shrink as wavelet threshold for grey scale image compression. In this algorithm, three level wavelet decomposition and reconstruction method is used with Debouches filters. The approximate subbands are coded by T-matrix coding and second and third level detailed subbands are tresholded with improved neigh shrink and then coded. This algorithm explores the redundancy in first level detail subbands and neglects them. The method uses arithmetic encoder along with run length coding in coding the compressed approximate and detail coefficients. The evaluated results show that the proposed algorithm show better compression performance in terms of PSNR and SSIM with small loss in image quality.

Secondly, a lossy compression algorithm using DWT and DFRCT was discussed. The two-level quantization and compact coding of DFRCT for low-frequency subband made this algorithm efficient in compression. This work is compared with basic DFrST and DFRCT compression.

The third one is a lossless compression algorithm, that uses DWT and DFRFT. This algorithm attempts to increase the compression performance without loss of image quality even at high compression percentage. Simulation results show that, the proposed DWT-DFRFT algorithm is significantly better than DWT-DFRCT algorithm. The extended version of this algorithm called, block based DFRFT is proposed for medical image compression. The method create blocks, and code the decomposed wavelet coefficients by one dimensional DFRFT, which makes this algorithm work as lossless compression algorithm.

6.3.2 Modified SVD in wavelet based progressive image compression

A lossy hybrid compression scheme, that uses a modified rank one updated SVD as the pre-processing operation for progressive image compression is proposed. Here SVD itself a lossy compression scheme, but a modification is made by subtracting image by its mean or median value and then apply the segmentation to that image matrix. This modified SVD increases the image quality and by passing this compressed image as input for wavelet-based progressive image compression methods, enhance the image quality. A hybrid compression of MSVD-ASPIHT is proposed and it shows improvement in performance over ASPIHT and is comparatively higher than JPEG2000 in terms of PSNR and SSIM. Similarly, another the proposed, MSVD-BTC compression algorithm is also better than BTC compression. Finally, another proposed, MNSVD-EZTW compression algorithm better than EZTW and also compete with JPEG at high compression ratio.

The results show that, each hybrid wavelet compression algorithm proposed, show a significant improvement from its conventional wavelet-based compression method.

6.4 Contribution

Some of the major contribution of the work involves in developing

- An optimal wavelet threshold in hybrid DWT-DCT was developed and explained with the help of experimental results. (chapter 3)
- An improved lossy and lossless compression algorithms using DWT-DFRCT and DFRFT are proposed and tested. (chapter 4)

- A hybrid compression method using MSVD and wavelet-based progressive image compressions like EZTW, ASPIHT and BTC is designed and simulated. (chapter 5)

Some minor contributions in the form of algorithms are listed as

- One dimensional coding of DCT as T- Matrix coding for grey scale image compression (section 3.3.2.3)
- One dimensional compression scheme of fractional transforms DFRST, DFRCT and DFRFT for grey scale image(section 4.2)
- New lossy image compression scheme by using median based rank one updated SVD(section 5.1).

6.5 Future work

On the basis of research work reported in this thesis, the hybrid wavelet-based image compression schemes have some limitations and there is a scope for improving these algorithms.

In case of threshold-based compression the performance of the algorithm can be improved, by using of different optimal threshold calculating methods like the visual shrink, sure shrink, buyers shrink in place of neigh shrink. The use of efficient encoder and header tags implementation can also enhance the bit rate of the algorithm. The algorithm can also be extended in compressing the color images with some modifications.

Another significant improvement in hybrid DWT and fractional transform is possible, by designing efficient quantization and encoding methods. The coding of an LL subband

before quantization process increases the number of zeroes and its encoding leads to the reduction in the size of compressed bit stream. Implementation of automatic optimal fractional order selection algorithm can add some improvement in the conventional method. These implementations possibly increase the compression ratio and bit rate.

The SVD based image compression algorithm has, its choices in selection of the optimal percentage of ranks for every set of image. Hence an algorithm that can select the optimal percentage of ranks automatically, will increase the efficiency of the compression algorithm. This work, has limited combination of SVD with EZTW, ASPIHT and BTC methods, however, the combination of SVD with remaining progressive image compression methods can also improve the compression performance. In this work compression algorithms are limited only for gray scale images. However, they can be extended for color images.

Finally, one more potential route intended for future work is to consider a hardware execution of proposed hybrid wavelet-based image compression system by using very large scale integrated (VLSI) chip. This hardware implementation can reveal the stability and suitability of algorithm for deferent applications.

The overall study concludes that, this thesis demonstrates signal analysis in time frequency plane and different approaches for signal compression in wavelet domain with significant improvements.

Bibliography

- [1] P. Khatwani, A. Tiwari, "A survey on different noise removal techniques of EEG signals" *Int. J. Adv. Res. Comput. Commun. Eng.*, Vol.2, No.2,pp.1091-1095,2013.
- [2] J.J. Grefenstette, "Optimization of Control Parameters for Genetic Algorithms", *IEEE Trans. Systems. Man. and Cybernetics*, Vol.16,pp.122-128,1986.
- [3] J. Moody and M. Saffell, "Learning to trade via direct reinforcement" *IEEE Trans. Neural. Netw.*, Vol.12, No.4, pp.875-889,2001.
- [4] R. Brette, W. Gerstner, "Adaptive exponential integrate and fire model as an effective description of neuronal activity" *J. neurophysiology*, Vol. 94,No.5, pp.3637-3642,2005.
- [5] P. Dayan, L.F. Abbott, "Theoretical Neuroscience: Computational and Mathematical Modeling of Neural Systems" The MIT Press, 1st edition, Cambridge, 2001.
- [6] Fausto Galvan, Giovanni Puglisi, Arcangelo Ranieri Bruna, and Sebastiano Battiato "First Quantization Matrix Estimation From Double Compressed JPEG Images" *IEEE Trans. on Inf. Forensics and Security*, Vol.9, No.8, pp.1200-1310,2014.

- [7] M. Kuuk and Y. Korkmaz, "The effect of physical parameters on sound absorption properties of natural fiber mixed non woven composites" *Textile Research Journal*, Vol.82,No.20, pp.2043-2053,2012.
- [8] F. Hlawatsch and G. F. Boudreaux-Bartels, "Linear and quadratic time-frequency signal representations" ,*IEEE Signal Processing Magazine*, Vol.9,No.4,pp.21-67,1992.
- [9] B.Barket Boashas, "A high resolution quadratic time-frequency distribution for multi-component signals analysis" *IEEE Trans. signal proc.*, Vol.49,pp.2232-2239,2001.
- [10] L. Cohen, "Time-frequency distributions - A review" *Proc. IEEE*, Vol.77,No.7, pp.941-981,2001.
- [11] O. A. Ahmed and M. M. Fahmy, "NMR signal enhancement via a new time-frequency transform" , *IEEE Trans. Med. Imag* , Vol.20,pp.1018-1025,1998.
- [12] B. Boshash, "Time frequency signal analysis, in Advances In Spectrum Analysis And Array Processing:" *S. Haykin (Ed.), vol. 1, Prentice-Hall, Englewood Cliffs, NJ*, 1991.
- [13] S.C.Pai, J.J.Ding, "Relations between fractional operations and time-frequency distributions and their applications" ,*IEEE Trans. Signal process.*,Vol.49, No.8,pp.1638-1655,2001.
- [14] A.Koc,H.M.Ozaktas, C.Candan, "Digital computation of Linear cononical transforms" ,*IEEE Trans. Signal process.*, Vol.56,No.6,pp.2384-2394,2007.

- [15] S. B. Suppappola S. Pon Varma, A. Papandreou-Suppappola, "Detecting faults in structures using time-frequency techniques", *Proc. IEEE Int. Conf. Acoust. Speech Signal Process.*, pp.3593 - 3596,2001.
- [16] O. Herrmann, "On the approximation problem in nonrecursive digital filter design, Circuit Theory", *IEEE Transactions on circuit theory*, Vol.18, No.3, pp.411-413, 1971.
- [17] K. G. Harish Kumar, Piyush Kumar, "Design and performance of finite impulse response filter using hyperbolic cosine window", *Int.jr.on Communication*, Vol.02, No.3, pp.45-49,2011.
- [18] C.Y. Chi, D. Wang, "An improved inverse filtering method for parametric spectral estimation", *IEEE Trans. Signal Process.*, Vol.40, No.7, pp.1807-1811,1992.
- [19] M.S. Panahi, K. Venkat, "A class of quadratic FIR filters with applications to spectral shaping and narrow-band generation", *in:IEEE/SP, 13th Workshop on IEEE Statistical Signal Process.*, pp. 817-822,2005.
- [20] C. T. Mullis, A. Roberts, "The use of second order information in the approximation of discrete-time linear systems", *IEEE Trans. Acoustics, Speech, Signal Process.*, Vol.24, No.3, pp. 226-238,1976.
- [21] B. Boashash, "Time-Frequency Signal Analysis and Processing: A Comprehensive Reference", *Oxford: Elsevier Science, ISBN 0-08-044335-4*,2003.
- [22] B. Boashash, P. Black, "An efficient real-time implementation of the Wigner-Ville distribution", *IEEE Trans. Acoust. Speech Signal Processing*, vol.35, pp.1611-1618, 1987.

- [23] D. Chan, "A non-aliased discrete-time Wigner distribution for time-frequency signal analysis", *ICASSP 82 Proc.*, pp. 1333-1336, 1982.
- [24] E. Jacobsen and R. Lyons, "The sliding DFT, Signal Processing Magazine", Vol. 20, No. 2, pp. 74-80, 2003.
- [25] T.M. Claasen and W.G. Mecklenbrauker, "Time-frequency analysis by means of the Wigner distribution", *Proc. of IEEE ICASSP, Atlanta, GA*, Vol. 81, pp. 69-72, 1981.
- [26] J. B. Allen, "Short-term spectral analysis and synthesis and modification by discrete Fourier transform", *IEEE Trans. Acoust. Speech Signal Processing*, vol.25, No.3, pp. 235-238, 1977.
- [27] J. Ville, "Theorie et Applications de la Notion de Signal Analytique", in *Cables et Transmissions*, Vol.2, pages 61-74, 1948.
- [28] T. M. Claasen and W.G. Mecklenbrauker, "The Wigner distribution - A tool for time-time frequency signal analysis, Part I: Continuous-time signals," *Philips J. Res.*, vol. 35, No. 3, pp. 217-250, 1980.
- [29] T. M. Claasen and W. G. Mecklenbrauker, "The Wigner distribution - A tool for time-time frequency signal analysis, Part III: Relations with other time-frequency signal transformations," *Philips J. Res.*, vol. 35, No. 6, pp. 372-389, 1980.
- [30] M. J. Bastiaans, "Wigner distribution function and its application to first-order optics", *J. Opt. Soc. Am.*, Vol.69, pp.1710-1716, 1979.

- [31] F. Hlawatsch and P. Flandrin, "The interference structure of the Wigner distribution and related time-frequency signal representations," *in: The Wigner Distribution-Theory and Applications in Signal Processing, Elsevier. Ed, Amsterdam, The Netherlands,*, pp. 59-133, 1997.
- [32] S. Pikula, P. Bene, "A new method for interference reduction in the smoothed pseudo Wigner-Ville distribution", *in: Proceedings of 8th International Conference on Sensing Technology*, pp. 599-603, 2014.
- [33] Williams W J, Jeong J., "Reduced interference time-frequency distributions.", *In: Boashash B, editors. Time-Frequency Signal Analysis: Methods and Applications, N.Y.: Wiley*, pp. 74-97, 1992.
- [34] Hlawatsch F, "Smoothed pseudo-Wigner distribution, Choi-Williams distribution, and cone-kernel representation: Ambiguity-domain analysis and experimental comparison", *J. Signal Process.*, Vol.43, pp.149-168, 1995.
- [35] De Lamare R.C., Sampaio-Neto R., "Reduced-Rank Space-Time Adaptive Interference Suppression With Joint Iterative Least Squares Algorithms for Spread-Spectrum Systems", *IEEE Trans. Veh. Technol.*, Vol.59, pp. 1217-1228, 2010.
- [36] H. M. Ozaktas, O. Ankan, M. Alper Kutay, and G. Bozdagi, "Digital computation of the fractional fourier transform", *IEEE Transactions on Signal Processing*, Vol. 44, No. 9, pp. 2141-2150, 1996.
- [37] Adhemar Bultheel, Hector , E. Martinez Sulbaran, "Computation of the fractional Fourier transform", *Appl. Comput. Harmon. Anal.*, Vol.16, pp.182-202, 2004.

- [38] B. Santhanam and J. H. McClellan, "The Discrete Rotational Fourier Transform", *IEEE Trans. Signal process.*, Vol. 44, pp. 994-998, 1996.
- [39] S.Chang,Ming-hung yen,Chian-chentseng, "Discrete Fractional Fourier Transform based on orthogonal projection",*IEEE Trans. on Signal processing*, Vol.47, No.5,pp.1335-1348,1999.
- [40] S. Mallat, W.L. Hwang, "Singularity detection and processing with wavelets", *IEEE Trans. Inform. Theory.*, Vol. 38, pp. 617-643,1992.
- [41] Akansu, A.N, Haddad, R.A.,"Multiresolution signal decomposition: transforms, sub-bands, and wavelets", *Academic Press*,ISBN 978-0-12-047141-6,1992.
- [42] A. Berkhout, D. de Vries, and P. Vogel.,"Acoustic control by wave field synthesis". *J. Acoustic Soc. America*, Vol.93, pp.2764-2778, 1993.
- [43] Nicolas Malyska and Thomas F. Quatieri., "Spectral representations of nonmodal phonation", *IEEE Transactions on Audio, Speech, and Language Processing*, Vol.16, No.1, pp. 34-46, 2008.
- [44] J.M.L. Bernard, "On the time-domain scattering by a passive classical frequency dependent wedge-shaped region in a lossy dispersive medium", *Ann. Telecom.*, Vol. 49, No.12, pp. 673-683, 1994.
- [45] W. Xu," Applying of steady-state harmonic distortion limits to the time-varying measured harmonic distortion", *IEEE Power Engineering Society Summer Meeting, Chicago, USA*, pp. 955-957, 2002.

- [46] Qian, S. and Chen, D., "Joint time-frequency analysis: methods and applications", *Prentice-Hall, Inc., New York, USA*, 1996.
- [47] Thayaparan, T., "Linear and quadratic time-frequency representations", *Defence R and D Canada, DREO TM 2000-080*, 2010.
- [48] P. R. Roth, "Effective measurements using digital signal analysis", *IEEE Spectrum*, Vol. 8, pp. 62-70, 1971.
- [49] A. H. Nuttall, G. C. Carter, E. M. Montavon, "Estimation of the two-dimensional spectrum of the space-time noise field for a sparse line array", *J. Acoust. Soc. Amer.*, Vol. 55, pp. 1034-1041, 1974.
- [50] R. J. McAulay, M. L. Malpass, "Speech enhancement using a soft-decision noise suppression filter", *IEEE Trans. Acoust. Speech Signal Processing*, Vol. 28, pp. 137-145, 1980.
- [51] S. P. Kim, W. Y. Su, "Recursive high-resolution reconstruction of blurred multiframe images", *IEEE Trans. Image Processing*, Vol. 2, pp. 534-539, 1993.
- [52] Bentley, J. L., Sleator, D. D., Tarjan, R. E., and Wei, V. K., "A Locally Adaptive Data Compression Scheme. Commun.", *J. ACM*, Vol. 29, No. 4, pp. 320-330, 1986.
- [53] Monsour, Robert A., and Whiting, Douglas L., "Data Compression Breaks Through to Disk Memory Technology", *Computer Technology Review*, Vol. 11, No. 6, pp. 39-45, 1991.

- [54] S.Kavitha,S.Mohammad mansoor roomi,N.Ramaraj, "Lossy compression through segmentation on low depth-of-field images",*int. J. Computer applications*, Vol.19, No.1, PP.59-65,2009.
- [55] A. Skodras, C. Christopoulos, T. EbrahimiThe, "JPEG 2000 still image compression standard", *IEEE Signal Process. Mag.*, Vol.18, No.5, pp. 36-58,2001.
- [56] X. Z. Xiong, Samuel Wu, Cheng, Jianping Hua, "Lossy-to-lossless compression of medical volumetric data using three-dimensional integer wavelet transforms", *IEEE Transactions on Medical Imaging*, Vol.22, No.3, pp. 459-470, 2003.
- [57] J. Kim, C.-M. Kyung, "A lossless embedded compression using significant bit truncation for HD video coding",*IEEE Trans. Circuits Syst. Video Technol.*, Vol.20,No.6, pp. 848-860,2010.
- [58] Paul G. Howard and Jeffrey Scott Vitter, "Arithmetic coding for Data Compression", *Proceeding of the IEEE*, Vol.82, No. 6, pp.445-459,1994.
- [59] ITU-T and ISO/IEC JTC 1, "Advanced video coding for generic audiovisual services," *ITU-T Recommendation H.264 and ISO/IEC14496-10 (MPEG-4 AVC)*, 2010.
- [60] Consultative Committee for Space Data Systems, CCSDS 100.0-G-1: Telemetry Summary of Concept and Rationale, Green Book, issue 1, December 1987. <http://www.ccsds.org/documents/100x0g1.pdf>.
- [61] Z. P. Liang, P. C. Lauterbur, "An efficient method for dynamic magnetic resonance imaging", *IEEE Trans. Med. Imag.*, Vol. 13, pp. 677-686, 1994.

- [62] D. Gibson, M. Spann, and S.I. Woolley, "A Wavelet-Based Region of Interest Encoder for the Compression of Angiogram Video Sequences", *IEEE Transaction on Information Technology in Biomedecine*, Vol. 18, No. 2, pp. 103-113, 2004.
- [63] K. Gerlach and S. D. Blunt, "Adaptive pulse compression repair." *IEEE Transactions on Aerospace and Electronic Systems*, Vol.43, pp. 1188-1195, 2007.
- [64] Beverly Jane Sharkey, "The Federal Aviation Administration Suspected Unapproved Parts Program: Th Need to Eliminate Safety Risks Posed by Unapproved Aircraft Parts", *J. Air L. and Com.*, Vol. 65, pp. 795-804, 2000.
- [65] C. Jung, L. Jiao, H. Qi, T. Sun, "Image deblocking via sparse representation", *Signal Processing: Image Communication*, Vol. 27, No. 6, pp. 663-677, 2012.
- [66] A high quality low complexity algorithm for packet loss concealment with G.711. 1999 ITU, Geneva, Switzerland. Rec. ITU-T G.711, App 1.
- [67] C. Perera, A. Zaslavsky, P. Christen, and D. Georgakopoulos, "Context aware computing for the internet of things: A survey.", *IEEE Commun. Surveys Tuts*. Vol. 16, No.1, pp. 414-454, 2014.
- [68] R.E.Learned and A.L. Willsky, "A wavelet packet approach to transient signal classification", *J. Applied and computational harmonics analysis*, Vol.1, No.2 pp.265-278,1995.
- [69] M. Rabbani, R. Joshi, "An overview of the jpeg2000 still image compression standard", *Signal Processing: Image Communication*, Vol. 17, No. 1, pp. 3-48, 2002.

- [70] H. Oh, A. Bilgin, M. W. Marcellin, "Visually lossless encoding for JPEG2000", *IEEE Trans. Image Process.*, Vol. 22, No. 1, pp. 189-201, 2013.
- [71] Dow JM, Neilan RE, Rizos C., "The international GNSS service in a changing landscape of global navigation satellite systems", *J. Geodesy*, Vol. 83, PP: 191-198, 1994.
- [72] James.R.Fleming, Josep Fourier, "The greenhouse effect, and quest for a universal theory of terrestrial temperatures", *J. of Endeavour*, Vol.23, No.2, pp.72-75, 1999.
- [73] Ramanathan, V., "The Greenhouse Theory of Climate Change: A Test by Inadvertent Global Experiment", *J. of Science*, Vol.240, pp. 293-299, 1988.
- [74] J. Goldstein, "An optimum processor theory for the central formation of the pitch of complex tones", *J. Acoust. Soc. Amer.*, Vol. 54, pp. 1496-1516, 1973.
- [75] J. F. James, "A Students Guide to Fourier Transforms", *Cambridge.Ed*, 1995.
- [76] Dym, H. and McKean, H. P., "Fourier Series and Integrals", *Academic Press, New York NY*, 1972.
- [77] Oppenheim, A. V., Willsky, A. S., Young, I. T., "Signals and Systems", *Prentice Hall Inc. Englewood Cliffs NJ*, 1983
- [78] J. W. Cooley, P. A. W. Lewis, P. D. Welch, "The finite Fourier transform", *IEEE Trans. Audio Electro-acoust.*, vol. AU-17, pp. 77-85, June 1969.
- [79] Jar-Ferr Yang, Fu-Kun Chen, "Recursive discrete Fourier transform with unified IIR filter structures", *Elsevier Science B.V. Signal Processing*, Vol. 82, No. 1, pp. 31-41, 2002.

- [80] I. S. Reed, D. W. Tufts, X. Yu, T. K. Truong, M.-T. Shih, X. Yin, "Fourier analysis and signal processing by use of the Mobius inversion formula", *IEEE Trans. Acoust. Speech Signal Processing*, Vol. 38, pp. 458-470, 1990.
- [81] W. M. Gentleman, G. Sande, "Fast Fourier transforms for fun and profit", *1966 Fall Joint Computer Conf. AFIPS Proc.*, Vol. 29, pp. 563-578, 1966.
- [82] J. W. Cooley, P. A. W. Lewis, P. D. Welch, "Historical notes on the fast Fourier transform", *IEEE Trans. Audio and Electroacoustics*, Vol. AU-15, pp. 76-79, 1967.
- [83] akahiro murakami, Yoshihisa Ishida, "Generalized Sliding Discrete Fourier Transform", *IEICE Transactions on Fundamentals of Electronics Communications and Computer Sciences*, Vol. E99.A, pp. 338, 2016,
- [84] S. G. Mallat, "A theory for multiresolution signal decomposition: The wavelet representation", *IEEE Trans. Pattern Anal. Machine Intell.*, Vol. 11, pp. 647-693, 1989.
- [85] Gilbert strang, "Wavelet and dilation equations: A Brief introduction", *SIAM reviews*, Vol. 31, No.4, pp.614-627, 1989.
- [86] Rao, R.M and Bopardikar, A.S," Wavelet transforms-Introduction to theory and applications", *Addison Wesley Longman, Inc.*,1998.
- [87] Najmi AH, Sadowsky J. "The continuous wavelet transform and variable resolution time- frequency analysis", *J. Hopkins APL Tech. Dig.*, Vol.18, No.1, pp.134-140, 1997.
- [88] S. Mallat, "A theory for multiresolution signal decomposition", *Univ. of Pennsylvania*, 1988.

- [89] Burrus,C.S,Gopinaath,R.A,Guo,H.,”Introduction to Wavelets and Wavelet transforms-A primer”, *New Jersey: prentise hall.*,1998.
- [90] Liu,C.S,Chan,A.K. ”Wavelet tool ware”, *London: Academic press lim.* , 1998.
- [91] I. Daubechies, ”Time-frequency localization operators, A geometric phase space approach”, *IEEE Trans. Inform. Theory*, Vol. 34, pp. 605-612, 1988.
- [92] Yanan Liu, Yinghua Liu, Zhangzhi Cen, Multi-scale ”Daubechies wavelet-based method for 2-D elastic problems, In Finite Elements in Analysis and Design”, Vol.47, No.4, PP. 334-341,2011.
- [93] D.L. Donoho, ”Denoising by soft-thresholding”, *IEEE Trans. Inform. Theory*, Vol.41, No.3, pp.613-627, 1995.
- [94] I. Daubechees, ”Where do wavelets come from?- A personal point of view”, *Proc. IEEE*, Vol.84, No.4, pp.510-513, 1996.
- [95] Jerome Lebrun and Martin Vetterli.,” Balanced multiwavelets theory and design”, *IEEE Transactions on Signal Processing*, Vol.46, No.4, pp.1119-1125, 1998.
- [96] Olivier Rioul, ”Regular wavelets: a discrete-time approach”, *IEEE Trans. on Signal Processing*, Vol.41, No.12, pp.3572-3579, 1993.
- [97] S. Mallat, ”Multi-frequency channel decompositions of images and wavelet models”, *IEEE Transactions on Acoustics, Speech, and Signal Processing*, Vol.37, pp.2091-2110 , 1989.
- [98] Vidyanathan.P.P, ”Multirate systems and Filter banks”,*Prentice Hall Inc.*, 1993.

- [99] Sweldens W., "The lifting scheme: A custom-design construction of biorthogonal wavelets", *J. Applied and Computational Harmonic Analysis*, Vol.3, No.2, pp.186-200, 1996.
- [100] R. Jain, H.-H. Nagel, "On the analysis of accumulative difference pictures from image sequences of real world scenes", *IEEE Trans. Pattern Anal. Mach. Intell.*, Vol. 1, No. 2, pp. 206-214, 1979.
- [101] J. Hao, C. Li, Z. Kim, Z. Xiong, "Spatio-temporal traffic scene modeling for object motion detection", *IEEE Trans. Intell. Transp. Syst.*, Vol. 14, No. 1, pp. 295-302, 2013.
- [102] De-Lee Fugal, "Conceptual Wavelet in DSP, An in depth practical approach for the Non- mathematician", *Space and signal Technical Publishing, Sandiago, California*,2009.
- [103] K. R. Rao, J. J. Hwang, "Techniques and Standards for Image Video and Audio Coding", *Prentice Hall*, 1996.
- [104] J. A. Richards, X. Jia," Remote Sensing Digital Image Analysis an Introduction", *Berlin, Germany:Springer-Verlag*, 1999.
- [105] T. Ning, C. H. Huang, J. A. Jenson, V. Wong, H. Chan, "Optical emission spectrum processing using discrete-wavelet transform compression", *Proc. IEEE/SEMI ASMC*, pp. 403-406, 2016.
- [106] A. Segall, "Bit allocation and encoding for vector sources", *IEEE Trans. Inform. Theory*, Vol. IT-22, pp. 162-169, 1976.

- [107] Burt P J and Adelson E H, "The Laplacian pyramid as a compact image code", *IEEE Transactions on Communications*, pp.532-540, 1983.
- [108] A. Croisier, D. Esteban, and C. Galand," Perfect channel splitting by use of interpolation/decimation /tree decomposition techniques", *in: Proceedings of the International Symposium on Information Circuis and Systems, Patras, Greece.,Vol.65,* pp.346-354, 1976.
- [109] M. J. T. Smith and S. L. Eddins, "Analysis/synthesis techniques for subband image coding", *IEEE Transactions on Acoustics, Speech, and Signal Processing*, Vol. 38, No. 8, pp. 1446-1456, 1990.
- [110] S.K. Mitra," Digital Signal Processing Computer-Based Approach", *2nd edition,* *Mc Graw-Hill,A New York*, 2001.
- [111] J. W. Woods and S. D. Neil, "Sub-band coding of images", *IEEE Transactions on Acoustics, Speech, and Signal Processing*, Vol. 34, No. 10, pp. 1278-1288, 1986.
- [112] I. Daubechies," Orthonormal bases of compactly supported wavelets", *Commun. Pure Appl. Math.*, Vol.41, No.4, pp.909-996,1998.
- [113] Stephen.G. Mallat, "A Theory for Multiresolution Signal Decomposition: The Wavelet Representation", *IEEE Trans. on Pattern Analysis and Machine Inteligence*, Vol. 11, No.7,pp.674-693.1989.
- [114] M. Jansen and A. Bultheel, "Multiple wavelet threshold estimation by generalized cross validation for images with correlated noise", *IEEE Transactions on Image Processing*, Vol. 8, No. 7, pp. 947-953, 1999.

- [115] S. G. Chang, B. Yu, and M. Vetterli, "Adaptive wavelet thresholding for image denoising and compression", *IEEE Transactions on Image Processing*, Vol. 9, No. 9, pp. 1532-1546, 2000.
- [116] D. L. Donoho and I. M. Johnstone, "Ideal spatial adaptation by wavelet shrinkage", *J. Biometrika*, Vol. 81, No. 3, pp. 425-455, 1994.
- [117] G. Gupta, "Algorithm for image processing using improved median filter and comparison of mean, median and improved median filter", *International Journal of Soft Computing and Engineering*, Vol. 1, No. 5, pp. 2231-2307, 2011.
- [118] H. C. Li, W. Hong, Y. R. Wu, and P. Z. Fan, "Bayesian wavelet shrinkage with heterogeneity-adaptive threshold for SAR image despeckling based on generalized gamma distribution", *IEEE Transactions on Geoscience and Remote Sensing*, Vol. 51, No. 4, pp. 2388-2402, 2013.
- [119] S.G. Chang, B. Yu. M. Vetterli, "Adaptive wavelet thresholding for image denoising and compression", *IEEE Trans. Image proce.*, Vol.9, pp.1532-1546, 2000.
- [120] F. Ruggeri, B. Vidakovic, "A Bayesian decision theoretic approach to wavelet thresholding", *J. Statist. Sinica*, Vol. 9, No. 1, pp. 183-197, 1999.
- [121] I. M. Johnstone, B. W. Silverman, "Wavelet threshold estimators for data with correlated noise", *J. R. Statist. Soc.*, Vol. 59, 1997.
- [122] Shapiro, J. M., "Embedded image coding using zero tree of wavelet coefficients", *IEEE Transactions on Signal Processing*, Vol. 41, No. 12, pp. 3445-3462, 1993.

- [123] Said, Amir; Pearlman, William A, "A new fast and efficient image codec based on set partitioning in hierarchical trees", *IEEE Transactions on Circuits and Systems for Video Technology*, Vol.6, No.3, pp. 243-250,1996.
- [124] Kassim A A, Lee W S, "Color image coding using SPIHT with partially linked spatial orientation trees", *IEEE Trans. on Circuit and System for Video Technology*, Vol. 2, No. 2, pp. 203-206, 2003.
- [125] W A Pearlman, A Islam, N Nagaraj, A Said, "Efficient low-complexity image coding with a set-partitioning embedded block coder", *Proc. IEEE Transactions on Circuits and Systems for Video Technology*, pp. 1219-1235, 2004.
- [126] J Y Kim, L S Kim, S H Hwang, "An advanced contrast enhancement using partially overlapped sub-block histogram equalization", *Proc. IEEE Transactions on Circuits and Systems for Video Technology*, pp. 475-484, 2001.
- [127] Tian J., Wells R.O. Jr.," Image Data Processing in the Compressed Wavelet Domain.", *3rd International Conference on Signal Processing Proc. Beijing, China*, pp.978-981,1996.
- [128] Jai A., Potnis A., "Wavelet Based Video Compression Using STW, 3D-SPIHT and ASWDR Techniques: A Comparative Study". *International Journal of Advances in Engineering and Technology*, Vol.3, No.2, pp.224-234, 2012.
- [129] S. Wang, A. Rehman, Z. Wang, S. Ma, and W. Gao, "SSIM-motivated rate distortion optimization for video coding", *IEEE Transactions on Circuits and Systems for Video Technology*, Vol. 22, No. 4, pp. 516-529, 2012.

- [130] Sonja Grgic, Mislav Grgic, "Performance Analysis of Image Compression Using Wavelets", *IEEE trans. on Industrial Electronics*, Vol.48,pp.354-366,2009.
- [131] Mohammed Mustafa Siddiq, E, "Using two level DWT with limited sequential search algorithm for image compression", *Journal of Signal and Information Processing*, Vol.3, pp. 51-62, 2012.
- [132] Strang. G and Nguyen.T, D., "Wavelets and Filter Banks", *Wellesly-Cambridge press, Wellesly, MA,,1996*. <http://www-math.mit.edu/gs/book/wfb.html>.
- [133] J. C. Goswami, A. K. Chan, "Fundamentals of Wavelets: Theory Algorithms and Applications", *Hoboken, NJ, USA:Wiley*, 1999.
- [134] A. Skodras, "Fast discrete cosine transform pruning", *IEEE Trans. Signal Process.*, Vol. 43, No. 2, pp. 197-205, 1995.
- [135] D. Marpe, H. Schwarz, T. Wiegand, "Context-based adaptive binary arithmetic coding in the H.264/AVC video compression standard", *IEEE Trans. Circuits Syst. Video Technol.*, Vol. 13, No. 7, pp. 620-636, 2003.
- [136] Zhou Dengwen, Chen Wengang, E., "Image denoising with an optimal threshold and neighboring window", *Pattern Recognition letters*, Vol. 29, pp.1694-1697, 2008.
- [137] Awal Mohammed Rufai, Gholamreza Anburjafri, Hasam Demirel," Lossy image compression using singular value decomposition and wavelet difference reduction", *Digital signal processing, Elsevier pub.*, Vol. 24, pp.117-123, 2014.
- [138] Akyildiz IF, Media T, Chowdhury KR," A survey on wireless multimedia sensor networks", *Journal of Computer Networks*, Vol.51, No.4, pp. 921-960,2007.

- [139] Khalid Sayood, "Introduction to data compression", 3rd edition, Morgan Kaufman publication, 2006.
- [140] L. Jones, T.W. Parks, "A high-resolution data-adaptive time-frequency representation", *IEEE Trans. Acoust. Speech Signal Process.*, Vol.38, pp.2127-2135, 1990.
- [141] E. Cands, J. Romberg, T. Tao, "Robust uncertainty principles: Exact signal reconstruction from highly incomplete frequency information", *IEEE Trans. Inform. Theory*, Vol.52, No.2, pp. 489-509, 2006.
- [142] Xiaoping Jiang, Hao Ding, HuaZhang, Chenghua Li, "Study on compressed sensing reconstruction algorithm of medical image based on curvelet transform of image block", *Journal of Neuro computing*, Vol. 220, No.12, pp. 191-198, 2017.
- [143] L. Yuan Hsu, Hwai Tsu Hu, "Blind watermarking via exploitation of inter block prediction and visibility threshold in DCT domain", *J. Visual comm. and image research*, Vol.32, pp. 130-143, 2015.
- [144] Bultheel A., Martinez H., "A shattered survey of the fractional Fourier transform". *TW Reports, TW337, 42 pages, Department of Computer Science, K.U. Leuven, Leuven, Belgium, 2002.*
- [145] V. Namias, "The fractional order Fourier transform and its application to quantum mechanics", *J. Inst. Math. Appl.*, Vol. 25, pp. 241-265, 1980.
- [146] G. W. Beakley, F. B. Tuteur, "Distribution-free pattern verification using statistically equivalent blocks", *IEEE Trans. Comput.*, Vol. C-21, pp. 1337-1347, 1972.

- [147] G. J. Sullivan, J. Ohm, W.-J. Han, T. Wiegand, "Overview of the high efficiency video coding (HEVC) standard", *IEEE Trans. Circuits Syst. Video Technol.*, Vol. 22, No. 12, pp. 1649-1668, 2012.
- [148] J. Han, A. Saxena, V. Melkote, K. Rose, "Jointly optimized spatial prediction and block transform for video and image coding", *IEEE Trans. Image Process.*, Vol. 21, No. 4, pp. 1874-1884, 2012.
- [149] J. C. Wood, D. T. Barry, "Radon transformation of time-frequency distributions for analysis of multicomponent signals", *IEEE Trans. Signal Process.*, Vol. 42, No. 11, pp. 3166-3177, 1994.
- [150] B. W. Dickinson, K. Steiglitz, "Eigenvectors and functions of the discrete Fourier transform", *IEEE Trans. Acoust. Speech Signal Process.*, vol. ASSP-30, no. 1, pp. 25-31, Feb. 1982.
- [151] F. A. Grnbaum, "The eigenvectors of the discrete Fourier transform: A version of the hermite functions", *J. Math. Anal. Appl.*, Vol. 88, No. 2, pp. 355-363, 1982.
- [152] D. Y. Wei, Q. W. Ran, Y. M. Li, J. Ma, L. Y. Tan, "Fractionalisation of an odd time odd frequency DFT matrix based on the eigenvectors of a novel nearly tridiagonal commuting matrix", *IET Signal Process.*, Vol. 5, No. 2, pp. 150-156, 2011.
- [153] B. Santhanan, T. S. Santhanan, "Discrete Gauss-Hermite functions and eigenvectors of the centered discrete Fourier transform", *Proc. IEEE Int. Conf. Acoust. Speech Signal Process.*, Vol. 3, pp. 1385-1388, 2007.

- [154] Yeh , M.H. Pei, S.C,”A method for the discrete fractional Fourier transform computation” , *IEEE Trans. Signal process.*, Vol.51, No.3, pp. 889-891, 2003.
- [155] Muhammad Irfan, Liying Zheng and Haroon Shahzad, ”Review of Computing Algorithms for Discrete Fractional Fourier Transform” , *Research Journal of Applied Sciences, Engineering and Technology*, Vol.6, No.11, pp. 1911-1919, 2013.
- [156] Cagatay candan, M.Alperkutay, Haldun.M.Ozakatas, ”The Discrete Fractional Fourier Transform” , *IEEE Trans. on signal processing*, Vol. 48, No. 5, pp.1329-1337, 2000.
- [157] Wilkinson.J.H, ”The Algebraic Eigenvalue problem”, *Oxford.pub, U.K.: Oxford*,1998.
- [158] Bradley, W.D. and S. Kenneth, ”Eigenvectors and functions of the discrete Fourier transform” , *IEEE Trans.Acoust. Speech*, Vol.30, No.1, pp.25-31, 1982.
- [159] W.B.Pennebaker,J.L. Mitchell,”JPEG still image data compression standard”, *1sted.,Kluwer Academic Publishers*,1992.
- [160] Singh. K,”Performance of discrete fractional fourier transform classes in signal processing applications”, (doctoral Thesis-2006),Retrieved from:dspace.http://thapar.edu:8080/jspui/bitstream/123456789/94/1/P92233.pdf.
- [161] Wang XW, Blostein SD, ”Video image transmission over mobile satellite channels”, *Signal processing: Image communication* Vol.16, pp. 531-540, 2001.
- [162] Vilchez FG, Mari JM, Zortea M, Blanes I, Ruiz VG, Valls GC, Plaza A, Sagrista JS, ”On the impact of lossy compression on hyperspectral image classification and

- unmixing", *IEEE Transmission Geoscience and Remote sensing Letter*, Vol.8, No.2, pp.253-257,2011.
- [163] Usevith BE, "A tutorial on modern lossy wavelet image compression: foundation of JPEG 2000", *IEEE signal processing Magazine*, pp. 22-35, 2001.
- [164] Taubman D, "High-performance scalable image compression with EBCOT", *IEEE Transaction on Image processing*, Vol.9, No.7, pp.1158-1170, 2001.
- [165] Neelamani RN, Fan Z, "JPEG Compression History Estimation for Color Images", *IEEE Transaction on Image processing*, Vol.15, No.6, pp.1365-1378, 2006.
- [166] Kim BJ, Xiong Z, Pearlman WA., "Low bit-rate scalable video coding with 3-D set partitioning in hierarchical trees (3-D SPIHT)", *IEEE Trans. On Circuits and Systems for Video Technology*, Vol.10, No.8, pp.1374-1387, 2003.
- [167] Golub GH, Van Loan, CF, "Matrix Computations", 3rd ed. *John Hopkins University Press*, 1996.
- [168] Waldemar P, Ramstad TA, "Hybrid KLT-SVD image compression", *IEEE International Conference on Acoustics, Speech, and Signal Processing*, Vol.4, pp.2713-2716, 2006.
- [169] Brand M, "Fast low-rank modifications of the thin singular value decomposition", *J. Linear Algebra and its Applications*, Vol.415, pp.20-30, 2006.
- [170] Kumar R, Kumar A, Singh GK, "Hybrid method based on singular value decomposition and embedded zero tree wavelet technique for ECG signal compression", *Computer methods and programs in biomedicine*, Vol.129, pp.135-148,2016.

- [171] An Investigation into using Singular Value Decomposition as a method of Image Compression. <http://www.haroldthecat.f2s.com/project>. Accessed on 12/2005.
- [172] Jha KS, Yadava RDS, "Denoising by Singular Value Decomposition and Its Application to Electronic Nose Data Processing", *IEEE Sensor Journal*, Vol.11, No.1, pp.35-44,2006.
- [173] Y. kiwon, C. Han, U. Kang, K. Sohan, "Embedded compression algorithm using error aware quantization and hybrid DPCM/BTC coding", *IEEE Int. conf. multimedia Expo. (ICME)*, pp. 1-6, 2011.
- [174] P.J.Burt, E.H.Adalson, "The Laplacian pyramid as a compact image code", *IEEE Trans. commun.*, Vol.31, pp.532-540,2011.
- [175] Naik AK, Holambe RS, "New Approach to the Design of Low Complexity 9/7 Tap Wavelet Filters With Maximum Vanishing Moments", *IEEE Transaction on Image processing*, Vol.23, No.12, pp.5722-5732,2014.
- [176] Artyomov E, Rivenson Y, Levi G, Pecht YO, "Morton (Z) Scan Based Real-Time Variable Resolution CMOS Image Sensor", *IEEE Transaction on Circuits and system for video technology*, Vol.15, No.7, pp.2345-2356, 2005.
- [177] Huang KK, Dai DQ, "A New On Board Image Codec Based on Binary Tree with Adaptive Scanning Order in Scan-Based Mode", *IEEE Transaction On geoscience and remote sensing*, Vol.50, No.10, pp.3737-3750, 2010.
- [178] E. J. Delp, O. R. Mitchell, "Image compression using block truncation coding", *IEEE Trans. Commun.*, vol.27, pp. 1335-1342, 1979.

- [179] F.W. Wheeler and W.A. Pearlman, "SPIHT image compression without list", *in Proc. ICASSP Istanbul, Turkey,, Vol.45*, pp. 2047-2050, 2000.
- [180] K. Ahmadi, A.Y. Javid and E. Salari," An efficient compression scheme based on adaptive thresholding in wavelet domain using particle swarm optimization", *Journal of Signal processing: Image Communication* , Vol.32,pp.33-39, 2012.
- [181] Kun KH,"Improved set Partitioning in hierarchical tree algorithm based on adaptive coding order", *Journal of computer applications*, Vol.32, No.3, pp.732-735, 2012.

Publications

1. *"Improved binary tree coding for image compression using modified singular value decomposition"*, **Naveen Kumar.R**,B.N.Jagadale, J.S.Bhat, Journal of informatics and mathematical science, **(Accepted)(2017)**.
2. *"Hybrid image compression using modified singular value decomposition and adaptive set partitioning in hierarchical tree"*, **Naveen Kumar.R**,B.N.Jagadale, J.S.Bhat, Indian Journal of Science and Technology, Vol. 10 No. 28, (2017) pp. 1-9.
3. *"An improved neigh shrink in hybrid wavelet transform for image compression"*,**Naveen Kumar .R**, B.N.Jagadale, J.S.Bhat, International Journal in Advanced Research in Computer Science, Vol. 8 No. 3, (2017) pp. 330-333.
4. *"A lossless image compression using one dimensional discrete fractional Fourier transform"*, **Naveen Kumar.R**,B.N.Jagadale, Sharvani.M,Nayana.B, Meghana.B.N, International Journal of Innovative Research in Science, Engineering and Technology, Vol. 6 No. 5, (2017) pp. 7828-7832.
5. *"An improved lossy image compression using wavelet and fractional cosine transforms"*, **Naveen Kumar.R**,B.N.Jagadale, J.S.Bhat, Communicated to an International Journal.

6. "An improved embedded zero tree coding using modified singular value decomposition for grayscale image compression", **Naveen Kumar.R**, B.N.Jagadale, J.S.Bhat, Communicated to an International Journal.
7. "Medical image compression using hybrid wavelet transform with block based fractional Fourier transform", **Naveen Kumar.R**, B.N.Jagadale, J.S.Bhat, Communicated to an International Journal.
8. "1D & 2D signal compression using discrete wavelet transform:A survey", **Naveen Kumar.R**, B.N.Jagadale, J.S.Bhat, Communicated to an International Journal.

Publications in International Conference proceedings

1. "Use of optimal threshold and T-Matrix coding in discrete wavelet transform for image compression", **Naveen Kumar.R**, B.N.Jagadale, J.S.Bhat, Sandeepa.K.S, IEEE sponsored , 3rd International Conference on Electronics and Communication System (ICECS-16), Vol. 3 No. 28, (2016) pp. 1462-1465..
2. "Performance evaluation of image compression in walsh wavelet transform using wavelet threshold", **Naveen Kumar.R**, B.N.Jagadale, J.S.Bhat, Sandeepa.K.S, IEEE sponsored , 3rd International Conference on Innovation in Information, Embedded and Communication System(ICIIECS-16), Vol. 4 No. 28, (2016) pp. 500-503.

Publications in National Conference proceedings

1. "Transform coding techniques for audio/speech signal: A survey", **Naveen Kumar.R**, B.N.Jagadale, Sandeepa.K.S, National Conference on Recent Trends in Electronics and its Application, GFGC, K.R.Puram-Bangalore (2014).

2. "*Wavelet based biomedical signal compression for telemedicine applications*", **Naveen Kumar.R**, B.N.Jagadale, Sandeepa.K.S, *JNANARJANA 2K14*, The Oxford college of science-Bangalore (2014).
3. "*ECG signal compression using wavelet transform*", **Naveen Kumar.R**, B.N.Jagadale, Sandeepa.K.S, *KSTA regional conference*, JSS College of Arts, Commerce and Science-Mysore, **Abstract proceedings**) (2016).